Master thesis

Real-Time Capable Vehicle and Driver Model for Traffic Flow Simulation

by Harald Kraus

Carried out at the Institute of Automotive Engineering
Member of Frank Stronach Institute

Head of the department: Univ.-Prof. Dipl.-Ing. Dr. techn. Wolfgang Hirschberg
Supervisors: Univ.-Doz. Dipl.-Ing. Dr. techn. Arno Eichberger
Univ.-Prof. Dr.-Ing. Martin Fellendorf

Graz, November, 2011

Statutory Declaration

I declare that I have authored this thesis independently, that I have not used other than the declared sources / resources, and that I have explicitly marked all material which has been quoted either literally or by content from the used sources.

date	(signature)

Abstract

In automotive engineering, computer aided numerical simulations gain more and more in importance. They have been used in order to reduce costs and time, and also to get information about the vehicle characteristics in early stages of the vehicle development process. Complex models which provide improved accuracy are a valuable tool for the development of the vehicle driving behavior. For traffic simulation and transport planning, the usage of simple vehicle models have often been sufficient.

For more advanced researches on traffic flow and transport planning, the usage of physically accurate vehicle models have become more important. One of these researches deals with so-called "shared spaces", which is about the efficient utilization of public places. In order to identify the potential of such a new road infrastructure, simulations with different types of vehicles with realistic driving behavior have to be carried out.

The aim of the present diploma thesis is the development of a suitable vehicle model for such simulations, which has to be physically accurate, but real-time capable as well. This high demand results in well-thought-out simplifications of the model complexity, in order to save resources and therefore meet the demand of real-time capability. Concurrently, this specification of the simulation model raises the problem of being too inaccurate. Hence, the emphasis of this thesis is put on the right compromise between model precision and necessary simplifications to meet all expectations.
In order to provide a variety of different vehicles, parameter sets of different vehicle classes are elaborated as well.

By implementing an additional driver model, the description of the desired course is simplified, since only position points are needed in order to follow a certain course instead of the needed driver control, which would require an extensive preprocessing. Moreover, the influence of different driving styles may also be studied by varying the driver parameters.

At the end of the present work, the potential of the elaborated vehicle and driver model in real-time traffic flow simulations is discussed by pointing out its main benefits and drawbacks. This is supported by a comparison study with more complex vehicle models in a variety of different driving maneuvers.

Kurzfassung

Die Bedeutung von komplexen, computer-unterstützten numerischen Simulationen hat im Bereich der Automobilindustrie in den letzten Jahren rapide an Bedeutung gewonnen. Ihr Einsatz hilft, Zeit und Kosten einzusparen, und nicht zuletzt liefern sie bereits während des Entwicklungsprozesses Kenntnisse über die Eigenschaften von Fahrzeugen. Während die Verwendung von simplen Fahrzeugmodellen oftmals für Verkehrssimulationen und Transportplanungen ausreicht, steigern komplexe Modelle die Genauigkeit und sind daher ein wertvolles Werkzeug, um das Fahrverhalten eines Fahrzeuges vorauszusagen.

Physikalisch akkurate Fahrzeugmodelle werden von Experten der Straßen- und Verkehrsplanung eingesetzt, um neue Forschungsprojekte umzusetzen und sich damit den Herausforderungen des Verkehrs von morgen zu stellen – etwa im Bereich der "Shared Spaces", einem Projekt, das sich mit der effizienten Nutzung öffentlicher Räume auseinandersetzt. Um das Potenzial solcher Infrastrukturen abzuschätzen, müssen verschiedene Arten von Fahrzeugen in den Simulationen einbezogen werden.

Das Ziel der vorliegenden Diplomarbeit ist die Entwicklung eines solchen Simulationsmodells, das sowohl physikalisch akkurat als auch echtzeitfähig sein soll. Je detaillierter die Simulation, desto aufwändiger ihre Berechnung; um die Echtzeit-Fähigkeit sicherzustellen, müssen daher einige Simplifikationen vorgenommen werden, ohne jedoch zu große Ungenauigkeiten in Kauf zu nehmen. Ziel ist es daher, einen Kompromiss zwischen diesen scheinbar widersprüchlichen Anforderungen zu finden.

Verschiedene Sets von Fahrzeugparametern wurden erarbeitet, um eine Vielzahl von verschiedenen Vehikel-Typen einzubeziehen. Durch die Implementierung eines zusätzlichen Fahrer-Modells kann die Beschreibung des gewünschten Kurses vereinfacht werden, da lediglich Positionspunkte statt des Lenkwinkels benötigt werden. Das Fahrer-Modell erlaubt außerdem die Analyse verschiedener Fahrer-Typen.

Abschließend soll das Potenzial des entworfenen Fahrzeug- und Fahrer-Modells in einer Verkehrsflussanalyse abgeschätzt werden. Dazu werden seine Vor- und Nachteile abgewogen und Vergleiche zwischen verschiedenen Fahrzeugdynamiken herangezogen. Unterstützend wird das Modell mit Fahrzeug-Modellen mit höherem Komplexitätsgrad in einer Vielzahl von verschiedenen Fahrmanövern verglichen.

Acknowledgement

The present thesis resulted from a project cooperation of the Institute of Automotive Engineering and the Institute for Highway Engineering and Transport Planning, both situated at the Graz University of Technology. At this point, I would like to thank all people, who supported me during the creation of this project.

I am deeply grateful to the head of the department of the Institute of Automotive Engineering, Mister Univ.-Prof. Dipl.-Ing. Dr. techn. Wolfgang Hirschberg who introduced me to this topic. His long lasting experience and the numerous helpful suggestions had a profound influence on this thesis. I consider myself truly lucky that I had the opportunity to share his experiences before his retirement.

Mister Univ.-Doz. Dipl.-Ing. Dr. techn. Arno Eichberger, who was the supervisor, is another person I would like to thank. His dedicated supervision made the whole project much easier. Although he is involved in many other projects, he always had the time to discuss the future procedure and unavoidable technical problems. Moreover, I appreciate the fact that he kindly did the proofreading.

Additionally, I am really happy to work together with all the other members of the Institute of Automotive Engineering, who always create a very friendly and productive working atmosphere. Particularly, I would like to point out two persons, first Dipl.-Ing. Daniel Wallner, with whom I had many prolifical discussions, and second Dipl.-Ing. Haymo Niederkofler, who gave an account of himself as far as the vehicle dynamics are concerned.

Moreover, I express my gratitude to Univ.-Prof. Dr.-Ing. Martin Fellendorf, head of the Institute of Highway Engineering and Transport Planning, who shared his experiences on the topic of traffic flow simulation.

Last but not least, I deeply thank my family and all my friends for their help and understanding.

Graz, October 2011 Harald Kraus

”The future belongs to those who believe in the beauty of their dreams.”

Eleanor Roosevelt (1884-1962)

Contents

Abbreviations

ABS	Anti-lock braking system
AWD	All wheel drive
CAD	Computer-aided design
CoG	Center of Gravity
DoF	Degrees of freedom
FWD	Front wheel drive
GPS	Global positioning System
KBA	Kraftfahrzeug-Bundesamt
NHTSA	National Highway Traffic Safety Administration
NLV	Non-linear vehicle model
R&D	Research and Development
RWD	Rear wheel drive
StVO	Straßenverkehrsordnung
VMU	Virtual mock up

Symbols

Coordinate systems

0	Index of the global coordinate system
V	Index of the vehicle coordinate system
W	Index of the wheel coordinate system
${}_0x$	Longitudinal axis of the global coordinate system
${}_0y$	Lateral axis of the global coordinate system
${}_0z$	Vertical axis of the global coordinate system
${}_Wx$	Longitudinal axis of the wheel-fixed coordinate system
${}_Wy$	Lateral axis of the wheel-fixed coordinate system
${}_Wz$	Vertical axis of the wheel-fixed coordinate system
0_0	Origin of the global coordinate system
C	Origin of the vehicle-fixed coordinate system
x	Longitudinal axis of the vehicle-fixed coordinate system
y	Lateral axis of the vehicle-fixed coordinate system
z	Vertical axis of the vehicle-fixed coordinate system

Parameters and constants

A	Coefficient of the tyre model
$a_{\psi,i}$	Weighting coefficients of the heading angle control
$a_{b,max}$	Maximum available vehicle deceleration
$a_{y,max}$	Maximum allowed lateral acceleration
a_1	Coefficient of the tyre model
a_2	Coefficient of the tyre model
A_x	Cross sectional area in x-direction
A_z	Cross sectional area in z-direction
A_y	Cross sectional area in y-direction
B	Coefficient of the tyre model
b_1	Coefficient of the tyre model
b_2	Coefficient of the tyre model
c_1	Coefficient of the tyre model
c_2	Coefficient of the tyre model
c_x	Aerodynamic coefficient in x-direction
c_y	Aerodynamic coefficient in y-direction

c_z	Aerodynamic coefficient in z-direction
D	Diameter of the tyre due to static deflection
d_f	Distance front axle to CoG
d_r	Distance rear axle to CoG
d_w	Diameter of the unformed tyre
e	Eccentricity
f_b	Proportional factor of the brake system
F_G	Weight
f_G	Proportional factor of the gearbox
G	Total vehicle weight
g	Gravitational acceleration
g_x	Fraction of gravity in x-direction
g_y	Fraction of gravity in y-direction
g_z	Fraction of gravity in z-direction
h_{CoG}	Height of CoG
I_{dt}	Mass inertia of the drivetrain
i_{fd}	Ratio of the finaldrive
I_{zz}	Yaw inertia of vehicle
I_a	Mass inertia about the rotational axis a
i_G	Gear ratio for the selected gear i
i_t	Total ratio of the drivetrain
I_W	Mass inertia of the wheel
K	Coefficient of the tyre model
$K_{p,\psi}$	Proportional gain of the heading angle control
$K_{p,d}$	Proportional gain of the position deviation control
K_p	Proportional factor of the state controller
L	Total vehicle length
l_{12}	Wheelbase
m	Total mass of a body
m_{lft}	Lifting height of the vehicle
m_i	Mass fraction of a body
m_v	Total vehicle weight
m_W	Mass of a wheel
n_{max}	Maximum engine speed
P_{rated}	Rated engine power
r	Tyre radius
r	Parameter of the desired path
R^{Oj}	Hazard radius of an object
r_d	Tyre radius
r_s	Static tyre radius
rd	Rolling torque distribution
s	Parameter of the actual path
T_N	Resetting time of the state controller

T_p	Preview time
trc	Track of the vehicle
w_c	Weighting coefficient
α_{tlt}	Static tilt angle
δ_{max}	Maximum allowed steering angle
η	Drivetrain efficiency
γ	Camber angle
κ	Curvature of the road ahead
κ_P	Curvature of the desired path
κ_t	Curvature of the trajectory
κ_V	Curvature of the path of the vehicle
λ	Rotational mass factor
ω_{rated}	Rated engine speed at rated power output
ψ_t	Tangent angle of the trajectory
θ_V	Path angle
ξ_a	Factor of driving torque distribution
ξ_b	Factor of braking torque distribution

Variables

${}_V a$	Vehicle's acceleration
a_y	Lateral vehicle acceleration
dY_0	Longitudinal/lateral initial tyre stiffness
$e(t)$	Control error
e_{rel}	Relative error
e_d	Position deviation error
$F_{d,y}$	Lateral aerodynamic force
F_{dwn}	Downforce
F_d	Aerodynamic drag
F_x	Longitudinal forces
F_y	Lateral forces
F_z	Tyre normal load
$K_{\dot{\psi},\delta}$	Relation factor between $\dot{\psi}$ and δ
p	Pedal position
s	Longitudinal slip
s^*	Longitudinal slip at maximum force
s_t	Distance covered along the path
s_x	Longitudinal slip
s_y	Lateral slip
t_{end}	End time of the simulation
t_0	Starting time of the simulation
T_e	Engine torque
T_r	Rolling torque

T_w	Driving/braking torque at wheels
v_s	Slide velocity
v_x	Longitudinal velocity
v_y	Lateral velocity
${}_W z$	Vertical movement of the wheels
X	Slip quantity
X^*	Slip quantity at maximum tyre force
Y	Tyre force (longitudinal or lateral)
Y_{inf}	Saturation value of the tyre force
Y_{max}	Maximum transferable tyre force
Y_0	Longitudinal/lateral tyre force for little slip values
Y_m	Maximum transferable tyre force
$\ddot{z}_W$	Acceleration of the wheel in z-direction
α	Slip angle
α^*	Slip angle at maximum lateral tyre force
β	Side slip angle
β_{lft}	Lifting angle of the vehicle
δ	Steering angle at tyre
δ_ψ	Steering angle due to the heading angle error
δ_{sw}	Steering angle at steering wheel
δ_d	Steering angle due to the position deviation
δ_t	Total steering angle
$\dot{\omega}_z$	Angular acceleration
μ	Slide friction coefficient
μ_0	Grip potential
ω_e	Engine speed
ω_x	Rotational speed about the x-axis
ω_y	Rotational speed about the y-axis
ω_z	Rotational speed about the z-axis
${}_W \omega$	Wheel rotation
ϕ	Roll angle
ψ	Yaw angle
θ	Pitch angle

Vectors

$d\mathbf{s}$	Differential vector of the vehicle path
$\mathbf{e}(t)$	Control deviation of a state controller
$\mathbf{e}_d$	Position deviation vector
$\mathbf{e}_\psi$	Heading angle error vector
$\mathbf{F}$	Force vector
$\mathbf{k}$	Gyro- and centrifugal forces
$\mathbf{n}$	External forces and resistances
$\mathbf{q}$	Impressed forces and moments due to the tyres
$\mathbf{r}$	Position vector
$\mathbf{r}(t)$	Reference input of a state controller
$\mathbf{r}_{CoG}$	Position vector of the CoG of a body
$\mathbf{r}_{CP}$	Position vector between the CoG and a point P
$\mathbf{r}_i$	Position vector of a specific part of a body
$\mathbf{s}$	Slip vector
$\mathbf{s}_{p,lat}$	Lateral preview vector
$\mathbf{u}(t)$	Regulating vector of a state controller
$\mathbf{v}$	Speed vector
${}_z\mathbf{v}$	Vehicle fixed velocity vector
$\mathbf{v}(t)$	Disturbance vector of a
$\mathbf{v}^{Oj}$	Velocity vector of an object
$\mathbf{v}_P$	Velocity vector of an arbitrary vehicle point P
$\mathbf{w}_d$	Weighting vector of the position deviation control
$\mathbf{w}_\psi$	Weighting vector of the heading angle control
$\mathbf{x}$	Current x-position of the vehicle
${}_0\mathbf{x}$	Position vector in the global reference system
$\mathbf{x}(t)$	State variables
$\mathbf{x}_f$	Future x-coordinates of the vehicle
$\mathbf{y}$	Current y-position of the vehicle
${}_0\mathbf{y}$	Position vector in the global reference system
$\mathbf{y}_f$	Future y-coordinates of the vehicle
$\dot{\mathbf{z}}$	Generalized acceleration vector

Matrices

$$ {}^{b}_{a}\mathbf{T} $$

a ...	Target reference
b ...	Initial reference

$\mathbf{I}_v$	Inertia matrix
$\mathbf{M}$	Mass matrix
$\mathbf{T}$	Transformation matrix
$\tilde{\omega}$	Skew symmetric tensor containing the angular speeds

Sub-/Superscripts

0	Global
crv	Curve
d	Desired
e	Engine
f	Front
i	Body index
L	Leveled
l	Left
lft	Lifting
max	Maximum
$mean$	Mean
min	Minimum
n	Needed
pyt	Pythagorean
r	Rear
r	Right
ref	Reference
rel	Relative
rot	Rotation
t	Trajectory
trn	Translation
trv	Traveled
var	Variable
w	Wheel
x	Longitudinal
y	Lateral
z	Vertical

1. Introduction

1.1. General Introduction

In the framework of a research project, the Institute of Highway Engineering and Transport Planning investigates the efficient utilization of road infrastructures. One research area deals with "shared space" areas. In this areas, all road users, such as pedestrians, bicyclists and car driver, are treated equally. According to [HFS11], neither traffic road signs nor crosswalks exist there. One example is situated in the city of Graz, Austria, at the Sonnenfelsplatz, according to [Ble11].

In order to study such "shared space" areas and its consequences in-depth, a simulation programme should be developed, which consists of an accurate vehicle and driver model amongst others. In order to design such a vehicle and driver model, a cooperation with the Institute of Automotive was introduced.

1.2. Motivation

The aim of the present diploma thesis is the composition of a real-time capable vehicle and driver model for application in traffic flow simulation. The detailed specifications are listed below.

- Real-time capability for both, the vehicle and the driver model, combined with an adequate and realistic reproduction of the vehicle dynamics and the driver behavior
- A vehicle model for non-critical driving maneuvers
- The limitation of the longitudinal speed to 50 [km/h], which meets almost all inner-city driving maneuvers
- The implementation of a suitable driver model
- The definition of suitable vehicle classes and the determination of its parameters

The consequences resulting from the model simplifications are discussed in detail and are compared with other simulation tools. Moreover, a complete vehicle parameter set of different kinds of vehicles is also presented in detail.

The result of the diploma thesis is a complete vehicle and driver model, and a suggestion how to use it. With the help of different testings done in the framework of this thesis, the user should gain knowledge how to ideally use the simulation tool .

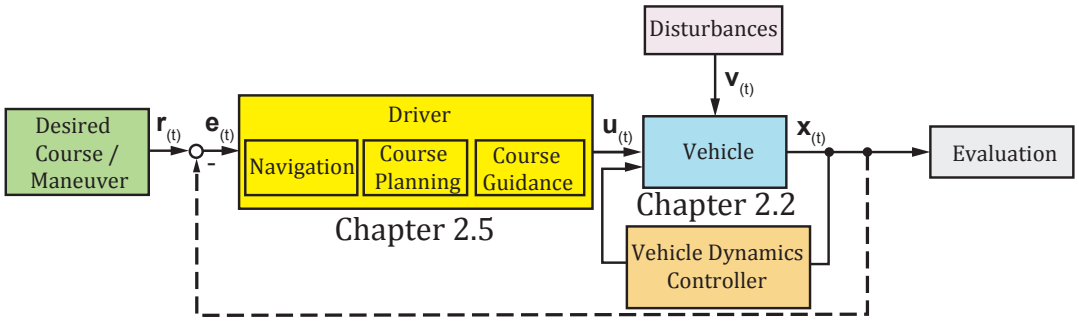

Figure 1.1.: Structure of the present thesis

1.3. Structure of the Thesis

At the beginning of this thesis, the theoretical fundamentals of vehicle dynamics are explained in general. Especially the definition of the coordinate systems and the needed mathematical background is mentioned. Afterwards, the implemented vehicle and driver model is described in detail. At the end of Section 2, the determination of the needed model parameters is discussed.

In Chapter 3, the evaluation scenarios are listed and discussed. This section is divided into two main parts: The first should allow a better understanding how well the driver model can follow a certain path. The second part deals with the evaluation of the vehicle model.

The closing chapter concludes the whole work and delivers prospects on possible future work.

Figure 1.1 illustrates in which chapter the main parts of the simulation tool can be found.

1.4. State of the Art

Traffic simulation is the mathematical modeling of transportation systems, freeway junctions and roundabouts. Such simulation programmes shall help to plan, design and operate different transportation systems. Simulation in transportation is becoming more and more important, since it can be used for experimental studies and can produce visualizations of present and future scenarios. A current example are the so-called ”shared space” areas.

Simulation software are becoming more accurate in a variety of different ways. In general,

simulation software for transportation can be divided into, according to [HW07]:

- **Macroscopic Simulations:**
  This simulations are able to represent a large geographic area, such as metropolitan region, but not to represent individual vehicles or people on the network.
- **Microscopic Simulations:**
  These are used to simulate only a certain segment of a road, such as the shared space area at Sonnenfelsplatz, Graz. They are rarely used for large geographic areas, since it would require a huge amount of input data and computational resources.
- **Mesoscopic Simulations:**
  These models are a combination of macro-/microscopic simulations. Thus, they can represent large geographic ares and allow more precise results than macro models

In the following, only microscopic models are considered. Micro-simulation models may track individual vehicle movements precisely. Today, such models are extensively used in order to analyze the implementation of innovative roadway management techniques. Such programmes are useful in analyzing key bottleneck roadways segments, where a better understanding of the impact on road conditions is needed, according to [FV10]. "AIMSIM", "DYNASIM", "SimTraffic" and "VISSIM" are only a few examples for such models. Vehicles move in a 1-dimensional world, and a vehicle's speed is determined by its current distance to its adjacent preceding vehicle [HFS11]. A more detailed listed can be found in [HW07].

Although microscopic models are widely spread, they are not suitable when pedestrians, bicycles, cars and heavy vehicles share the same space, since they are based on car-following modes with limited consideration of lateral interaction [HFS11]. However, in recent years, the concept of shared space has become popular as a way of creating more livable environments. For that reason, heterogeneous traffic models or 2-dimensional models are growing in interest.

2. Methodology

2.1. Fundamentals of Vehicle Simulation

The first chapter deals with the fundamental knowledge of vehicle simulation, which is an essential prerequisite to understand the mathematical part of the vehicle model. This includes, among other subjects, the definition of the vehicle coordinate system.

2.1.1. Standardized Coordinate System

In order to describe the movement of vehicles, it is helpful to use a predefined coordinate system, which helps other users to understand what exactly the programm is doing. Nowadays, two different standards are common: First, the standard according to DIN ISO 70000, which is shown in Figure 2.1.

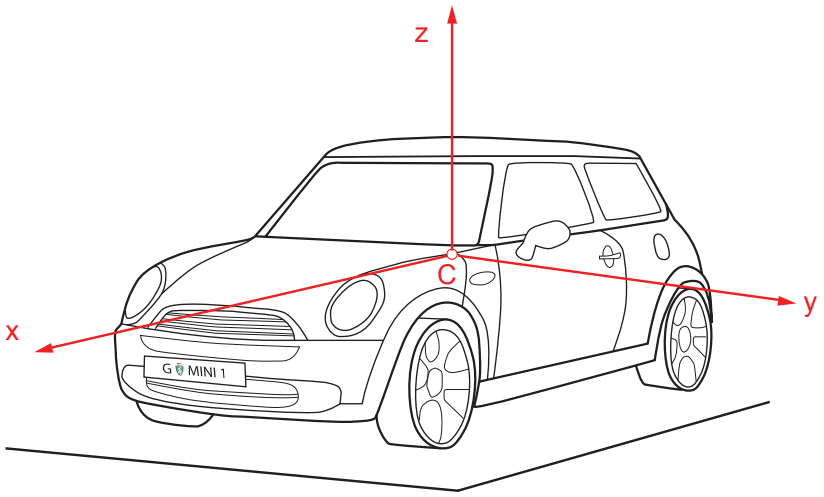

Figure 2.1.: Standardized coordinate system according to DIN ISO 70000 [HW10a]

The second standard that defines the position of the coordinate system is the standard according to SAE, which is shown in Figure 2.2. The two systems differ due to historic reasons as far as the direction of the y- and z-axes is concerned. The standards according to SAE was firstly used in the area of aviation. In order to prevent misunderstandings, it is therefore necessary to point out which standard is used. If not stated otherwise, the standard according to DIN ISO 70000 is used in this work.

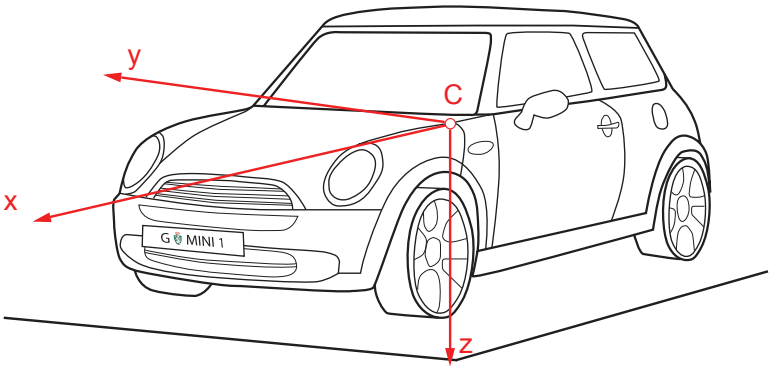

Figure 2.2.: Standardized coordinate system according to SAE[HW10a]

Moreover, there are more types of coordinate systems which are essential to understand the derivation of a vehicle model. These are:

- **Global defined Coordinate System** $\{O_0; x_0, y_0, z_0\}$
  This reference system is earth-based and globally fixed. Normally, the position of the vehicle is given in this system, since it is easier to handle - especially if more vehicles interact.
- **Vehicle-fixed Coordinate System** $\{C; x, y, z\}$
  As the name of the coordinate system tells, it is fixed to an arbitrary point of the car's body, normally to the CoG. This reference system is moving together with the vehicle's body, as shown in Figure 2.1 and 2.2. The CoG is not always feasible, since the loading conditions may change in multidimensional vehicle models. The benefits of such a coordinate system are according to [SHB+10b]:
  - Newton's law is still applicable easily ($F = m \cdot a$).
  - The movement is divided in a translation and a rotation.
  - The state variables are directly measurable with suitable measurement arrangements.
- **Leveled Vehicle Coordinate System** $\{C; x_L, y_L, z_L\}$
  It is comparable with the leveled vehicle coordinate system, but the z_L-axis is always parallel to the z_0-axis of the inertial frame.

2.1.2. Movement of the Vehicle

In general, a unrestrained rigid body possesses six degrees of freedom in a multidimensional space, three translational and three rotational [SHB+10d]. Accordingly, a simple

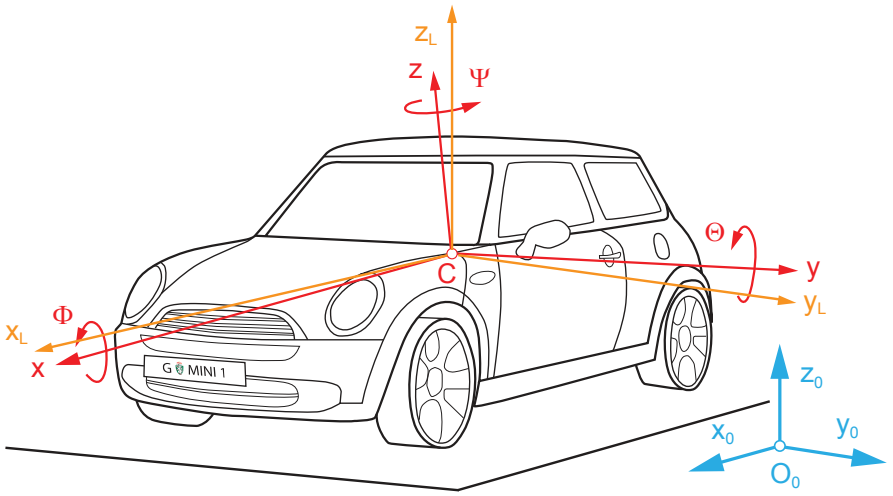

Figure 2.3.: Vehicle movement according to DIN ISO 70000[HW10a]

representation of a vehicle can be interpreted as a rigid body with six degrees of freedom.

Considering the DIN ISO standard mentioned in Chapter 2.1.1, the movement of the vehicle can be divided as shown in Figure 2.3:

According to [MW04a], the three translations in the DIN ISO 70000 reference system are called:

- in x-direction:
  Driving
- in y-direction
  Lateral movement
- in z-direction
  Lifting

The rotational portion can be divided in:

- Yaw angle (ψ):
  Describes the rotation about the z-axis
- Pitch angle(θ):
  Depicts the rotation about the y-axis
- Roll angle (ϕ):
  Presents the rotation about the x-axis

All other coordinate systems for specific vehicle parts (tyre, etc.) used in connection with this master thesis are introduced in the relevant chapter.

2.1.3. Mathematical and Kinematical Fundamentals

This chapter explains the required basics of vector analysis.

Vector Product

The vector product creates a vector $\mathbf{c}$, which is orthogonal to the vectors $\mathbf{a}$ and $\mathbf{b}$. It can be calculated by:

$$\mathbf{c} = \mathbf{a} \times \mathbf{b} = \tilde{\mathbf{a}}\mathbf{b},$$

where $\mathbf{a}$, $\mathbf{b}$, $\mathbf{c}$ are vectors of the same length and $\tilde{\mathbf{a}}$ correlates with the operator of the vector product $\mathbf{a}\times ...$ and is a skew symmetric tensor. If vector $\mathbf{b}$ is the vector of angular speed ω, $\tilde{\omega}$ is defined as:

$$\tilde{\omega} = \begin{bmatrix} 0 & -\omega_z & \omega_y \\ \omega_z & 0 & -\omega_x \\ -\omega_y & \omega_x & 0 \end{bmatrix},$$

where $\omega_{x,y,z}$ are the rotation velocities about the x-, y-, z-axis of a specific reference system.

Multidimensional Rotation and Angular Speed

According to [SHB+10b], there are two possibilities to create a multidimensional rotation:

1. The multidimensional rotation is handled like a single rotation about a single spatial rotational axis with a corresponding rotation angle.

2. The rotation is divided into three consecutive plane elementary rotations. This method is used in this thesis and therefore, explained further.

Figure 2.4 shows how to derive a elementary rotational matrix. The detailed derivation may be seen in [SHB+10b].

The first plane rotational fraction is about the a_1-axis, with the rotation angle ψ in [rad]. The corresponding transformation matrix is:

$$\mathbf{T}_\psi = \begin{bmatrix} \cos\psi & -\sin\psi & 0 \\ \sin\psi & \cos\psi & 0 \\ 0 & 0 & 1 \end{bmatrix},$$

The second plane rotational fraction is about the a_2-axis, with its rotation angle θ in [rad]:

$$\mathbf{T}_\theta = \begin{bmatrix} \cos\theta & 0 & \sin\theta \\ 0 & 1 & 0 \\ -\sin\theta & 0 & \cos\theta \end{bmatrix},$$

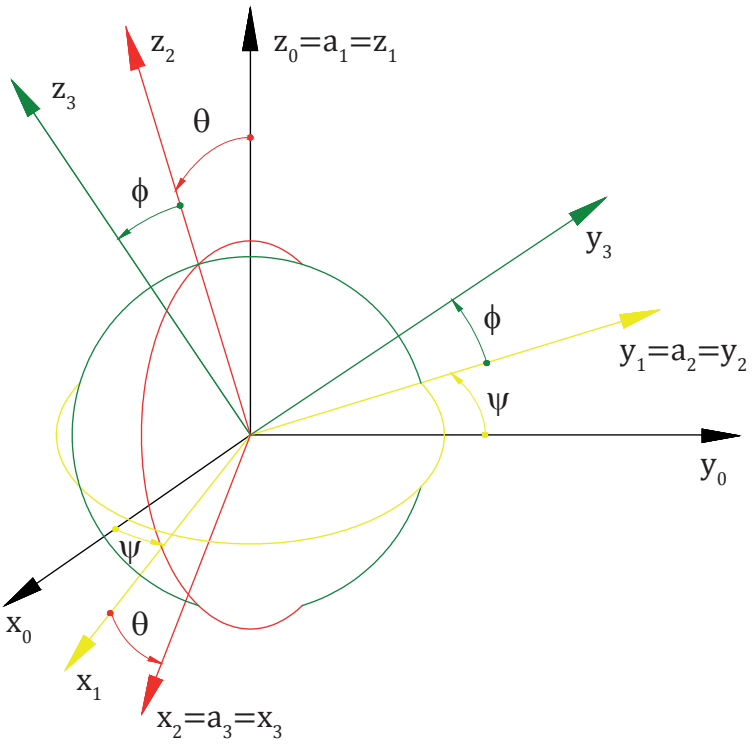

Figure 2.4.: Deriving the multidimensional transformation matrix

The final plane rotation is about the a_3-axis, with the corresponding rotation angle ϕ also in [rad]:

$$\mathbf{T}_\phi = \begin{bmatrix} 1 & 0 & 0 \\ 0 & \cos\phi & -\sin\theta \\ 0 & \sin\theta & \cos\theta \end{bmatrix},$$

By multiplying these elementary transformation matrices in a certain order, the multidimensional rotational matrix is obtained, and describes the transformation from a body fixed coordinate system to the global reference system.

$$\begin{aligned} {}^{V}_{0}\mathbf{T} &= \mathbf{T}_\psi\ \mathbf{T}_\theta\ \mathbf{T}_\psi = \begin{bmatrix} \cos\psi & -\sin\psi & 0 \\ \sin\psi & \cos\psi & 0 \\ 0 & 0 & 1 \end{bmatrix} \begin{bmatrix} \cos\theta & 0 & \sin\theta \\ 0 & 1 & 0 \\ -\sin\theta & 0 & \cos\theta \end{bmatrix} \begin{bmatrix} 1 & 0 & 0 \\ 0 & \cos\phi & -\sin\theta \\ 0 & \sin\theta & \cos\theta \end{bmatrix} \\ &= \begin{bmatrix} \cos\theta\cos\psi & \sin\phi\sin\theta\cos\psi - \cos\phi\sin\psi & \cos\phi\sin\theta\cos\psi + \sin\phi\sin\psi \\ \cos\theta\sin\psi & \sin\phi\sin\theta\sin\psi + \cos\phi\cos\psi & \cos\phi\sin\theta\sin\psi - \sin\phi\cos\psi \\ -\sin\theta & \sin\phi\cos\theta & \cos\phi\cos\theta \end{bmatrix} \end{aligned} \quad (2.1)$$

Last but not least, the relationship between the rotational tensor and its angular speed is shown. The vector ${}_0\mathbf{r}$ is defined in the global reference system $\{0_0, x_0, y_0, z_0\}$, but the

vector ${}_V\mathbf{r}$ is defined in a moving body fixed coordinate system $\{0_V, x_V, y_V, z_V\}$. According to [SHB+10b], it holds that

$$\tilde{\omega} = {}^0_V\mathbf{T}\ {}^V_0\dot{\mathbf{T}} = \begin{bmatrix} 0 & -\omega_z & \omega_y \\ \omega_z & 0 & -\omega_x \\ -\omega_y & \omega_x & 0 \end{bmatrix}, \tag{2.2}$$

where ${}^0_V\mathbf{T}$ is the transformation matrix of the global coordinate system relative to the vehicle-fixed axis system, and ${}^V_0\dot{\mathbf{T}}$ is the derivation of the inverse transformation matrix of ${}^0_V\mathbf{T}$.

2.2. Vehicle Models

This chapter describes some possible vehicle models suitable for a traffic flow simulation software. Their main difference lies within their complexities, which may influence the computational time directly. In the following subsections, the single track model is compared with the four wheel model, also called double track model.

2.2.1. Single Track Model

This model was introduced by Riekert and Schnuck in the 1940s for analyzing the steering- and disturbance response of vehicles [RS40]. In the course of time, this original single track model was extended. In this thesis, the non-linear (extended) single track model is discussed when talking about this reference model. The vehicle model can be described with a different amount of degrees of freedom. Within the framework of this paper, two types are explained: the five degrees of freedom model and the three degrees of freedom model. In both cases, the chassis is modeled as a rigid body with three DoF, the yaw angle and the lateral and longitudinal displacements. The two additional DoF of the five DoF model can be explained with the consideration of the tyre model.

2.2.1.1. Linear Single Track Model

The single track model is a real-time capable reference model according to [HW10b]. To ensure the models' real-time capability, some simplifications have to be made, which should be mentioned in the following according to [SHB+10a]:

- The vehicle's velocity is assumed to be constant along a given trajectory.
- Lifting, pitching and rolling movement are neglected.
- The total vehicle mass acts in the CoG.
- The front and rear wheels are combined per axle, in other words there is only one wheel at the front and the rear axle.

- The wheel contact point at the front and the rear axle is always in the middle of the corresponding axle.
- Inclinations of the wheels are not considered.
- The distribution of vertical tyre loads at the front and rear are always considered to be constant.

According to these simplifications, there exist four constraints. Since every rigid body has got six degrees of freedom in a multidimensional area, these constraints result in two degrees of freedom: the yaw angle ψ and the side slip angle β, as it can be seen in Figure 2.7. This original vehicle model is applicable for investigation of the vehicle dynamics until a lateral vehicle acceleration a_y of four [m/s^2], according to [Amm97]. As mentioned before, the help of the linear single track model makes it possible to analyze the behavior of the vehicle sufficiently, as long as the lateral vehicle acceleration a_y is smaller than four [m/s^2] and the steering angle δ is $\ll 1$ [rad], because then $\cos\delta \sim 1$ and $\sin\delta \sim \delta$, according to [HW10b]. Moreover, the influence of the drivetrain is not considered. For that reason, a non-linear single track model is introduced in the following.

2.2.1.2. Non-linear Single Track Model

The characteristics of this model are:

- The vehicle consists of a single a rigid vehicle body with three DoF, as explained in Section 2.2.1.
- There is only one front and one rear wheel, with its imposed forces acting at the wheel.
- The aerodynamic drag is considered in this model.
- The torque T_w acting at the wheels is a function of the engine torque T_e, the current selected gear i_G, the tyre radius r_d, the axle ratio i_{fd} and the efficiency η. The engine torque T_e is again a function of the current engine speed ω_e and the pedal position p, which can vary between [-1;1].
- The total driving / braking torque at the wheels, T_w, is dependent on the distribution of the torque between the front and rear axle. With the factor of the driving torque ξ_a, alternatively the factor of the braking torque ξ_b, the total driving / braking torque can be written:

$$T_w = \xi_a \cdot T_{w,f} + (1 - \xi_a) \cdot T_{w,r}, \tag{2.3}$$

  where T_w is the total driving torque, $T_{w,f}$ is the driving torque acting on the front wheel, $T_{w,r}$ is the driving torque acting on the rear wheel, and ξ_a is the distribution

factor of the driving torque between front and rear. When braking the total torque is calculated by:

$$T_w = \xi_b \cdot T_{w,f} + (1 - \xi_b) \cdot T_{w,r}, \tag{2.4}$$

where ξ_b is the distribution factor of the braking torque.

- The dynamic axle load transfer is considered, that means that with changing vehicle acceleration, the vertical tyre load moves from the front to the rear, according to the following equations:

$$F_{z,f} = m_v \frac{g \cdot d_r - a_x \cdot h_{CoG}}{d_r + d_f} + F_{dwn,f}, \tag{2.5}$$

$$F_{z,r} = m_v \frac{g \cdot d_f + a_x \cdot h_{CoG}}{d_r + d_f} + F_{dwn,r}, \tag{2.6}$$

where $F_{z,f,r}$ is the acting force on the front or rear axle in [N], m_v is the total vehicle mass in [kg], g is the gravitation in [m/s^2], $d_{f,r}$ is the distance of the CoG to the front or rear axle in [m], a_x is the longitudinal acceleration in [m/s^2] and $F_{dwn,f,r}$ is the downforce at the front and rear axle.

- By using the equations below, the tire lateral load transfer is also taken into account:

$$F_{z,f,r} = \frac{1}{2} F_{z,f} + T_{r,f} \cdot trc_f, \tag{2.7}$$

$$F_{z,f,l} = \frac{1}{2} F_{z,f} - T_{r,f} \cdot trc_f, \tag{2.8}$$

$$F_{z,r,r} = \frac{1}{2} F_{z,r} + T_{r,r} \cdot trc_r, \tag{2.9}$$

$$F_{z,r,l} = \frac{1}{2} F_{z,r} - T_{r,r} \cdot trc_r, \tag{2.10}$$

where the indices f or r denotes the front or rear axle moreover the indices l and r denote the left or the right wheel on a specific axle. The parameter trc is the track of the vehicle in [m].

- The position of the CoG is above the ground that means that external forces acting on the CoG result in corresponding torques.

In the following, only the non-linear single track model is treated.

2.2.1.3. Single Track Model

In this section, all forces and loads acting externally on the vehicle are explained further, before the mathematical part shows their influence on the vehicle dynamics. Furthermore, the main control variables shall be discussed briefly.

Aerodynamic Drag

The higher the vehicle velocity becomes, the bigger is the influence of the aerodynamic on the power and the driving behavior of the vehicle. Especially the aerodynamic drag, respectively its parameter, the aerodynamic coefficient c_x, is earning more and more intention, since they directly affect the amount of fuel consumption and the CO_2-emission. In the present vehicle model, the aerodynamic coefficient c_x in longitudinal vehicle direction is assumed to be constant over the whole velocity area, as well as for the lift coefficient c_z at the front and rear of the car. According to [MW04a], the reference point is in the middle of the track and wheelbase, since the coefficients are not depending on the distribution of mass. Corresponding to the DIN ISO 7000 coordinate system, mentioned in Section 2.1.1, three aerodynamic forces are existing:

- **Aerodynamic Drag**

$$F_d = c_x A_x \frac{\rho}{2} v_x^2, \tag{2.11}$$

  where F_d is the aerodynamic drag in [N], c_x is the aerodynamic coefficient, A_x is the cross sectional area in x-direction in [m^2], ρ is the density of the ambient air in [kg/m^3] and v_x is the vehicle speed in x-direction in [m/s].

- **Lateral Aerodynamic Force**

$$F_{d,y} = c_y A_y \frac{\rho}{2} v_{d,y}^2, \tag{2.12}$$

  where $F_{d,y}$ is the lateral aerodynamic force in [N],c_y is the aerodynamic coefficient in lateral direction of the vehicle, A_y is the cross sectional area in y-direction in [m^2] and $v_{d,y}$ is the lateral flow velocity in [m/s].

- **Downforce**

$$F_{dwn} = c_z A_z \frac{\rho}{2} v_x^2, \tag{2.13}$$

  where F_{dwn} is the downforce in [N], A_z is the cross sectional area in z-direction in [m^2] and c_z is the aerodynamic coefficient in z-direction. All other values are explained above.

The moments resulting from the aerodynamic forces are neglected in the vehicle model and are not explained in this thesis. Figure 2.5 shows the cross sectional areas mentioned above.

Tyre Forces

The tyre forces are affecting the vehicle dynamics to a large extent. The wheel transfers forces and moments in tyre contact zone to the road [MW04d]. In order to calculate tyre forces in longitudinal and lateral direction, a modification of the semi-empirical tyre model TM Easy is used [HRW07]. The used tyre model is not considering any inclination of the wheel, for example camber angle, toe angle and caster angle. Depending on the complexity of the tyre model, the lateral slip and/or the longitudinal slip are considered. The difference will be explained later in Section 2.3.5.

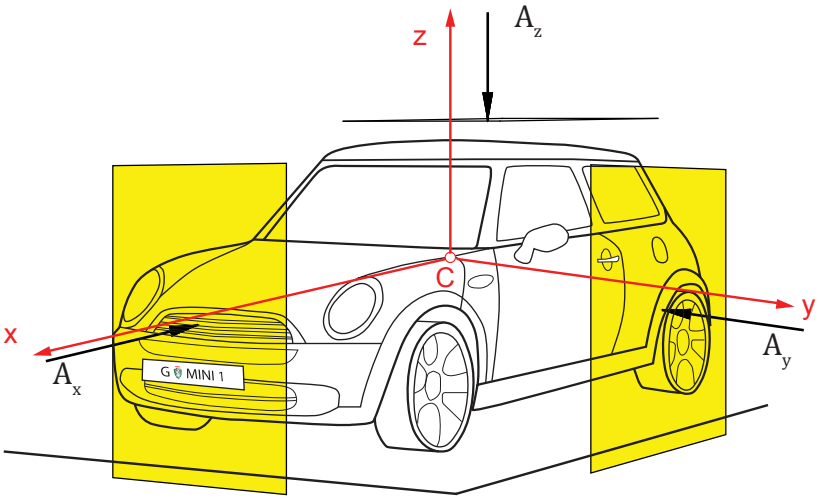

Figure 2.5.: Cross sectional areas for the air resistance

Wheel Vertical Loads

The wheel vertical loads are depending on the vehicle acceleration or deceleration. That means that the dynamic axle load transfer due to different different longitudinal driving maneuver is considered in the vehicle model. In addition, the aerodynamic downforce at the front and rear at the vehicle may be also considered. Additionally, the lateral load transfer is also taken into account.

Lateral Control Variable

The lateral control variable is the tire steering angle δ, which influences the position of the front wheel. A rear steering mechanism is not considered. Moreover, there is no ratio between the steering angle δ at the wheel and the steering angle δ_{sw} at the steering wheel implemented in the vehicle simulation.

Longitudinal Control Variable

The second control variable is the pedal position p, which determines the driving or braking torque. Depending on the drivetrain concept the driving torque is either applied on the front wheel, also called Front Wheel Drive (FWD), on the rear wheel, Rear Wheel Drive (RWD), or on all wheels, which is called All Wheel Drive (AWD). If AWD is simulated, the torque distribution can be chosen arbitrarily. But the braking torque distribution is always fixed to 70:30 front/rear, to avoid rear wheel locking due to dynamic axle loads. Nowadays, the braking torque distribution is also variable and is regulated that no wheel locking is occurring in any situation.

A gearbox is simulated in order to make the vehicle model more realistic, it selects the gear upon the vehicle velocity. The rotational mass factor λ is introduced to the model. This factor characterizes the rotational inertia faction of the drivetrain and contributes significantly, especially when the vehicle is accelerating in low gears. Typical values for λ are between about 1.06 in the highest gear and 1.75 in the lowest gear, but this varies for different cars. Last but not least, a characteristic braking behavior is implemented in the model and described in the following.

2.2.2. Derivation of the Non-linear Single Track Model

After the theoretical explanation in Section 2.2.1.3, the mathematical implementation is pointed out in this chapter. First of all, the kinematics is described, and after that, the vehicle dynamics is explained.

Vehicle Kinematics

At the very beginning, it is useful to introduce a position vector ${}_0\mathbf{y}$, which defines the position of the specific vehicle in the global coordinate system $\{O_0; x_0, y_0, z_0\}$.

$$ {}_0\mathbf{y} = \begin{matrix} \\ 0 \end{matrix} \begin{bmatrix} x \\ y \\ \psi \end{bmatrix} \tag{2.14} $$

Moreover a generalized velocity vector ${}_V\mathbf{z}$ is introduced, which is defined as follows:

$$ {}_V\mathbf{z} = \begin{matrix} \\ V \end{matrix} \begin{bmatrix} v_x \\ v_y \\ \omega_z \end{bmatrix} \tag{2.15} $$

Between Equation (2.14) and (2.15), there exists a simple relationsship according to Equation (2.16):

$$ {}_0\dot{\mathbf{y}} = {}^V_0\mathbf{T}\ {}_V\mathbf{z} \tag{2.16} $$

where ${}^V_0\mathbf{T}$ is the transformation matrix from the vehicle-fixed coordinate system $\{C; x, y, z\}$ to the global coordinate system $\{O_0; x_0, y_0, z_0\}$.

With

$$ {}^V_0\mathbf{T} = \begin{bmatrix} \cos\psi & -\sin\psi & 0 \\ \sin\psi & \cos\psi & 0 \\ 0 & 0 & 1 \end{bmatrix} $$

and

$$ {}_0\dot{\mathbf{y}} = \frac{d}{dt}{}_0\mathbf{y} = \begin{bmatrix} \dot{x} \\ \dot{y} \\ \dot{\psi} \end{bmatrix} $$

Equation 2.16 can be rewritten to:

$$ {}_0\begin{bmatrix}\dot{x}\\ \dot{y}\\ \dot{\psi}\end{bmatrix} = \begin{bmatrix}\cos\psi & -\sin\psi & 0\\ \sin\psi & \cos\psi & 0\\ 0 & 0 & 1\end{bmatrix} {}_V\begin{bmatrix}v_x\\ v_y\\ \omega_z\end{bmatrix} \tag{2.17} $$

This approach seems to be detailed, but this method contains an advantage. First of all, the related equation of motion gets quite compact and straightforward, since external forces are easier describable in the vehicle-fixed coordinate system, for instance the tyre forces or the aerodynamic drag according to [HW10b].

In order to get the vehicle's acceleration ${}_V\mathbf{a}$, the acceleration in the fixed reference system is calculated first according to (2.18) using the chain rule:

$$ {}_0\mathbf{a} = \frac{d}{dt}({}_0\dot{\mathbf{y}}) = \frac{d}{dt}\left({}^V_0\mathbf{T}\ {}_0\mathbf{z}\right) = {}^V_0\mathbf{T}\ {}_V\dot{\mathbf{z}} + {}^V_0\dot{\mathbf{T}}\ {}_V\mathbf{z} \tag{2.18} $$

The acceleration in the moving coordinate system is derived similarly like the velocity in the moving system in Equation (2.16), but by using the inverse transformation matrix ${}^0_V\mathbf{T}$.

$$ {}_V\mathbf{a} = {}^0_V\mathbf{T}\ {}_0\mathbf{a} = \underbrace{{}^0_V\mathbf{T}\ {}^V_0\mathbf{T}}_{\mathbf{I}}\ {}_V\dot{\mathbf{z}} + \underbrace{{}^0_V\mathbf{T}\ {}^V_0\dot{\mathbf{T}}}_{\tilde{\omega}}\ {}_V\mathbf{z}, \tag{2.19} $$

where ${}_V\mathbf{a}$ is the vector with the vehicle's accelerations, ${}^V_0\mathbf{T}$ is the transformation matrix, ${}^0_V\mathbf{T}$ is its inverse, $\mathbf{I}$ is the identity matrix, ${}_V\mathbf{z}$ is the vector with the generalized velocities, ${}_V\dot{\mathbf{z}}$ is the derivative vector of ${}_V\mathbf{z}$ and $\tilde{\omega}$ is the matrix consisting of the angular speeds in all directions, which is further explained in the following. If there are rotations about all three vehicle axis, the vector ω reads:

$$ \omega = \begin{bmatrix}\omega_x\\ \omega_y\\ \omega_z\end{bmatrix}, $$

the corresponding matrix $\tilde{\omega}$ is then

$$ \tilde{\omega} = \begin{bmatrix}0 & -\omega_z & \omega_y\\ \omega_z & 0 & -\omega_x\\ -\omega_y & \omega_x & 0\end{bmatrix}. $$

A simplification can be done, if there is only one rotational freedom about the z-axis, which is the case in the present vehicle model. That means that the vector ω can be rewritten to

$$ \omega = \begin{bmatrix}0\\ 0\\ \omega_z\end{bmatrix}, $$

the corresponding matrix $\tilde{\omega}$ is then

$$ \tilde{\omega} = \begin{bmatrix}0 & -\omega_z & 0\\ \omega_z & 0 & 0\\ 0 & 0 & 0\end{bmatrix}. $$

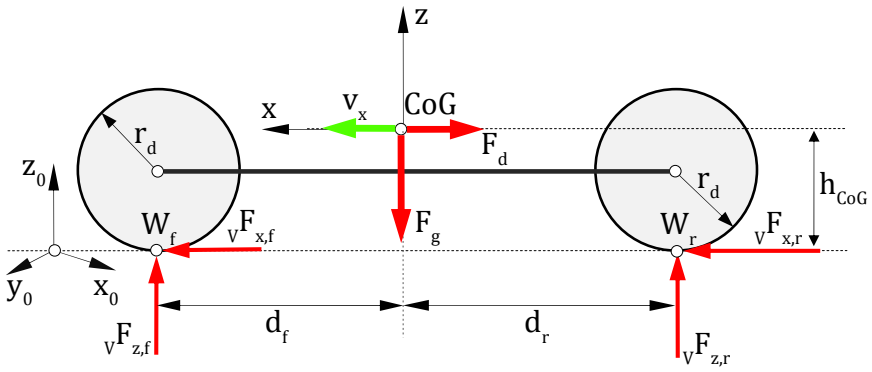

Figure 2.6.: Side view of the non-linear single track model

Now it is possible to rearrange (2.19):

$$ {}_V\mathbf{a} = \underbrace{\begin{bmatrix} 1 & 0 & 0 \\ 0 & 1 & 0 \\ 0 & 0 & 1 \end{bmatrix}}_{\mathbf{I}} \underbrace{\begin{bmatrix} \dot{v}_x \\ \dot{y}_v \\ \dot{\omega}_z \end{bmatrix}}_{{}_V\dot{\mathbf{z}}} + \underbrace{\begin{bmatrix} 0 & -\omega_z & 0 \\ \omega_z & 0 & 0 \\ 0 & 0 & 0 \end{bmatrix}}_{\tilde{\omega}} \underbrace{\begin{bmatrix} v_x \\ v_y \\ \omega_z \end{bmatrix}}_{{}_V\mathbf{z}} = \begin{bmatrix} \dot{v}_x - \omega_z v_y \\ \dot{v}_y + \omega_z v_x \\ \dot{\omega}_z \end{bmatrix} \tag{2.20} $$

By taking a closer look at (2.20), it can be rewritten to (2.21):

$$ {}_V\mathbf{a} = {}_V\dot{\mathbf{z}} + \omega \times {}_V\mathbf{z}, \tag{2.21} $$

where $\omega \times {}_V\mathbf{z}$ is a vector consisting the the gyroscopic and centrifugal acceleration in $[\mathrm{m/s^2}]$ and ${}_V\dot{\mathbf{z}}$ is the vehicle acceleration in $[\mathrm{m/s^2}]$.

Vehicle Dynamics

After deriving the kinematics of the vehicle model, the dynamics is discussed in detail. Figure 2.6 and Figure 2.7 show the side view alternatively the top view of the non-linear single track model and its important mathematical quantities.

In order to derive the equation of motion, all external forces acting on the vehicle have to be transformed to the vehicle-fixed coordinate system, since in this reference system the principle of linear momentum and the principle of angular momentum are applicable.

The principle of linear momentum, stated in general:

x-direction:

$$ m_v \; {}_V a_x = \sum {}_V F_x = {}_V F_{x,f} + {}_V F_{x,r} - F_d, \tag{2.22} $$

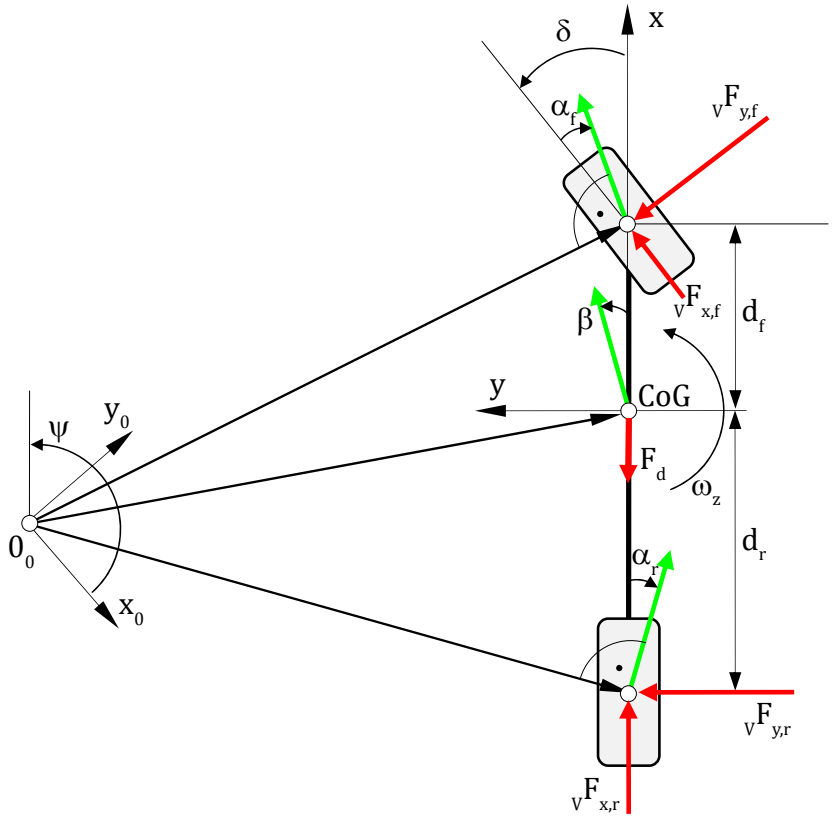

Figure 2.7.: Top view of the non-linear single track model

y-direction:

$$m_v \, {}_V a_y = \sum {}_V F_y = {}_V F_{y,f} + {}_V F_{y,r} - \underbrace{F_{d,y}}_{=0}, \tag{2.23}$$

z-direction:

$$\underbrace{m_v \, {}_V a_z}_{=0} = \sum {}_V F_z = {}_V F_{z,f} + {}_V F_{z,r} - F_G, \tag{2.24}$$

where m_v is the total mass of the vehicle in [kg], ${}_V a_i$ is the acceleration of the vehicle in x-, y-, z-direction of the vehicle-fixed reference system in [m/s^2], ${}_V F_{x,f}$ is the force acting on the front wheel in x-direction in [N], ${}_V F_{x,r}$ is the force at the rear wheel in x-direction in [N], ${}_V F_{y,f}$ is the force acting in y-direction at the front wheel in [N], ${}_V F_{y,r}$ is the force acting at the rear wheel in y-direction in [N], F_d is the aerodynamic drag in x-direction in [N], F_G is the weight in [N], I_{zz} is the moment of inertia around the vehicle's vertical axis in [kgm^2] and d_f, d_r are the distances from the CoG to the front axle respectively to the rear axle in [m]. Equation (2.23) neglects the lateral aerodynamic force.

The principle of angular momentum about the z-axis can be defined by Equation (2.23):

$$I_{zz}\ \dot{\omega}_z = \sum {}_V M^{(CoG)} = {}_V F_{y,f}\ d_f - {}_V F_{y,r}\ d_r, \tag{2.25}$$

The insertion of the specific terms of the acceleration in Equation (2.22) to (2.25) leads to the general equation of motion of the single track model. In Equation (2.26), the three main important equations are combined to a well-arranged system of equations.

$$\underbrace{\begin{bmatrix} m_v & 0 & 0 \\ 0 & m_v & 0 \\ 0 & 0 & I_{zz} \end{bmatrix}}_{\mathbf{M}} \underbrace{\begin{bmatrix} \dot{v}_x \\ \dot{v}_y \\ \dot{\omega}_z \end{bmatrix}}_{\dot{\mathbf{z}}(t)} = \underbrace{m_v \begin{bmatrix} \omega_z\ v_y \\ -\omega_z\ v_x \\ 0 \end{bmatrix}}_{\mathbf{k}(t)} + \underbrace{\begin{bmatrix} {}_V F_{x,f} + {}_V F_{x,r} \\ {}_V F_{y,f} + {}_V F_{y,r} \\ {}_V F_{y,f}\ d_f - {}_V F_{y,r}\ d_r \end{bmatrix}}_{\mathbf{q}(t)} + \underbrace{\begin{bmatrix} -F_d \\ 0 \\ 0 \end{bmatrix}}_{\mathbf{n}(t)}, \tag{2.26}$$

where
M is a [3x3] mass matrix
$\dot{\mathbf{z}}$ is a [3x1] vector containing the generalized accelerations
k is a [3x1] vector describing the gyro- and centrifugal forces
q is a [3x1] vector containing all impressed forces and moments due to the tyres
n is a [3x1] vector contain all other external forces and resistances

The acting tyre forces, which are needed to solve the system of equations of motion in (2.26), are in detail discussed in Section 2.3.

2.2.3. Double Track Model

Although the present master thesis focuses on the single track model for reasons of minimal simulation time, the double track model shall not be left unmentioned. This section deals with a simple double track model, which does not consider the kinematics of the wheel suspension, compare [SHB+10d].

In Figure 2.8, the homologous model is shown. As it does not model any kinematics of the wheel suspension, the wheels are only attached via spring- and damper forces to the vehicle body. Another assumptions of that model is that the center point of the tyres is only moving vertically relative to the vehicle body. That means that no multidimensional movements, like camber angle change etc., are considered. According to Figure 2.8, the homologous model has got fourteen degrees of freedom:

- Three body translations: x, y, z
- Three body rotations: pitch angle(θ), roll angle (ϕ), yaw angle (ψ)
- Four wheel rotations: ${}_W\omega_i$
- Four vertical movements of the wheels: ${}_W z_i$

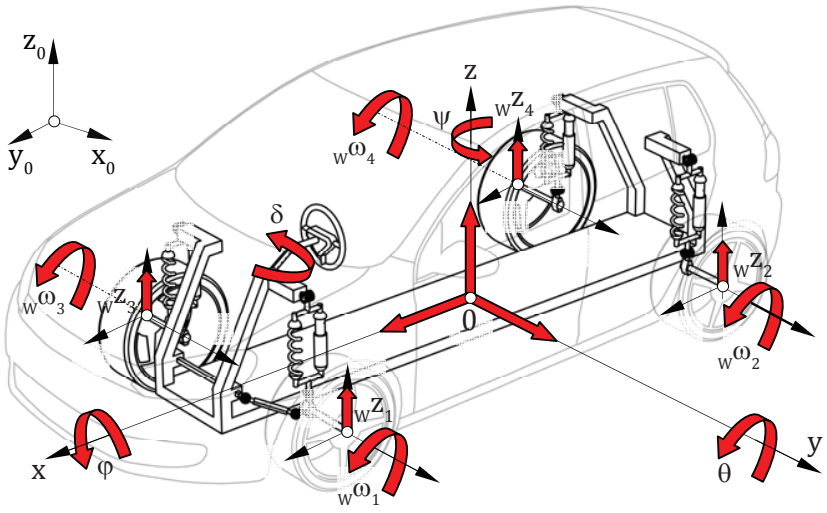

Figure 2.8.: Homologous model of the double track model [SHB+10d]

Kinematics of the Double Track Model

In order to describe the vehicle movement in the inertial coordinate system $\{0_0, x_0, y_0, z_0\}$, the motion of the vehicle body has to be transformed about the three rotational axis x, y, z. This is done by using the transformation matrix ${}^{V}_{0}\mathbf{T}$ explained in Section 2.1.3 for the multidimensional case:

$$ {}^{V}_{0}\mathbf{T} = \mathbf{T}_z(\psi) \cdot \mathbf{T}_y(\phi) \cdot \mathbf{T}_x(\theta) = $$

$$ = \begin{bmatrix} \cos\theta\cos\psi & \sin\phi\sin\theta\cos\psi - \cos\phi\sin\psi & \cos\phi\sin\theta\cos\psi + \sin\phi\sin\psi \\ \cos\theta\sin\psi & \sin\phi\sin\theta\sin\psi + \cos\phi\cos\psi & \cos\phi\sin\theta\sin\psi - \sin\phi\cos\psi \\ -\sin\theta & \sin\phi\cos\theta & \cos\phi\cos\theta \end{bmatrix} $$

Next, the kinematics have to be derived. In (2.27), the angular speed of the vehicle body is shown. Starting with the relationship that

$$ \tilde{\omega} = {}^{0}_{V}\mathbf{T}\ {}^{V}_{0}\dot{\mathbf{T}} = \begin{bmatrix} 0 & -\omega_z & \omega_y \\ \omega_z & 0 & -\omega_x \\ -\omega_y & \omega_x & 0 \end{bmatrix}, $$

the angular speed can be written:

$$ {}_{V}\omega = {}_{V}\begin{bmatrix} \omega_x \\ \omega_y \\ \omega_z \end{bmatrix} = \begin{bmatrix} \dot{\phi} - \dot{\psi}\sin\theta \\ \dot{\theta}\cos\phi + \dot{\psi}\cos\theta\sin\phi \\ -\dot{\theta}\sin\phi + \dot{\psi}\cos\theta\cos\phi \end{bmatrix} = \underbrace{\begin{bmatrix} -\sin\theta & 0 & 1 \\ \cos\theta\sin\phi & \cos\phi & 0 \\ \cos\theta\cos\phi & -\sin\phi & 0 \end{bmatrix}}_{\mathbf{T}_\omega} \begin{bmatrix} \dot{\psi} \\ \dot{\theta} \\ \dot{\phi} \end{bmatrix} \qquad (2.27) $$

Moreover, the movement of the tyres can be described by the rotational matrix ${}^{W}_{0}\mathbf{T}$ in Equation (2.28). Note that the rotation about the tyre axis is not considered. It should also be stated that this transformation matrix is similar to the one mentioned in Section 2.2.1.

$$ {}^{W}_{0}\mathbf{T} = \mathbf{T}_z(\psi+\delta) = \begin{bmatrix} \cos(\psi+\delta) & -\sin(\psi+\delta) & 0 \\ \sin(\psi+\delta) & \cos(\psi+\delta) & 0 \\ 0 & 0 & 1 \end{bmatrix}, \tag{2.28} $$

where δ is the steering angle in [rad].
It is assumed that the steering mechanism is mounted at the front axis only:

$$ \delta_{r,l} = \delta_{r,r} = 0, $$

where $\delta_{r,l}$ is the steering angle at the rear at the left rear wheel in [rad] and $\delta_{r,r}$ is the steering angle at the right rear wheel also in [rad].

Additionally, it has to be mentioned that it is assumed that the steering angle at the left and right front axis is always equal.

$$ \delta_{f,l} = \delta_{f,r}, $$

where $\delta_{f,l}$ is the steering angle at the left front wheel in [rad] and $\delta_{f,r}$ is the steering angle at the right front wheel in [rad].
The rotation of the wheel-fixed coordinate system $\{{}_W0, {}_Wx, {}_Wy, {}_Wz\}$ relatively to the vehicle-fixed reference system can be calculated by Equation (2.29):

$$ {}^{W}_{V}\mathbf{T} = \mathbf{T}^T_x(\phi)\cdot\mathbf{T}^T_y(\theta)\cdot\mathbf{T}_z(\delta) = $$

$$ = \begin{bmatrix} \cos\delta\cos\theta & -\sin\delta\cos\theta & -\sin\theta \\ \sin\phi\sin\theta\cos\phi\sin\delta & -\sin\phi\sin\theta\sin\delta+\cos\phi\cos\delta & \sin\phi\cos\theta \\ \cos\phi\sin\theta\cos\delta-\sin\phi\sin\delta & -\cos\phi\sin\theta\sin\delta-\sin\phi\cos\delta & \cos\phi\cos\theta \end{bmatrix} \tag{2.29} $$

Consequently, if the steering angle δ is zero, as it is the case at the rear axle, the transformation matrix simplifies to:

$$ {}^{W}_{V}\mathbf{T} = \mathbf{T}^T_x(\phi)\cdot\mathbf{T}^T_y(\theta) = \begin{bmatrix} \cos\theta & 0 & -\sin\theta \\ \sin\phi\sin\theta & \cos\phi & \sin\phi\cos\theta \\ \cos\phi\sin\theta-\sin\phi & -\sin\phi & \cos\phi\cos\theta \end{bmatrix} \tag{2.30} $$

It is also possible to introduce generalized position vector ${}_0\mathbf{y}$, which refers to the global coordinate system and a generalized velocity vector ${}_V\mathbf{z}$, as it is done in Section 2.2.2.

With

$$ {}_0\mathbf{y} = {}_0\begin{bmatrix} x & y & z & \phi & \theta & \psi & {}_Wz_1 & {}_Wz_2 & {}_Wz_3 & {}_Wz_4 & {}_W\omega_1 & {}_W\omega_2 & {}_W\omega_3 & {}_W\omega_4 \end{bmatrix}^T, \tag{2.31} $$

and

$$ {}_V\mathbf{z} = {}_V\begin{bmatrix} v_x & v_y & v_z & \omega_x & \omega_y & \omega_z & {}_W\dot{z}_1 & {}_W\dot{z}_2 & {}_W\dot{z}_3 & {}_W\dot{z}_4 & {}_W\dot{\omega}_1 & {}_W\dot{\omega}_2 & {}_W\dot{\omega}_3 & {}_W\dot{\omega}_4 \end{bmatrix}^T, \tag{2.32} $$

where the parameters x, y, z, ϕ, θ, ψ depict the position of the vehicle body in [m] or in [rad],respectively, ${}_W z_i$ are describing the position of the suspension in [m] and ${}_W\omega_i$ is the angular speed of a specific wheel in [rad/s]. Vector ${}_V\mathbf{z}$ shows the derivatives of the quantities explained before.

The relation between ${}_0\mathbf{y}$ and ${}_V\mathbf{z}$ is stated in equation with the help of the block diagonal matrix ${}^V_0\mathbf{K}$ (2.33):

$$ {}_0\dot{\mathbf{y}} = \underbrace{\begin{bmatrix} {}^V_0\mathbf{T}_{[3x3]} & 0 & 0 & 0 \\ 0 & \mathbf{T}^{-1}_{\omega,[3x3]} & 0 & 0 \\ 0 & 0 & \mathbf{I}_{[4x4]} & 0 \\ 0 & 0 & 0 & \mathbf{I}_{[4x4]} \end{bmatrix}}_{= {}^V_0\mathbf{K}} {}_V\mathbf{z} \tag{2.33} $$

The procedure is now the same as described for the single track model. The acceleration in the global coordinate system can be calculated by Equation (2.34)

$$ {}_0\mathbf{a} = \frac{d}{dt}({}_0\dot{\mathbf{y}}) = \frac{d}{dt}\left({}^V_0\mathbf{K}\ {}_V\mathbf{z}\right) = {}^V_0\ \mathbf{K}\ {}_V\dot{\mathbf{z}} + {}^V_0\ \dot{\mathbf{K}}\ {}_V\mathbf{z} \tag{2.34} $$

By using the inverse transformation matrix ${}^0_V\mathbf{K}$, the acceleration in the vehicle-fixed coordinate system may be derived:

$$ {}_V\mathbf{a} = {}^0_V\ \mathbf{K}\ {}_0\mathbf{a} = \underbrace{{}^0_V\mathbf{K}\ {}^V_0\mathbf{K}}_{\mathbf{I}}\ {}_V\dot{\mathbf{z}} + {}^0_V\ \mathbf{K}\ {}^V_0\dot{\mathbf{K}}_V\mathbf{z}. \tag{2.35} $$

Dynamics of the Double Track Model

The principle of linear momentum of the vehicle body can be written in general:

x-direction:

$$ m_v\ {}_V a_x = \sum_{i=1}^{4} {}_V F_{i_x} + m_v\ g_x + F_d, \tag{2.36} $$

y-direction:

$$ m_v\ {}_V a_y = \sum_{i=1}^{4} {}_V F_{i_y} + m_v\ g_y + \underbrace{F_{d,y}}_{=\,0}, \tag{2.37} $$

z-direction:

$$ m_v\ {}_V a_z = \sum_{i=1}^{4} {}_V F_{i_z} + m_v\ g_z + F_{dwn}, \tag{2.38} $$

where m_v is the total vehicle mass in [kg], ${}_V a_{x,y,z}$ are the vehicle acceleration in x-, y-, and z-direction in [m/s^2], ${}_V F_{i\ x,y,z}$ are the forces in x-, y- , z-direction acting between the suspension and the vehicle body in [N], $g_{x,y,z}$ are the fractions of gravity in x-, y-, z-direction due to rotation in [m/s^2], F_d is the aerodynamic drag in [N], $F_{d,y}$ is the lateral aerodynamic force in [N], which is neglected and finally F_{dwn} is the downforce in [N].

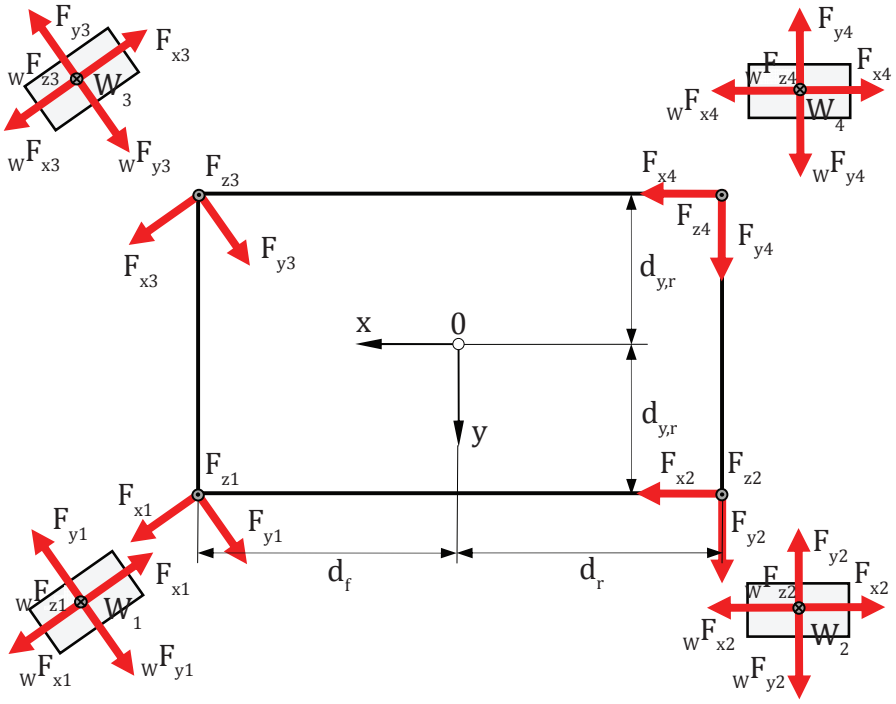

Figure 2.9.: Top view the double track model [SHB+10d]

According to Figure 2.9, the principle of conservation of angular momentum can be generally written:

$$\mathbf{I}_v \, {}_V\dot{\omega} + {}_V\omega \times (\mathbf{I}_v \, {}_V\omega) = \sum_i M^{(CoG)} = \sum_{i=1}^{4} {}_V\mathbf{r}_{P\,i} \times {}_V\mathbf{F}_i, \tag{2.39}$$

with

$${}_V\mathbf{F}_i = \begin{matrix} \\ V \end{matrix} \begin{bmatrix} F_{i\ x} \\ F_{i\ y} \\ F_{i\ z} \end{bmatrix}$$

and

$$\mathbf{I}_v = \begin{bmatrix} I_{v,xx} & 0 & 0 \\ 0 & I_{v,yy} & 0 \\ 0 & 0 & I_{v,zz} \end{bmatrix}$$

where $\mathbf{I}_v$ is the inertia matrix in [kgm^2], ${}_V\dot{\omega}$ is the angular acceleration in [rad/s^2], ${}_V\omega$ is the angular speed in [rad/s], ${}_V\mathbf{r}_{Pi}$ is the position vector from the CoG to the suspension in [m] and ${}_V\mathbf{F}_i$ is the force vector containing the forces acting on the suspension in x-, y-, and z-direction in [N].

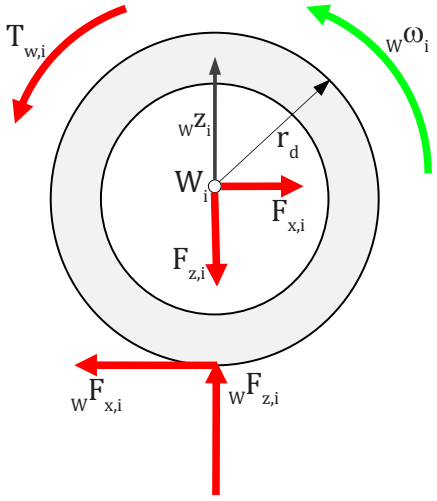

Figure 2.10.: Forces and momentum acting on the wheels
[SHB+10d]

In Equation (2.39), some assumptions are made. Firstly, all the momentum due to aerodynamic drag is neglected. Additionally, the inertia matrix $\mathbf{I}_v$ does not consider the moments of deviation, since the mass inertia is evaluated in its principle axis. In such principle axis, the moments of deviations equal zero, according to [SGHW08b]. Consequently, the structure of the inertia matrix depends on the chosen reference point and the orientation of the coordinate axis.

The principle of impulse and momentum for the wheels may be calculated with the help of Figure 2.10 according to (2.40) and (2.41):

$$m_W \ddot{z}_{W,i} = {}_W F_{z,i} - {}_V F_{z,i} - m_W g, \tag{2.40}$$

$$I_W \; {}_W\dot{\omega} = T_w - r_d \; {}_W F_{i\;x}, \tag{2.41}$$

where I_W is the mass inertia about the y-axis of the wheel in [kgm^2], m_W is the mass of the wheel in [kg], $\ddot{z}_{W,i}$ is the acceleration of the wheel in [m/s^2], ${}_W F_{z,i}$ is the force acting on the wheel contact in [N], ${}_V F_{z,i}$ is the force due to the suspension in [N], g is the gravity in [m/s^2], ${}_W\dot{\omega}$ is the angular acceleration of the wheel in [rad/s^2], r_d is the dynamic tyre radius in [m], ${}_W F_{i\;x}$ is the longitudinal tyre force in [N] and T_w is the driving or braking torque in [Nm]. Moreover, the subindex i names the different wheels.

The modeling of the anti-roll bar, the springs and dampers and the drivetrain in detail is not part of this work. The tyre forces in the wheel contact can be calculated with the approach shown in Section 2.3.

2.2.4. Full Vehicle Model

The full vehicle model is a complex approach to simulate the full vehicle dynamics in detail. Due to its complexity, it promises to reproduce the most realistic assumptions

of the vehicles' behavior. However, a detailed description would go beyond the scope of this thesis. Nonetheless, it shall be mentioned that the major part of these models is the detailed description of non-linear kinematics of wheel suspensions. The high model complexity can result in problems as far as real-time capability is concerned [SHB+10c].

2.3. Tyre Models

In order to receive a realistic assumption of the vehicles' behavior, the modeling of the tyre is essential. Therefore, the following sections shall explain tyres in general, introduce two tyre models, differing in complexity and accuracy. Finally, the different application of a tyre model in a three and a five degrees of freedom model are shown.

2.3.1. Fundamentals of Tyres

Since tyres are deformable elements, the classical rigid body mechanics can only be applied within limits. In the literature, tyre models are often modeled as a combination of springs and dampers with a polymer border.

Consequently, due to the tyre deflection several losses occur, which are described in the following:

Rolling Resistance a_R:

The antisymmetrical pressure distribution $p(x)$ results in a displacement of the total vertical tyre force in the tyre contact zone. Consequently, a rolling resistance momentum M_R is caused by the combination of the vertical tyre force F_z and its eccentricity e, which is stated in Equation (2.60) and in Figure 2.11:

$$\begin{aligned} \sum M_y^{(C)} &= 0 \\ F_R r_s - F_z e &= 0 \\ F_R &= \underbrace{\frac{e}{r_s}}_{a_R} F_z, \end{aligned} \tag{2.42}$$

where r_s is the static tyre radius in [m], F_z is the total vertical tyre load in [N], e is the eccentricity in [m], and F_R is the rolling resistance in [N]. In the literature, a tyre may be modeled as a combination of springs and dampers, according to [MW04d]. With such tyre models, the rolling resistance can be explained as follows:
The tyre circumference compresses and expands alternately in the tyre contact zone, that means that the springs and dampers are also compressed and expanded, which leads to heat losses [MW04d]. Consequently, the rolling resistance grows smaller, the smaller the compression of the tyre is. A high tyre pressure reduces the rolling resistance, but also reduces the driving comfort. The rolling resistance is also dependent on the driving

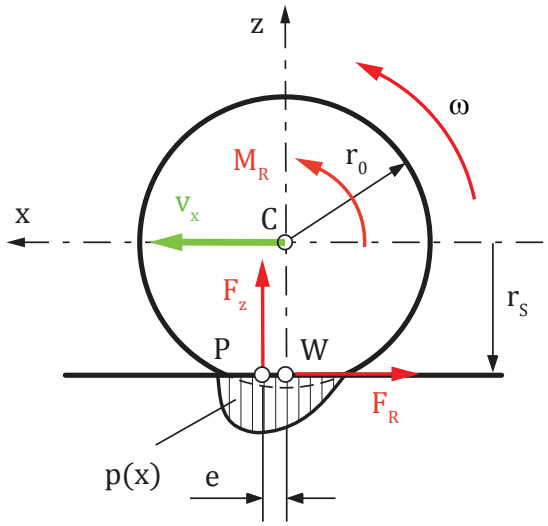

Figure 2.11.: Rolling resistance [HW10a]

velocity and increases with the following approximation according to [MW04d]:

$$a_R = a_{R0} + a_{R1}\left(\frac{v}{100km/h}\right) + a_{R4}\left(\frac{v}{100km/h}\right)^4,$$

where v is the driving velocity in [km/h].
According to [MW04d] typical values for the rolling resistance are:

$$a_R = \begin{cases} < 0.01, & \text{for passenger cars,} \\ < 0.005, & \text{for trucks.} \end{cases}$$

Another rolling resistance occurs due to the water displacement, the rolling resistance inside the bearings and the deformation of the road.

Longitudinal Slip s and characteristic Force-Slip Curve

The longitudinal slip s is one of the main parameters to describe maximum transferable longitudinal tyre forces. It is defined as follows:

$$s = \begin{cases} \frac{{}_W\omega \cdot r_d - v_x}{v_x}, & \text{if braking,} \\ \\ \frac{{}_W\omega \cdot r_d - v_x}{{}_W\omega r_d}, & \text{if accelerating.} \end{cases}$$

where v_x is the longitudinal vehicle velocity in [m/s], ${}_W\omega$ is the angular speed of the wheel in [rad/s] and r_d is the dynamic tyre radius in [m].

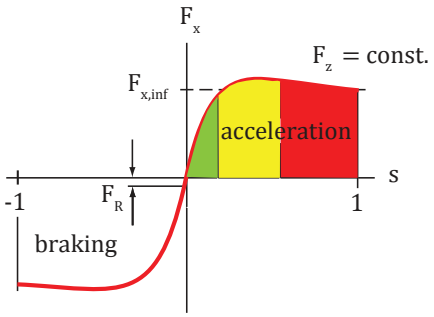

Figure 2.12.: Characteristic tyre force-slip curve[HW10a]

With the help of this definition, the characteristic force-slip curve can be displayed as in Figure 2.17. Three areas can be distinguished:

- The green marked block represents the area of linear relationship between the slip and tyre force. In this area, adhesion is predominant in the contact zone of the tyre, according to Equation (2.61).

$$F_x \leq \mu_0 F_z, \tag{2.43}$$

  where F_x is the transferable tyre force due to adhesion in [N], μ_0 is the grip potential [-] and F_z is the tyre vertical load in [N].

- The yellow area is the transition zone. In this section, the longitudinal slip increases, and adhesion and slipping occur simultaneously. After reaching the maximum transferable tyre force, the force is decreasing according to Equation (2.44).

$$F_x \leq \mu F_z \text{sign} v_s, \tag{2.44}$$

  where F_x is the transferable longitudinal tyre force in [N], μ is the slide friction coefficient [-], F_z is the tyre vertical load in [N] and $v_s = r\omega - v$ is the slide velocity in [m/s]. Moreover, it holds that

$$\mu_0 > \mu$$

- The red area is characterized by a decrease of the maximum transferable tyre force until its saturation value. The slide friction is predominant at very high slip values.

Additionally, it has to be mentioned that a hysteresis effect occurs due to the fact that tyres are elastomers. Nonetheless, this fact will not be considered in this thesis.

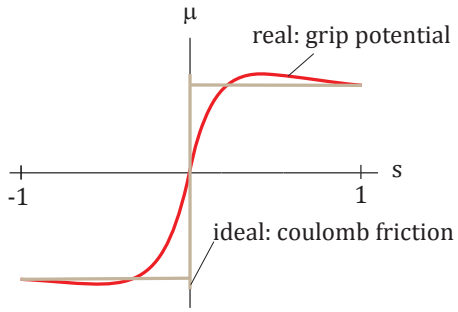

Figure 2.13.: Difference between the coulomb friction and the grip potential

Grip Potential μ_0

The grip potential μ_0 defines the the maximum transferable tyre force in the tyre contact zone. According to [MW04d], the grip potential is defined as follows:

$$\mu_0 = \frac{F_x}{F_z},$$

where F_x is the transferable longitudinal tyre force in [N] and F_z is the tyre vertical load in [N]. In Figure 2.13, the difference between the ideal coulomb friction in grey and the grip potential in red is illustrated. But the grip potential μ_0 strongly depends on many factors. Some of these factors should be listed below:

- Road conditions: wet, dry, or bitumen, country road,
- tyre air pressure,
- temperature of road and tyre respectively,
- tyre dimension,
- surface profile and elastomer mixture of the tyre,
- age of the tyre,
- slide velocity v_s or slip s respectively,
- tyre vertical load F_z.

All factors mentioned above but the slip s, the tyre vertical load F_z and the grip potential μ_0 can be fixed. Thus, these factors have little relevance as far as the dynamical analysis in the area of few seconds is concerned. Consequently, the transferable tyre force F_x in longitudinal direction can be calculated by Equation (2.69):

$$F_x = f(s, F_z, \mu), \tag{2.45}$$

where s is the longitudinal slip of the tyres in [%], F_z is the tyre vertical load in [N] and μ is the grip potential. In the following, μ denotes the grip potential, instead of μ_0.

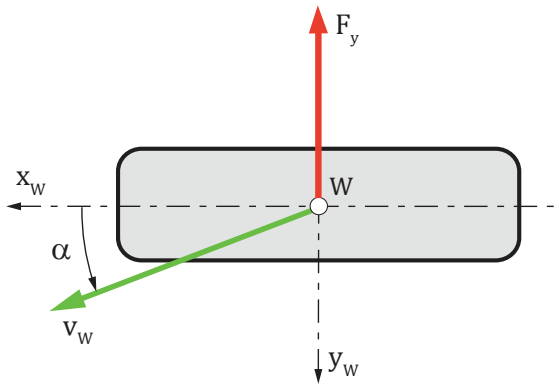

Figure 2.14.: Wheel coordinate system according to ISO 8855

Lateral Slip Angle α:

The transferable lateral tyre force acts quite similar to the longitudinal one. The lateral slip is defined with its slip angle α according to Equation (2.63):

$$\alpha = \underset{W}{} \left(\frac{v_y}{v_x} \right), \tag{2.46}$$

where α is the lateral slip angle in [rad], v_x is the longitudinal tyre velocity in [m/s] and v_y is the lateral tyre velocity also in [m/s].
Next, the wheel coordinate system has to be defined according to ISO 8855 standards, which can be seen in Figure 2.14. It is obvious, that if there is a positive slip angle α, the lateral forces F_y acts in negative y-direction of the wheel coordinate system.

A typical tyre force-slip curve in lateral direction is stated in Figure 2.15. If this characteristic curve is compared with the curve of the longitudinal tyre characteristics in Figure 2.17, the lateral tyre features a lower tyre stiffness and a less dominant peak characteristics. This is because of the tyre design and important for a predictable driving behavior. The characteristic curve can again be described with a few parameters as displayed in (2.64).

$$F_y = f(\alpha, F_z, \gamma, \mu), \tag{2.47}$$

where F_y is the transferable lateral tyre force in [N], α is the slip angle in [rad], F_z is the tyre vertical load in [N], γ is the camber angle in [rad] and μ is the grip potential.
It should be pointed out clearly that only the lateral tyre force F_y depends on the camber angle γ not the longitudinal tyre force stated in Equation (2.69). The camber angle γ , as well as the pneumatic trail, are not considered in the scope of this work; the latter creates a tyre aligning torque in combination with the lateral tyre force F_y.

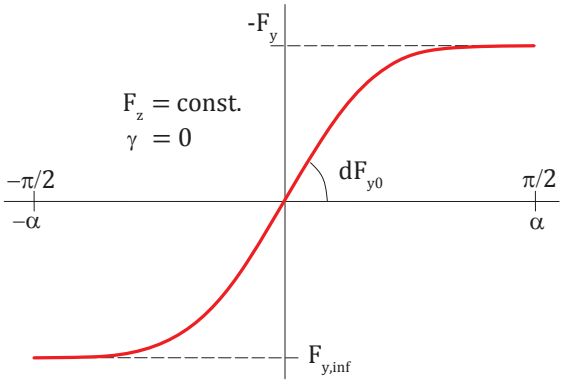

Figure 2.15.: Characteristic lateral tyre force-slip curve

Influence of the Vertical Tyre Load F_z:

The vertical tyre load on each single wheel has an important impact on the maximum transferable tyre force in longitudinal and also in lateral tyre direction. The transferable tyre force decreases relatively to the vertical tyre load when the load increases. This characteristics have to be considered in every tyre model, and are thus integrated in the implemented tyre model explained later on.

2.3.2. Basics of Tyre Models

According to [HW10a], there are three types of tyre models:

1. **Physical Tyre Models**
   are based on an in-depth description of the physical effects appearing within the tyres. That means that adhesion and deflection mechanisms are modeled approximately. The obvious advantage is that it helps to understand the nature of tyres and results can be interpreted easier. However, this model requires significantly more computational resources due to the high degree of detail. Therefore, physical tyre models are rather used for R&D applications than for real-time simulations.

2. **Empirical-Mathematical Tyre Models**
   The measurement of the forces and moments acting on the wheel leads to a mathematical function, which is capable of simulation, but requires the effort of the measurements. It is capable for simulation, but on the other hand the quality of the model depends on accurate measurements of the tyre characteristics.

3. **Semi-Empirical Tyre Models**
   These models are a combination of the two models explained above. This type is implemented in the present vehicle model.

In Figure 2.16, the input-output structure of a tyre model is shown.

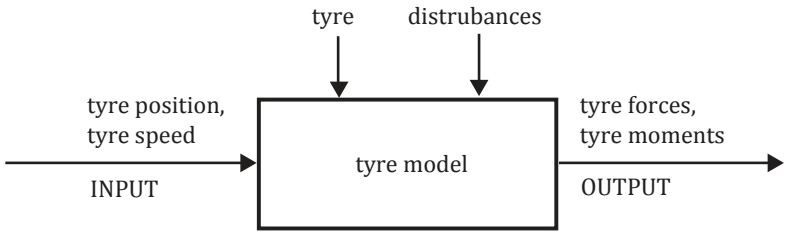

Figure 2.16.: Input-Output structure of a tyre model

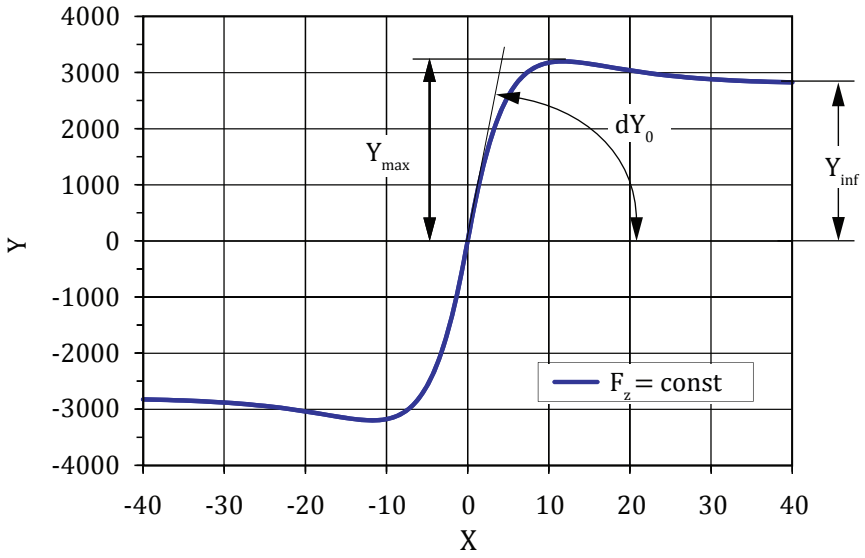

Figure 2.17.: Typical force-slip development

2.3.3. Detailed Tyre Model

The explained tyre model is a derivation of the tyre model "TM Easy" [HRW07]. Aim of this section is to derive a real-time capable tyre model, which is easy to handle on the one hand, and sufficiently accurate on the other hand. A typical force-slip development is shown in Figure 2.17. The symbol Y is in that case either the longitudinal tyre force ${}_W F_x$ or the lateral tyre force ${}_W F_y$ both in [N], the symbol X is either the corresponding longitudinal slip s in [%] or the corresponding lateral slip angle α in [rad]. As the figure points out, this curve is only valid for a specific tyre vertical load F_z.

The following tyre model, called "TM-Simple", is taken from lecture notes according to [HW10a].

"TM-Simple" neglects the influence of the camber angle γ, and the road has to be even. With the help of the nominal road-tyre grip potential μ, the transferable longitudinal and lateral tyre forces ${}_W F_x$ and ${}_W F_y$ for a given vertical tyre load F_z, can be calculated. The main input of the model is the longitudinal slip s in [%] and the lateral slip angle α in [rad], which are defined in Section 2.3.1. The force Y in Figure 2.17 acting on the tyre at the wheel point W can be calculated by (2.48)

$$Y = K \underbrace{\sin[B \overbrace{(1 - e^{\frac{-|X|}{A}})}^{\text{term 2}} \text{ sign } X]}_{\text{term 1}}, \tag{2.48}$$

where Y is the force in [N] and X is the related slip quantity either expressed in [%] or in [rad]. Moreover, term 1 creates the characteristic cutout and term 2 in (2.48) serves that the curve closes asymptotic to the maximum transferable force Y_{max}. The parameters K, B and A are coefficients which are derived in the following:

Determination of the Coefficients A, B, K :

First case: $X \longrightarrow 0$:
If $X \longrightarrow 0$, the $\sin(x)$ can be linearized to its argument x. By doing a Taylor series expansion, which is canceled after the first order, the exponential function in Equation (2.48) can be rewritten to:

$$e^{\frac{-|X|}{A}} \approx 1 + \frac{1}{1!}\frac{-|X|}{A}, \tag{2.49}$$

Inserting (2.49) in (2.48) results in:

$$Y_0 = \underbrace{K\frac{B}{A}}_{dY_0} X,$$

where Y_0 is the transferable longitudinal/lateral tyre force for little slip values in [N] and dY_0 is the initial tyre stiffness either expressed in [N/%] or [N/rad].

Second case: $X \longrightarrow \infty$:

$$Y_{inf} = K \ \sin[B \ (1 - \underbrace{e^{\frac{-|X|}{A}}}_{=\,0}) \ \text{sign } X], \tag{2.50}$$

leads to:

$$Y_{inf} = K \ \sin[B \ \text{sign } X] \tag{2.51}$$

According to Figure 2.17 and (2.50) to (2.51) the coefficients are given by:

$$K = Y_{max},$$

$$B = \underbrace{\Pi-}_{1} \arcsin \frac{Y_{inf}}{Y_{max}},$$

$$A = K \frac{B}{dY_0},$$

where Y_{max} is the maximum transferable tyre force in [N], dY_0 is the initial tyre stiffness in [N/rad] or [N/%], respectively, and Y_{inf} is the saturation value of Y in [N]. Term 1 is added in order to get the correct result, since $\arcsin(x)$ is an arc-trigonometric function. In order to consider the declining degressive influence of the vertical tyre load F_z, mentioned in Section 2.3.1, the following polynomials are introduced:

$$Y_{max}(F_z) = a_1 \frac{F_z}{F_{z\ nom}} + a_2 \left(\frac{F_z}{F_{z\ nom}} \right)^2,$$

$$dY_0(F_z) = b_1 \frac{F_z}{F_{z\ nom}} + b_2 \left(\frac{F_z}{F_{z\ nom}} \right)^2,$$

$$Y_{inf}(F_z) = c_1 \frac{F_z}{F_{z\ nom}} + c_2 \left(\frac{F_z}{F_{z\ nom}} \right)^2,$$

where $F_{z\ nom}$ is the nominal tyre load in [N] and a_1, a_2, b_1, b_2, c_1 and c_2 are coefficients which can be calculated by:

$$a_1 = Y_{F_z nom} - \frac{1}{2} Y_{2 \cdot F_z nom},$$

$$a_2 = \frac{1}{2} Y_{2 \cdot F_z nom} - Y_{F_z nom},$$

the other coefficients can be obtained similarly by inserting the corresponding values. That means, for getting b_1 and b_2 $dY_{0F_z nom}$ and $dY_{0\ 2 \cdot F_z nom}$ alternatively; $Y_{inf\ F_z nom}$ and $Y_{inf\ 2 \cdot F_z nom}$ for calculating c_1 and c_2.

With the help of this mathematical approach, it is possible to describe the physical characteristics of tyres in longitudinal and lateral direction by using the corresponding values for Y_{max}, dY_0 and Y_{inf}.
In normal driving situations, acceleration as well as braking maneuvers occur combined with steering activities. In other words, at the contact point W of the tyre, there are both longitudinal and lateral tyre forces.
To consider this, the similarity of the longitudinal and lateral slip can be used [HW10a]. The aim is to create to the resultant tyre force vector ${}_W\mathbf{F}$

$${}_W\mathbf{F} = {}_W \begin{bmatrix} F_x \\ F_y \end{bmatrix}$$

and the corresponding resultant slip vector s

$$\mathbf{s} = \begin{bmatrix} s_x \\ s_y \end{bmatrix},$$

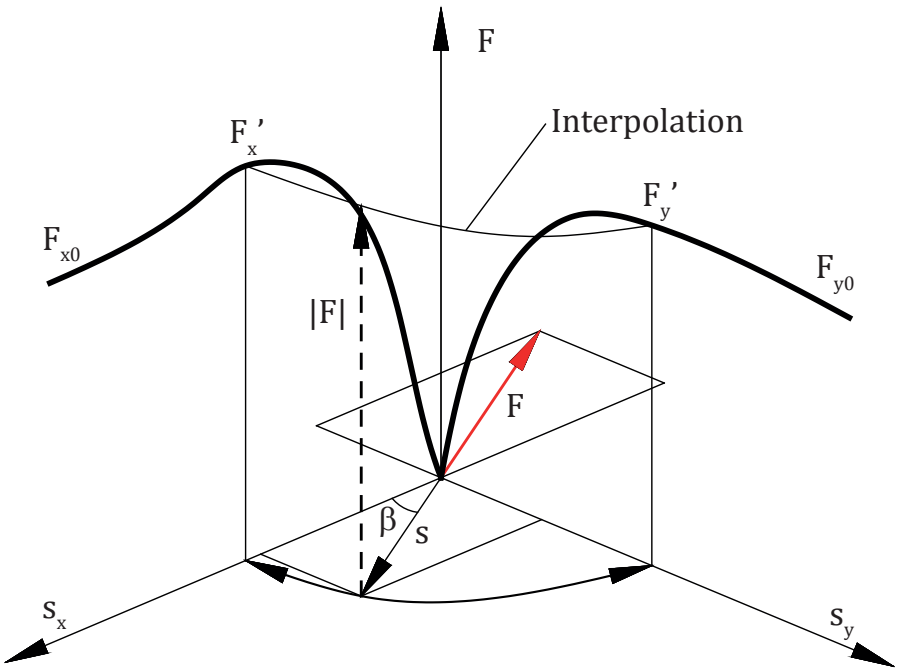

Figure 2.18.: Interpolation of the combined tyre forces
[HW10a]

where the slip angle α is transformed to a lateral slip s_y, such that an equivalent initial stiffness is reached. This can be done by using a weighting function $G(F_z)$:

$$s_y := \frac{\alpha}{G(F_z)}$$

where $G(F_z)$ is defined by:

$$G(F_z) = \frac{dF_{x0}(F_z)}{dF_{y0}(F_z)} = \frac{A_y}{A_x}\frac{K_x B_x}{K_y B_y}.$$

In Figure 2.18, the applied superposition can be seen. The magnitude of the resulting force vector ${}_W F = |\mathbf{F}|$ can be calculated according to Equation 2.52.

$${}_W F = \frac{1}{2}\left[F'_x + F'_y + \left(F'_x - F'_y\right)\cos 2\beta\right], \tag{2.52}$$

where ${}_W F$ is the magnitude of the resulting force vector $\mathbf{F}$ in [N], F'_x and F'_y are the related base values of the longitudinal and lateral force in [N]. At the end the maximum transferable tyre forces under a certain driving situation may be written as:

$${}_W\mathbf{F} = {}_W\begin{bmatrix} F_x \\ F_y \end{bmatrix} = {}_W F \begin{bmatrix} \cos\beta \\ \sin\beta \end{bmatrix} \tag{2.53}$$

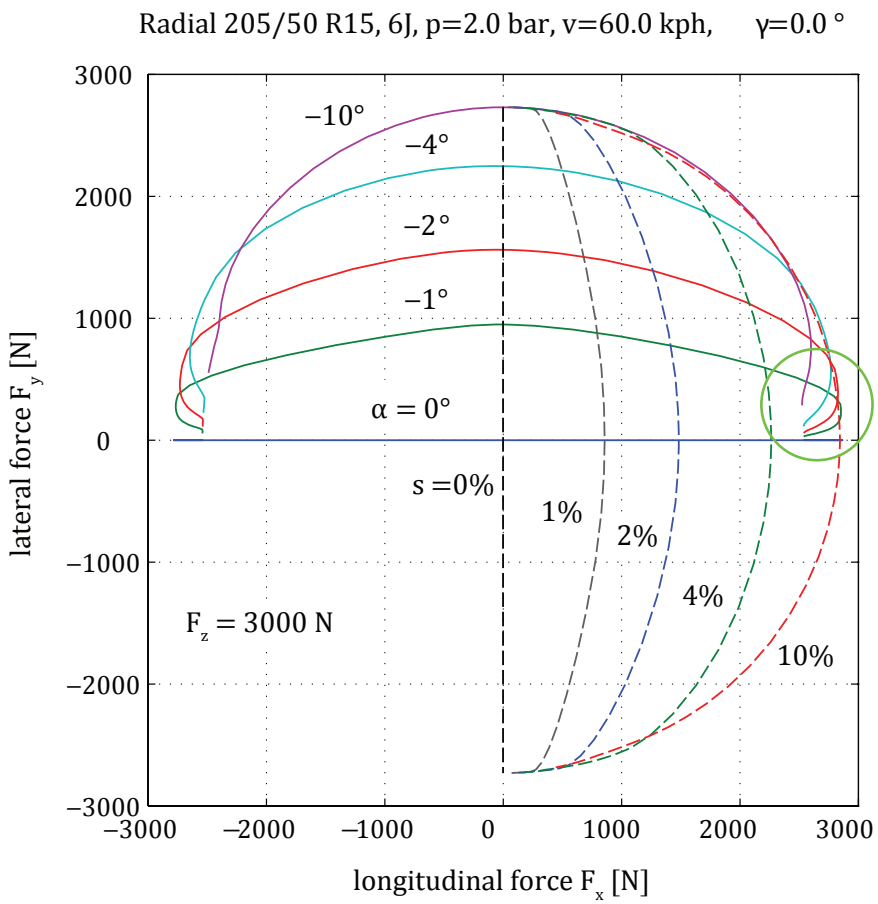

Figure 2.19.: Visualization of the combined tyre forces in different driving situations [HW10a]

According to Figure 2.19, it can be seen that combined driving maneuvers result in reduced tyre forces with respect to the longitudinal and lateral direction. The higher the longitudinal acceleration is, the less lateral force can be transferred. For instance, if the driver slams on the brakes, the maximum transferable lateral tyre force becomes almost zero . The so-called "Kamm'scher Kreis" is not a perfect circle, since normally the tyre profile is designed to assist longitudinal tyre maneuvers more than the lateral ones. The reduction of the lateral forces described above can be seen in the green marked area.

2.3.4. Simplified Tyre Model

Due to the specification to optimize the simulation time of the whole vehicle model for real-time performance, a simplified tyre model is introduced. It is based on the ideas

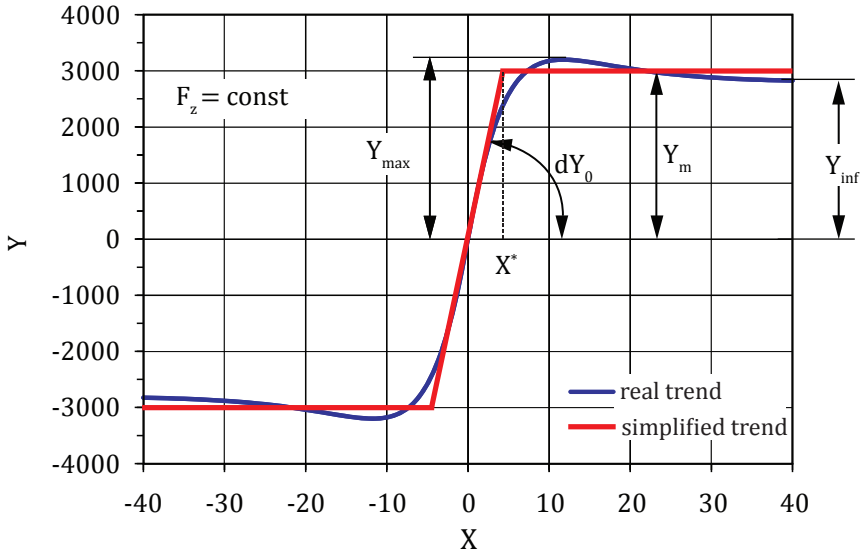

Figure 2.20.: Simplified tyre model and its parameters

of the approach described in Section 2.3.3. The simplified approach is accurate in non-critical driving maneuvers up to six [m/s^2] lateral acceleration and uses physical tyre parameters as model input. These specifications lead to the following model, which output is shown in Figure 2.20.

The implemented tyre model consists of only one linear area which is cut beyond a certain slip value X^*. That means that the maximum transferable force of a specific slip value X is calculated by:

$$Y(F_z) = \begin{cases} dY_0 \cdot X, & \text{if } X < X^* \\ Y_m, & \text{if } X \geq X^* \end{cases}, \tag{2.54}$$

where X is the slip value either in [%] for the longitudinal slip or in [rad] for the lateral slip quantity, dY_0 is the initial tyre stiffness in [N/%] or in [N/rad], X^* is the slip value at the maximum tyre force either in [%] or [rad] and Y_m is the maximum transferable tyre force in [N]. The force Y_m may be calculated by the mean of Y_{max} and Y_{inf}:

$$Y_m = \frac{1}{2}(Y_{max} + Y_{inf}), \tag{2.55}$$

where Y_{max} is the maximum transferable tyre force in [N] and Y_{inf} is the saturation value also in [N].

With the help of that idea and the definition of the longitudinal slip s in [%] and the lateral slip α in [rad], the tyre forces for different driving situations may be calculated.

2.3.5. Difference to the Single Track Model with five Degrees of Freedom

After the detailed explanation of a specific tyre model and its modification, its application in the vehicle model shall be discussed. The amount of DoF of the vehicle, the detailed determination of a tyre model and its parameters, have a great impact on the accuracy of the simulation model.
The three degrees of freedom model explained in this work has only DoF in x, y and ψ, that means that there is no DoF for the rotation of the wheels. This fact makes it impossible to evaluate the angular speed of the wheels ${}_W\omega$ and thus the longitudinal slip s. So with the used three DoF single track model only, the lateral tyre forces are a function of the slip angle α.

$$ {}_W F_y = f(F_z, \alpha) = \begin{cases} dF_{y0}(F_z) \cdot \alpha, & \text{if } \alpha < \alpha^*, \\ F_{ym}, & \text{if } \alpha \geq \alpha^*, \end{cases} \tag{2.56} $$

where F_z is the vertical tyre load in [N], α is the slip angle in [rad], α^* is the slip angle where the maximum transferable tyre forces is reached in [rad], dF_{y0} is the initial lateral tyre stiffness in [N/rad] and F_{ym} is the maximum transferable lateral tyre force in [N].

Here, the longitudinal tyre forces is a function of the engine torque and the gear ratio i_G.

$$ {}_W F_x = f(T_e, i_G) = \frac{T_e}{r_d} i_G \cdot i_{fd}, \tag{2.57} $$

where ${}_W F_x$ is the longitudinal tyre force in [N], T_e is the engine torque in [Nm], r_d is the dynamic tyre radius in [m], i_G is the gear ratio of the selected gear [-] and i_{fd} is the ratio of the finaldrive [-].

With the help of this approach, a consideration of the longitudinal slip s and longitudinal tyre forces is not possible. Only used within uncritical driving maneuvers, the error should be marginal. An application of the detailed tyre model "TM-Simple" explained in Section 2.3.3 is not possible, since the longitudinal slip s is not calculated.

A vehicle model with five degrees of freedom provides, the longitudinal and lateral displacement x, y, and the rotation about the yaw axis and the front and rear wheel rotation ${}_W\omega$. Thus, a calculation of all slip quantities is possible. The longitudinal tyre force ${}_W F_x$ can be calculated by (2.58):

$$ {}_W F_x = f(s, F_z), \tag{2.58} $$

where s is the longitudinal slip in [%] and F_z is the vertical tyre load in [N]. By using the simplified tyre model, Equation (2.58) can be rewritten to:

$$ {}_W F_x = \begin{cases} dF_{x0}(F_z) \cdot s, & \text{if } s < s^*, \\ F_{xm}, & \text{if } s \geq s^*, \end{cases} \tag{2.59} $$

where dF_{x0} is the initial longitudinal tyre stiffness in [N/%], s is the longitudinal tyre slip in [%], s^* is the slip value where the maximum transferable longitudinal tyre force F_{xm} in [N] is reached.

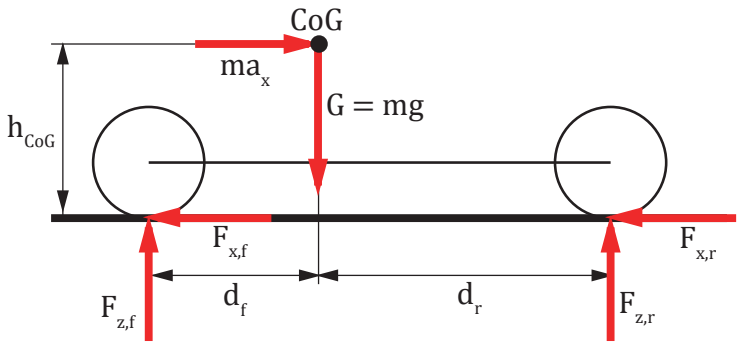

Figure 2.21.: Quasi-static pitching model

The transferable lateral tyre force ${}_W F_y$ can be similarly calculated to Equation (2.56).

In order to consider the dynamic load transfer between front and rear axle, as well as the load transfer between the left and right vehicle side, an approach has to be found which is able to represent this influence, while it has to be ensured that the consideration of these effects does not slow down the simulation program. Therefore, a computational time efficient quasi-static model is preferred to a dynamic one like in [SHB+10a].

Longitudinal Load Transfer

The longitudinal load transfer arises due to braking or acceleration maneuvers. If the vehicle accelerates more, load acts on the rear axle, and vice versa. This fact strongly influences the tyre vertical load, and consequently the maximum transferable tyre forces. In order to consider this effect, a simple quasi-static approach is used according to Figure 2.21 and Equations (2.60) to (2.61).

$$F_{z,f} = m_v \frac{g \cdot d_r - a_x \cdot h_{CoG}}{d_r + d_f} + F_{dwn,f}, \tag{2.60}$$

$$F_{z,r} = m_v \frac{g \cdot d_f + a_x \cdot h_{CoG}}{d_r + d_f} + F_{dwn,r}, \tag{2.61}$$

where $F_{z,f,r}$ is the acting force on the front or rear axle in [N], m_v is the total vehicle mass in [kg], g is the gravitation in [m/s^2], $d_{f,r}$ is the distance of the CoG to the front or rear axle in [m], a_x is the longitudinal acceleration in [m/s^2] and $F_{dwn,f,r}$ is the downforce at the front and rear axle in [N].

Lateral Load Transfer

If the simulation model should also describe effects caused by steering or cornering maneuvers, a so-called rolling model has to be applied. During a cornering scenario, more

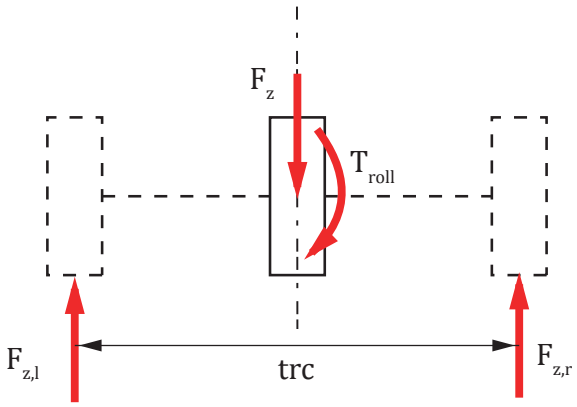

Figure 2.22.: Quasi-static rolling model

load is transferred to the outer curve wheel. Since the vertical tyre load has a major influence on the longitudinal and lateral tyre forces, it is important to implement such a model. However, the emphasis remains on the real-time capability, thus again a quasi-static roll model is preferred to a dynamic one as described in [SHB+10a]. According to Figure 2.22 and (2.65) through (2.68), the load on a single wheel can be calculated as follows:

The total rolling torque T_r is defined as in Equation (2.69):

$$T_r = m_v \cdot a_y \cdot h_{CoG}, \tag{2.62}$$

where m_v is the total vehicle mass in [kg], a_y is the lateral vehicle acceleration due to a steering maneuver in [m/s^2] and h_{CoG} is the height of the center of gravity in [m]. The lateral acceleration a_y is defined according to Equation (2.19). By assuming that the distribution of the rolling torque between front and rear is known, the front and rear rolling torque can be calculated according to Equation (2.63) to (2.64):

$$T_{r,f} = T_r \cdot rd_f, \tag{2.63}$$

$$T_{r,r} = T_r \cdot rd_r, \tag{2.64}$$

where T_r is the total rolling torque in [Nm], $T_{r,f,r}$ is the rolling torque at the front or rear axle in [Nm] and $rd_{f,r}$ is the rolling torque distribution between front and rear axle in [%/100].

The vertical tyre load due to lateral load transfer can be calculated according to Equation (2.65) to (2.68).

$$F_{z,f,r} = \frac{1}{2} F_{z,f} + T_{r,f} \cdot trc_f, \tag{2.65}$$

$$F_{z,f,l} = \frac{1}{2} F_{z,f} - T_{r,f} \cdot trc_f, \tag{2.66}$$

$$F_{z,r,r} = \frac{1}{2} F_{z,r} + T_{r,r} \cdot trc_r, \tag{2.67}$$

$$F_{z,r,l} = \frac{1}{2} F_{z,r} - T_{r,r} \cdot trc_r, \tag{2.68}$$

where the indices f or r denotes the front or rear axle. Moreover, the indices l and r denote the left or the right wheel on a specific axle. The parameter trc is the track of the vehicle in [m].

By looking at (2.65) through (2.68), it can be seen that some assumptions are made:

- The lateral force due to the lateral acceleration a_y is calculated with the total vehicle mass instead of a certain fraction.
- The load distribution between left and right wheel at one axle is equal when the car is not cornering.
- The influence of the suspension and other devices is neglected.
- The rolling torque distribution is known and constant for each vehicle.

In order to derive the tyre parameters, they are summed vectorially on the left and the right side of a certain axle. This means that, for example, the lateral tyre force acting in the single track model on the front wheel can be calculated by (2.44):

$$F_{y,f} = F_{y,f,l} + F_{y,f,r}, \tag{2.69}$$

where $F_{y,f}$ is the total acting lateral tyre force of the front wheel for the single track model in [N], $F_{y,f,l}$ is the lateral tyre force of the left front wheel in [N] and $F_{y,f,r}$ is the lateral tyre force of the right front wheel also in [N].
The rolling torque distribution can be chosen according to [MW04e] and strongly affects the maximum reachable lateral acceleration. The default calibration for the present simulation programme is 60% rolling torque at the front axle. This results in understeering behavior of the vehicle with such a rolling torque distribution.

Thus, the main differences between the three and five DoF single track models concerning the tyre models are easily summarized:
First of all, the three DoF model is not considering the longitudinal tyre force as a function according to (2.59). That is why the detailed tyre model is more accurate, but it also needs more computational resources, which makes the simulation model not that time efficient. On the other hand, the three DoF model disclaims a detailed description of the tyre characteristics, which makes almost no difference in non-critical driving maneuvers. Additionally, the five DoF model allows the application of the tyre model "TM-Simple".

2.4. Applied Vehicle and Tyre Model

Before starting to describe the driver model approach, the used vehicle model with the applied tyre model is stated in detail using the information in Chapter 2.2 to 2.3. Since the emphasis is to develop a real-time capable vehicle model with adequate accuracy, the non-linear vehicle model with a simplified tyre model is chosen. The following explains the main mathematical steps in detail.

According to Equation (2.26), the three relevant equations of motion can be written to:

$$\begin{aligned}
\dot{v}_x &= \omega_z v_y + \frac{1}{m_v}\left({}_V F_{x,f} + {}_V F_{x,r} - F_d\right) \\
\dot{v}_y &= -\omega_z v_x + \frac{1}{m_v}\left({}_V F_{y,f} + {}_V F_{y,r}\right) \\
\dot{\omega}_z &= \frac{1}{I_{zz}}\left({}_V F_{y,f} \cdot d_f - {}_V F_{y,r} \cdot d_r\right)
\end{aligned}$$

where $\dot{v}_{x,y}$ and $\dot{\omega}_z$ are accelerations of the vehicle in [m/s^2] or [rad/s^2], respectively. The variables ${}_V F_{x,y,f,r}$ are the acting forces relative to the vehicle coordinate system in x- and y-direction in [N], m_v is the total vehicle mass in [kg] and d_f and d_r are the distances from the center of gravity to the front or rear axle in [m], respectively.

By integration, the vehicle velocities as well as the angular speed of the vehicle body can be obtained.

$$v_x = \int_{t_0}^{t_{end}} \dot{v}_x \, dt, \tag{2.70}$$

$$v_y = \int_{t_0}^{t_{end}} \dot{v}_x \, dt, \tag{2.71}$$

$$\omega_z = \int_{t_0}^{t_{end}} \dot{\omega}_z \, dt, \tag{2.72}$$

where v_x and v_y are the velocities of the vehicle in the vehicle-fixed coordinate system in [m/s], and ω_z is the angular speed of the vehicle in [rad/s].

Repeated integration leads to the vehicle's covered distance in the vehicles coordinate

system:

$$ {}_V x = \int_{t_0}^{t_{end}} v_x \, dt, \tag{2.73} $$

$$ {}_V y = \int_{t_0}^{t_{end}} v_y \, dt, \tag{2.74} $$

$$ {}_V \psi = \int_{t_0}^{t_{end}} \omega_z \, dt \tag{2.75} $$

where x and y are the position of the vehicle in the vehicle reference system $\{0, x, y, z\}$ in [m], ψ is the rotation of the vehicle coordinate system relative to the global reference system in [rad].

In order to receive the vehicle's position in global coordinates directly, the rotational angle ψ has to be considered in the x and y equation above.

$$ {}_0 \begin{bmatrix} x \\ y \end{bmatrix} = \int_{t_0}^{t_{end}} \begin{bmatrix} \cos\psi & -\sin\psi \\ \sin\psi & \cos\psi \end{bmatrix}_V \begin{bmatrix} v_x \\ v_y \end{bmatrix} \, dt, \tag{2.76} $$

Now, only those forces needed to calculated the accelerations a_x, a_y and $\dot{\omega}_z$ of the vehicle in Equation (2.26) have to be taken into account.

Aerodynamic Forces

The aerodynamic forces are calculated according to (2.11) and (2.13). The aerodynamic drag is modified so that it is also valid for both directions:

$$ F_d = \frac{1}{2} \rho A_x c_x v_x \, \mathrm{sign} v_x, $$

where F_d is the aerodynamic drag in longitudinal vehicle direction in [N], ρ is the density of the ambient air in [kg/m^3], A_x is the cross sectional area of the car in x-direction in [m], c_x is the aerodynamic coefficient [-], v_x is the longitudinal vehicle velocity in [m/s]. With the sign-function, the driving direction is also considered.

Moreover, the downforce F_{dwn} is directly influencing the tyre vertical load ${}_W F_z$. Thus, it also influences the vehicle dynamics. It is calculated by:

$$ F_{dwn} = \frac{1}{2} \underbrace{c_z A_z}_{C_{dwn}} \rho v_x^2, $$

where F_{dwn} is the downforce in [N], c_z is the aerodynamic coefficient in vertical direction [-], A_z is the cross sectional area in z-direction in [m], ρ is the density of the air in [kg/m^3]

and v_x is the vehicle speed in longitudinal direction in [m/s]. The product $c_z \cdot A_z$ are combined to the constant C_{dwn} in [m^2], since it is hard to evaluate A_z or c_z without doing any flow analysis.

Longitudinal and Lateral Forces

According to Chapter 2.3.5, the longitudinal slip s and the lateral slip angle α have to be determined in order to calculate the acting tyre forces. Only the definition of the slip angle α has to be considered, since only the lateral slip angle α can be calculated in the applied three DoF vehicle model.

$$\alpha = {}_{W}\left(\frac{v_y}{v_x}\right)$$

Therefore, the longitudinal and lateral tyre velocity has to be calculated. According to [SGHW08d], the velocity vector of a arbitrary point P of a body $\mathbf{v}_P$ may be determined by equation (2.77):

$$\mathbf{v}_P = \mathbf{v}_C + \omega \times \mathbf{r}_{CP}, \tag{2.77}$$

where $\mathbf{v}_P$ is the speed vector of a arbitrary point of the body in [m/s], $\mathbf{v}_C$ is the speed vector of the point C of the body in [m/s] where only a rotation exists relative to the initial coordinate system, ω is the rotational speed in [rad/s] and $\mathbf{r}_{CP}$ is the distance vector of point P relative to point C in [m].

By applying Equation (2.77) on the vehicle model, the tyre velocity can be calculated by:

$$\begin{bmatrix} v_{x,f} \\ v_{y,f} \\ 0 \end{bmatrix} = \begin{bmatrix} v_x \\ v_y \\ 0 \end{bmatrix} + \begin{bmatrix} 0 \\ 0 \\ \omega_z \end{bmatrix} \times \begin{bmatrix} d_f \\ 0 \\ 0 \end{bmatrix} = \begin{bmatrix} v_x \\ v_y - \omega_z d_f \\ 0 \end{bmatrix}, \tag{2.78}$$

$$\begin{bmatrix} v_{x,r} \\ v_{y,r} \\ 0 \end{bmatrix} = \begin{bmatrix} v_x \\ v_y \\ 0 \end{bmatrix} + \begin{bmatrix} 0 \\ 0 \\ \omega_z \end{bmatrix} \times \begin{bmatrix} -d_r \\ 0 \\ 0 \end{bmatrix} = \begin{bmatrix} v_x \\ v_y + \omega_z d_r \\ 0 \end{bmatrix}, \tag{2.79}$$

where $v_{x,y,f,r}$ are the tyre velocities at the front and rear wheels in [m/s], $v_{x,y}$ are the velocity of the vehicle also in [m/s], ω_z is the angular speed in [rad/s], and $d_{f,r}$ are the distances of the CoG relative to the front and rear wheel in [m].
Since the front wheel is steered, the velocities $v_{x,y,f}$ have to be transformed into the front wheel coordinate system with the help of the inverse transformation matrix ${}^{V}_{W}\mathbf{T} = {}^{W}_{V}\mathbf{T}^{-1}$.

$${}_{W}\begin{bmatrix} v_{x,f} \\ v_{y,f} \\ 0 \end{bmatrix} = \underbrace{\begin{bmatrix} \cos\delta & \sin\delta & 0 \\ -\sin\delta & \cos\delta & 0 \\ 0 & 0 & 1 \end{bmatrix}}_{{}^{V}_{W}\mathbf{T}} {}_{V}\begin{bmatrix} v_x \\ v_y - \omega_z d_f \\ 0 \end{bmatrix} \tag{2.80}$$

Now, it is possible to calculate the lateral tyre forces at the front and rear wheel by using the simplified tyre model. The lateral slip angle α at the front and rear wheel is obtained by using Equation (2.81) :

$$\alpha_{f,r} = {}_{W}\left(\frac{v_{y,f,r}}{v_{x,f,r}}\right), \tag{2.81}$$

According to Equation (2.56), the lateral tyre forces relative to to wheel coordinate system can be obtained by:

$${}_{W}F_y = f(F_z, \alpha) = \begin{cases} dF_{y0}(F_z) \cdot \alpha, & \text{if } \alpha < \alpha^*, \\ F_{ym}, & \text{if } \alpha \geq \alpha^*, \end{cases}$$

The needed tyre vertical force F_z at the every single wheel can can be calculated according to Equation (2.65) to (2.68).

Moreover, the driving force ${}_{W}F_x$ acting on the wheel has to be evaluated. Depending on the drivetrain concept and the driving situation, ${}_{W}F_x$ may be calculated according to (2.82) and (2.83):

$${}_{W}\begin{bmatrix} F_{x,f} \\ F_{x,r} \end{bmatrix} = \begin{bmatrix} \xi_a \\ 1-\xi_a \end{bmatrix} \frac{T_w}{r_d} - {}_{W}\begin{bmatrix} F_{z,f} \\ F_{z,r} \end{bmatrix} a_R \ \text{sign} v_x, \text{if driving}, \tag{2.82}$$

$${}_{W}\begin{bmatrix} F_{x,f} \\ F_{x,r} \end{bmatrix} = \begin{bmatrix} \xi_b \\ 1-\xi_b \end{bmatrix} \frac{T_w}{r_d} - {}_{W}\begin{bmatrix} F_{z,f} \\ F_{z,r} \end{bmatrix} a_R \ \text{sign} v_x, \text{ if braking}, \tag{2.83}$$

where ${}_{W}F_{x,f,r}$ are the tyre longitudinal forces in [N], ξ_a is the driving torque distribution of the front and rear wheel in [%/100], ξ_b is the braking torque distribution in [%/100], T_w is the total driving/braking torque at the wheels in [Nm], r_d is the dynamic tyre radius in [m] and $F_{z,f,r}$ is the tyre vertical load at the wheels in [N].
It should also be mentioned that in this simulation model, simultaneous acceleration and deceleration is not possible, since there is only one pedal for both maneuvers.
Finally, the tyre forces acting on the front wheel have to transformed to the vehicle-fixed coordinate system according to Equation (2.84):

$${}_{V}\begin{bmatrix} F_{x,f} \\ F_{y,f} \\ 0 \end{bmatrix} = \underbrace{\begin{bmatrix} \cos\delta & -\sin\delta & 0 \\ \sin\delta & \cos\delta & 0 \\ 0 & 0 & 1 \end{bmatrix}}_{{}^{W}_{V}\mathbf{T}} {}_{W}\begin{bmatrix} F_{x,f} \\ F_{y,f} \\ 0 \end{bmatrix}, \tag{2.84}$$

2.5. Driver Model

After deriving a complete three DoF vehicle model with a suitable tyre model, the behavior of a driver has to be modeled. The driver model has to follow a certain speed profile and it also has to follow a certain path.
Driving a car belongs to one of the goal-oriented, consciously controlled activities of

humans, where people have to perform self-chosen or predetermined tasks.
Several driver models can be found in the literature, which differ mainly in complexity and thus in real-time capability. But in all models, the driver is represented by one or more state controllers. The control activities of the driver can be divided into three main tasks, according to [Kra08] and [HW10a]:

1. **Navigation**
   In this layer, the desired path is adopted to the specific transportation task. Moreover, all other anticipated activities belong to that group. For example, the planning of the travel time, determination of driving rests, etc.

2. **Course Planning**
   Course planning is the second level of a driver model. Here, the strategic decisions, made in the navigation layer, are realized to operative actions. For instance, the needed traveling velocity results from the time management and the choice of course. Simultaneously, the choice of course directly influences the distance to the road borders.

3. **Course Guidance**
   The last layer consists of the lane keeping and the control of traveling velocity. This layer can be simulated with different controllers for the longitudinal and lateral vehicle control, which are explained in detail in the following sections.

In Figure 2.23, the drivel model with its three main tasks is implemented in the vehicle system. Where $\mathbf{r}_{(t)}$ is the reference input vector, $\mathbf{e}_{(t)}$ is the vector of control deviation, $\mathbf{v}_{(t)}$ is the disturbance vector, $\mathbf{u}_{(t)}$ is the regulating vector and $\mathbf{x}_{(t)}$ is the state vector. Disturbances in a simulation may be irregularities of the road, wind, or other users of the road. The driver in this model is the outer controlling circuit, which is always a level above the inner controlling circle, also vehicle dynamics controller, which can be some assisting systems like ABS, or ASR. If only the solid lines are considered, the system is called an open loop control system, since the course is not controlled by the driver model. In the scope of this thesis, only closed loop maneuvers are considered, since the driver is always comparing the vehicle output $\mathbf{x}_{(t)}$ with the reference input vector $\mathbf{r}_{(t)}$.

According to [Kra08], three effects have to be considered when describing a driver.

1. **Reaction Time**
   No driver is able to react directly, if the environment changes. They need a certain reaction time, which differs from driver to driver.

2. **Reaction Speed**
   The driver is not able to follow a changing situation with arbitrary reaction speed. This effect also varies with different drivers.

3. **Accuracy**
   The accuracy of controlling strongly depends on the driver and is not arbitrary.

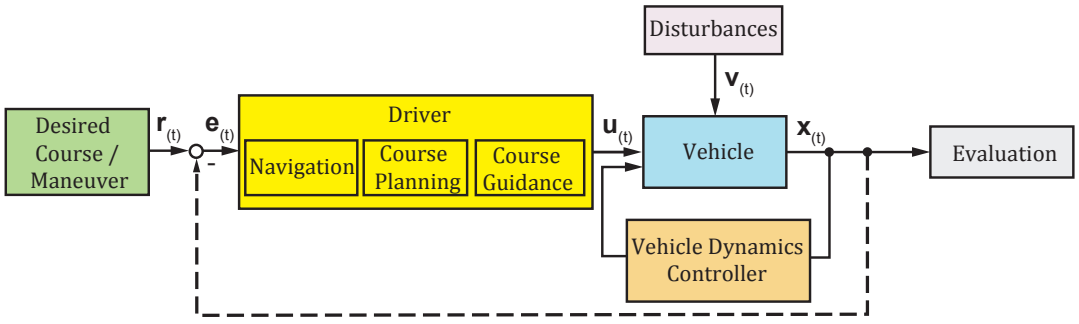

Figure 2.23.: Principle of a driver model implemented in a vehicle system

In order to consider these three important human effects, the driver controller consists mainly of a delay unit for the human reaction time, a low pass filter for the limited reaction speed, and some remnants for the accuracy. It can be assumed that a driver model becomes quite complex and time inefficient when considering all the human effects. This fact is shown in Equation (2.85), where the transfer function according to [Joh77] is derived. As described before, this driver model consists of a delay unit in order to consider the reaction time. Moreover, neuromuscular effects are also taken into account.

$$H(s) = K \cdot \underbrace{e^{-s\tau}}_{\text{delay time}} \cdot \underbrace{\left(\frac{1}{(1+sT_N) \cdot \left(1 + \frac{2\zeta_N}{\omega_N} s + \left(\frac{s}{\omega_N}\right)^2\right)} \right)}_{\text{neuromuscular fraction incl. low pass filter}} \cdot \underbrace{\frac{1+sT_L}{1+sT_I}}_{\text{adaption term}} \cdot \underbrace{\frac{1+sT_K}{1+sT_K}}_{\text{term for low freq.}} , \tag{2.85}$$

where $\tau, T_N, T_L T_I, \zeta_N, \omega_N$ are parameters to describe the performance of a single human being.

It is the aim of this thesis to find a driver model which is real-time capable; exact description of human behavior is not considered as necessary. Thus, mathematical models which only fulfill the driver task of course guidance are introduced in the next section. Due to clear arrangement, the driver model is distinguished into a longitudinal driver model, which should follow a certain speed profile, and a lateral driver model, which should follow a specific path by steering.

2.5.1. Longitudinal Driver Model

The first part of the driver model is the longitudinal driver. The main task of this model is to keep the traveling speed of the vehicle on a certain desired level. Moreover, the driver should be able to brake or to accelerate whenever it is necessary. This simulated driver should also be able to perform a deceleration until the stop of the vehicle, and a

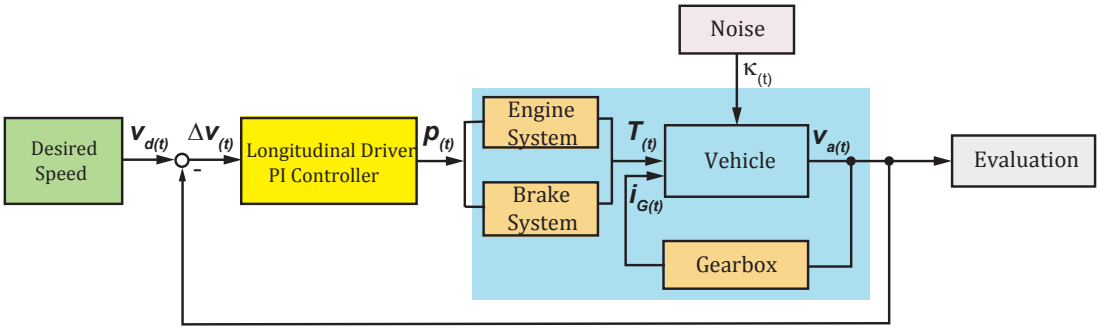

Figure 2.24.: Principle of the used longitudinal driver model

following acceleration maneuver. In Figure 2.24, the used principle of the longitudinal driver is shown. As mentioned above, the driver model consists of one or more state controller. The state controller in the used simulation model is a PI-controller, because the testings have shown that with such a controller, the speed profile can be followed. The I-term should reduce fluctuations in the speed profile. The controller compares the vehicle's actual speed v_a with the desired speed v_d at the same moment. If there is a little difference, the driver model reacts by either accelerating or braking. In order to make the longitudinal driver model work, some parts of the drivetrain are simulated, as well. That means that the complete longitudinal control system consists of:

- PI-Controller
- Engine System
- Brake System
- Gearbox

Of course, these four components are not all parts of a real longitudinal driver system. Especially parts of the drivetrain are not considered in the framework of this thesis, like the clutch, the cardan shaft, the drive shaft etc. Moreover, the modeled parts are simplified, in order to reduce computing time. In the following subchapters, the modeled parts are discussed in detail, and afterwards, the operating mode of the complete longitudinal controller is explained further.

2.5.1.1. Engine System

In order to generate propulsion, a simplified engine model is implemented in the vehicle simulation environment. As the previous modeled parts, it should be not too complex, so that the real-time capability is not endangered. Thus, an approach according to [Gen97] is used. The full-load curve of the engine is thereby approximated with two parameters:

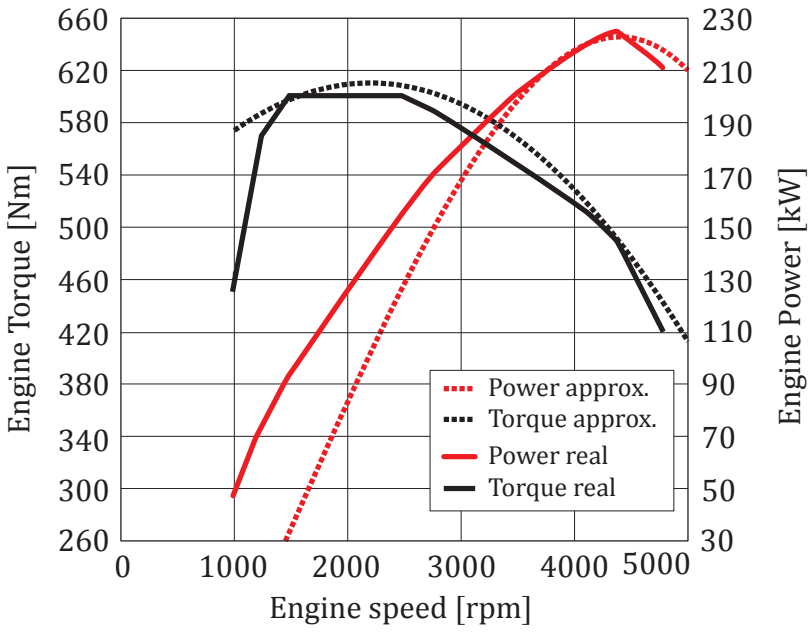

Figure 2.25.: Comparison of the power map of a BMW X5 40d

The rated engine power P_{rated} and the corresponding rated engine speed ω_{rated}. The engine's characteristic curve may be approximated with Equation (2.86):

$$P_e = \sum_{i=0}^{3} P_i \, \omega_e^i, \tag{2.86}$$

with

$$\begin{aligned} P_0 &= 0, \\ P_1 &= \frac{P_{rated}}{\omega_{rated}}, \\ P_2 &= \frac{P_{rated}}{\omega_{rated}^2}, \\ P_3 &= -\frac{P_{rated}}{\omega_{rated}^3}, \end{aligned}$$

where P_i are fixed coefficients for a specific engine type, P_{rated} is the maximum engine power in [kW], ω_{rated} is the engine's angular speed at maximum engine power in [rad/s] and i is an index from 0 to 3.

In order to get the produced engine torque, Equation (2.86) has to be divided by the angular speed of the engine ω_{rated}:

$$T_e = \frac{P_e}{\omega_e} = \sum_{i=1}^{3} P_i \ \omega_e^{i-1}. \tag{2.87}$$

According to Figure 2.25, the approximation of the engine power and the engine torque are good relative to the original engine data of a BMW X5 40d. Especially with higher engine speed, the estimated data, displayed with the dashed lines, is almost congruent with the original data, displayed with solid lines. Since the applied vehicle model has only three DoF, the engine speed is a function of the vehicle speed according to (2.88):

$$\begin{aligned} \frac{\omega_e}{{}_W\omega} &= \underbrace{i_G \cdot i_{fd}}_{i_t} \\ \omega_e &= i_t {}_W\omega \\ \omega_e &= i_t \frac{v_x}{r_d \cos\delta}, \end{aligned} \tag{2.88}$$

where ω_e is the engine speed in [rad/s], ${}_W\omega$ is the angular speed of the wheel in [rad/s], i_G is the gear ratio of the selected gear [-], i_{fd} is the ratio of the finaldrive [-], i_t is the total ratio of the drivetrain [-], r_d is the dynamic tyre radius in [m] and δ is the steering angle in [rad].

The engine torque is transferred via the drivetrain to the front and/or rear wheels, depending on the configuration of the drivetrain. Since every transfer is coupled with an energy loss, the simulation model considers a drivetrain efficiency η. Thus, the total driving torque at the wheels can be written according to Equation (2.89):

$$T_w = \eta T_e. \tag{2.89}$$

where the drivetrain efficiency η is between the interval [0;1].

The pedal position p or the throttle position, respectively, is also considered. It is assumed that a pedal position unequal to 100% moves the full load curve in Figure 2.25 to lower levels as it is shown in Figure 2.27.

$$T_{e,n} = p \cdot T_{e,max},$$

where $T_{e,n}$ is the needed engine torque in [Nm], p is the pedal position in [%] and $T_{e,max}$ is the maximum available engine torque at a certain engine speed in [Nm].

2.5.1.2. Brake System

Every vehicle needs to have a well working braking system, else a safe driving is not ensured. For that reason, a braking system is implemented in the vehicle simulation, which tries to be sufficiently accurate and real-time capable. Consequently, some simplifications have to be made which are listed in the following:

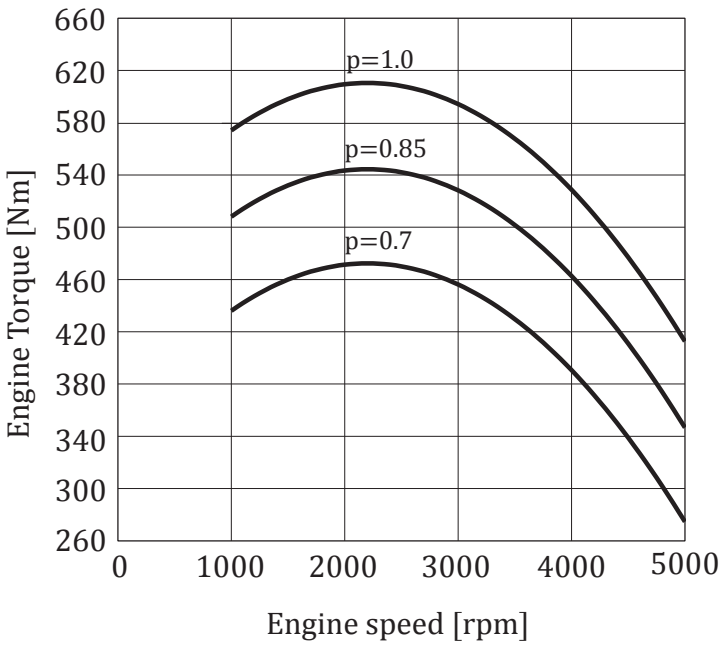

Figure 2.26.: Influence of the pedal position on the actual engine torque

Simplifications of the Brake System:

Hydraulic braking systems are state of the art in passenger vehicles and in light-duty trucks. The standard braking system consists of the following parts according to [Wal05]:

- Pedal Mechanism
- Brake Force Booster
- Main Cylinder
- Wheel Cylinder

In the used brake system model, the brake force booster is idealized by not limiting the booster. This results in a linear relationship between the acting pedal force and the force after the brake force booster according to Equation (2.90).

$$F_{out} = c_1 \cdot F_{pedal}, \tag{2.90}$$

where F_{out} is the resulting force after the brake force booster in [N] and F_{pedal} is the force due to the prying effect in [N] and c_1 is a constant value in [-].
What is more, the braking force hysteresis, shown in [ESP11], is not considered in this

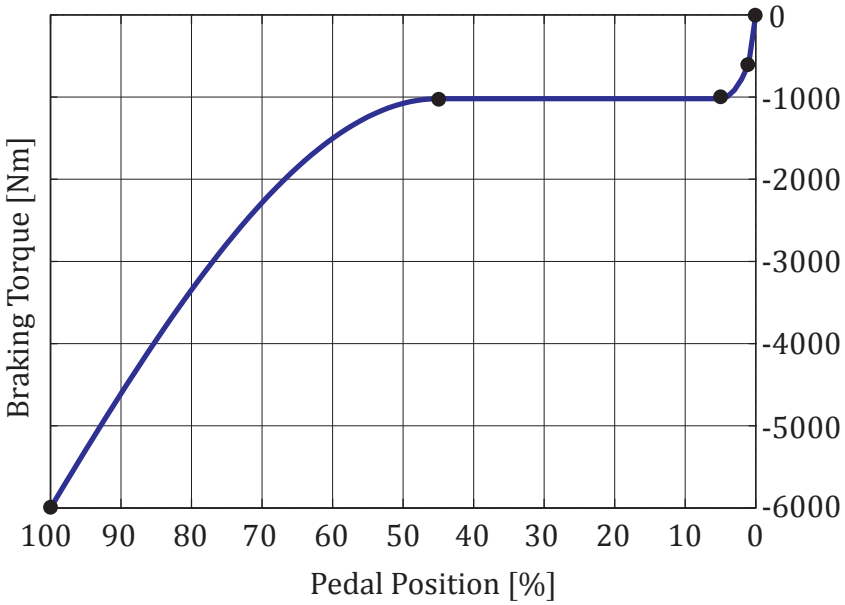

Figure 2.27.: Brake system model with $T_{e,max} = 600$ Nm and $f_b = 10$

simple brake system model, and the speed dependance of the real brake system is neglected. All these simplifications lead to the characteristic brake curve, shown in Figure 2.27. It shows the pedal position-torque relationship where the black dots display the support points to create the shape of the curve. With the help of the maximum engine torque $T_{e,max}$ and a proportional factor f_b, the performance of the brake system can be adjusted according to Equation (2.91):

$$T_b = f_b \cdot T_{e,max} \cdot p, \tag{2.91}$$

where T_b is the braking torque in [Nm], f_b is a proportional factor [-], $T_{e,max}$ is the maximum engine torque in [Nm] and p is the pedal position which may reach values between the area [-1;0]. In comparison to a real braking curve according to [Zot11] the applied one shows quite a good accordance. Finally, the braking torque has to be distributed to the wheels. In order to avoid unstable driving behavior due to locking of the rear wheels, a fixed braking torque distribution of 70% at the front wheels and 30% at the rear wheels is chosen.

2.5.1.3. Gearbox

A gear box model is used in the applied driver model. Thus, a driver is able to select a suitable gear for a certain traveling speed. Depending on the driving style, one driver shifts rather at low engine speed, others may shift shortly before the engine speed limiter

interferes. This fact is considered in the gearbox model. The user of the simulation programme can choose at which engine speed the driver should shift. Figure 2.28 shows an example of a gearbox model. The vehicle velocity at which the driver shifts may be calculated by Equation (2.92):

$$v_x = f_G \cdot \frac{n_{max}}{2\pi \cdot 60}\ r_d\ \frac{1}{i_G \cdot i_{fd}}, \tag{2.92}$$

where v_x is the traveling speed in [m/s], f_G is a proportional factor in [%] relative to the maximum engine speed n_m in [rpm], r_d is the dynamic tyre radius in [m], i_G is the gear ratio of the selected gear [-] and i_{fd} is the ratio of the finaldrive [-].
In Figure 2.28 the red line shows the rotational mass factor λ. It is assumed that this factor is between 1.75 for the lowest gear and 1.06 for the highest gear according to [HW10a]. The values of the different gears between are linearly interpolated. The rotational mass factor is defined according to Equation (2.93):

$$\lambda = \frac{I_{dt}}{r^2}, \tag{2.93}$$

where I_{dt} is the mass inertia of the drivetrain in [kgm^2], r is the tyre radius in [m]. The rotational mass factor influences the longitudinal vehicle dynamics by considering the changing rotational mass fraction of the complete drivetrain.

2.5.1.4. PI-Controller

As displayed in Figure 2.24, the controller compares the actual vehicle velocity v_x with the desired vehicle speed v_d. Normally, this results in a control error $e_{(t)}$, which is defined as follows:

$$e_{(t)} = v_d - v_x.$$

A PI-controller is considered to be sufficient in order to follow a certain speed profile, because it can follow a certain speed profile sufficiently and fluctuations in the speed profile are reduced. Thus, the control error consists of a proportional and an integral term, shown in Equation (2.94):

$$u_{(t)} = K_p \cdot e_{(t)} + \frac{1}{T_N} \int e_{(t)}\ dt, \tag{2.94}$$

where $u_{(t)}$ is the regulating variable which corresponds to the pedal position p in [%], K_p is the proportional factor of the P-term in [s%/m], T_N is the resetting time in [m/%] and $e_{(t)}$ is the control error in [m/s].
Since the pedal position p has to be between $\pm 100\%$, the manipulated variable is limited according to Equation (2.95):

$$p_{(t)} = min\left(\text{abs}(u_{(t)}), 1\right) \cdot \text{sign}(u_{(t)}) \cdot 100\%. \tag{2.95}$$

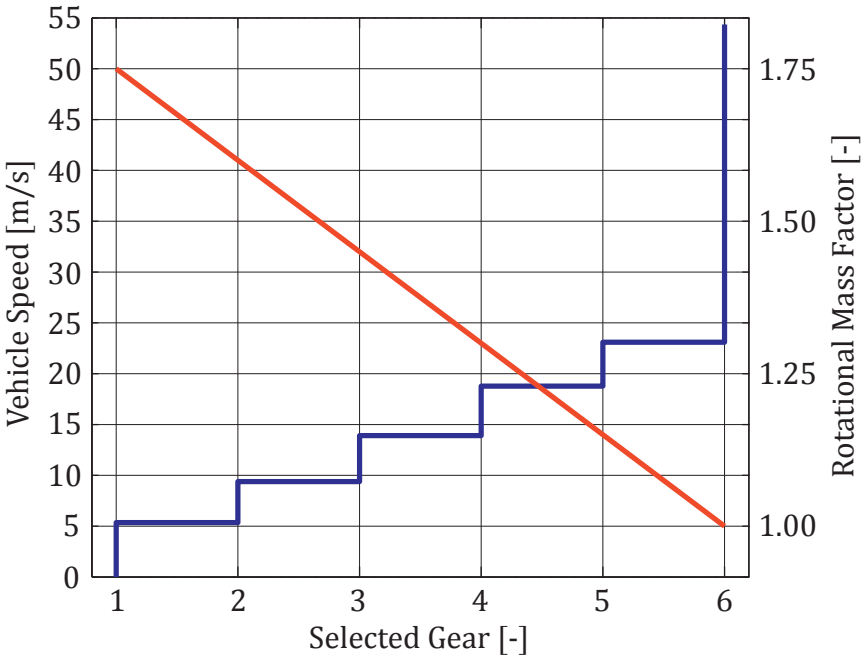

Figure 2.28.: Gearbox model with a shifting point at 2500 [rpm]

2.5.1.5. Operation Method of the Longitudinal Driver Model

Finally, the driving strategy of the longitudinal driver model is explained in detail. The chosen velocity of the driver depends on several factors, listed below:

- Desired speed v_d,
- curvature κ of the road ahead,
- grip potential μ,
- acceleration / deceleration potential of the vehicle.

During normal driving, the driver tries to achieve the desired velocity. In case that the curve of the desired path is too radical for the actual speed, the longitudinal driver model slows the vehicle down. So the first task of the longitudinal driver model is to ensure that the vehicle speed is appropriate when entering a corner. For that reason, the driver model uses the preview distance $d_{p,l}$ in order to find the highest curvature κ of the desired path.

Longitudinal Preview Distance $d_{p,l}$:

The longitudinal preview distance is defined so that the driver is always able to stop the car within this distance. Equation (2.96) shows how to calculate this longitudinal preview distance $d_{p,l}$:

$$d_{p,l} = \frac{v_x^2}{2a_{b,max} \cdot \mu}, \tag{2.96}$$

where v_x is the vehicle's longitudinal speed in [m/s], $a_{b,max}$ is the maximum available vehicle deceleration in [m/s^2] and μ is the grip potential [-].

Maximum Vehicle Speed through a Corner $v_{x,max}$:

By knowing the longitudinal preview distance, the driver model can estimate the maximum speed within this distance by using the definition of the centrifugal acceleration a_c according to [SGHW08a]:

$$a_c = \omega^2 R \underset{v=\omega R}{=} \frac{v^2}{R},$$

where a_c is the centrifugal acceleration in [m/s^2], ω is the angular speed in [rad/s], R is the distance of the object to the rotational axis in [m] and v is the tangential velocity in [m/s].
Applying the definition of a_c combined with the definition of the curvature κ

$$\kappa = \frac{1}{R},$$

the maximum longitudinal vehicle speed can be calculated by Equation (2.97):

$$v_{x,crv} = \left(\frac{a_{y,max} \cdot \mu}{\kappa}\right)^{\frac{1}{2}}, \tag{2.97}$$

where $v_{x,crv}$ is the maximum vehicle longitudinal speed in order to manage a corner ahead in [m/s], $a_{y,max}$ is the maximum allowed vehicle lateral acceleration in [m/s^2], μ is the grip potential of the road tyre contact [-] and κ is the curvature of the desired path ahead in [1/m].
In order to manage the corner without any problems, the driver model chooses the highest curvature κ and the lowest grip potential μ within the longitudinal preview distance $d_{p,l}$. Moreover, the maximum lateral vehicle acceleration $a_{y,max}$ may be chosen arbitrarily. In this vehicle model, the threshold is set to five [m/s^2], since up to this value, the tyre characteristics are still linear according to [HW10b], and, as mentioned above, the used tyre model is a simplified linear tyre model with a upper threshold.
Finally, the maximum longitudinal vehicle speed within a certain preview distance, chosen by the driver model can be calculated with Equation (2.98):

$$v_{x,max} = min(v_d, v_{x,crv}). \tag{2.98}$$

Calculation of the Road Curvature κ:

Since both, the longitudinal driver model as well as the lateral driver model, are using the curvature κ of the desired path as an input parameter, the approach to get the magnitude of κ for a discrete number of data points is described.

As mentioned above, the curvature κ is defined as:

$$\kappa = \frac{1}{R}$$

Using the equation of a circle in order to evaluate the distance of the object to its instantaneous center of rotation R. The equation of a circle is shown in (2.99):

$$(x - x_M)^2 + (y - y_M)^2 = R^2, \tag{2.99}$$

where x, y are the coordinates of arbitrary points on the circle in [m], x_M, y_M are the coordinates of the instantaneous center of rotation also in [m] and R is the radius of the circle in [m].
Thus, this equation has three parameters. In order to calculate the radius R, three different points on the circle are needed. The following equations show the starting point of the calculation:

$$\begin{aligned}(x_1 - x_M)^2 + (y_1 - y_M)^2 &= R^2\\ (x_2 - x_M)^2 + (y_2 - y_M)^2 &= R^2\\ (x_3 - x_M)^2 + (y_3 - y_M)^2 &= R^2\end{aligned}$$

where the indices 1 to 3 show the different points on the circle. After eliminating x_M and y_M the radius R can be calculated. Finally, the curvature κ is obtained by calculating the inverse of R as shown above.

2.5.2. Lateral Driver Model

Not only does the driver model have to perform the longitudinal control of the vehicle, it also has to keep the vehicle on a certain path, which ensures a safe travel. According to Figure 2.23, the final task, course guidance, is discussed in detail. Although there are numerous of different lateral driver models, only a few are described in this section. For the lateral driver model, as well, the real-time capability is the main criterion. Figure 2.29 shows the principle of this controller.

In order to choose a suitable lateral controller, the following main criteria are considered:

- Real-time capability,
- simple implementation,
- velocity dependent preview distance,

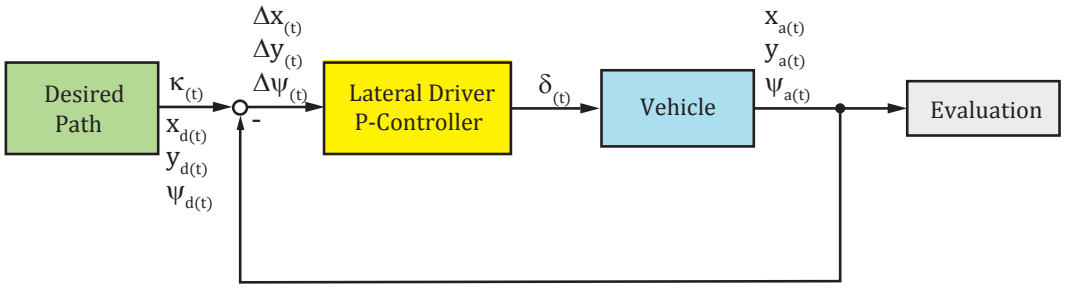

Figure 2.29.: Principle of a lateral driver model

s_t [m]	κ_t [1/m]	ψ_t [rad]	x_t [m]	y_t [m]	v_d [m/s]	μ_t [ ]

Table 2.1.: Look up table for the lateral driver model

- easy reproducible.

All driver models discussed in this thesis are using the curvature κ and the global position of the desired trajectory to describe the road. The approach to determine the curvature is described in the previous section.

2.5.2.1. Lateral Driver Model Type I

The approach is based on the ideas of [CS09]. This driver model uses the heading and position deviation between the vehicle and road as controller input in order to steer.

Description of the desired path

The main part of the model is a look-up table, see Table 2.1, where all needed values are stored. In Figure 2.30, all values belonging to this look-up table are illustrated.

This table contains all values for describing the desired path. Where s_t is the distance covered along the path in [m] and is also used as an unique index for look-up purposes. The symbol κ_t is the curvature of the path in [1/m], ψ_t is the tangent angle of the desired trajectory in [rad], x_t and y_t are the position coordinates of the path [m], v_d is the desired speed in [m/s] and μ is the grip potential [−]. Between certain data points, values are linearly interpolated. It should also be noted that only the position values x_t and y_t, the desired speed v_d and the grip potential μ have to be known, all others can be calculated from the position data according to Equation (2.100) to (2.101):

$$s_t = \sum_{i=1}^{N-1} \left[(x_{t(i+1)} - x_{t(i)})^2 + (y_{t(i+1)} - y_{t(i)})^2 \right]^{\frac{1}{2}}, \tag{2.100}$$

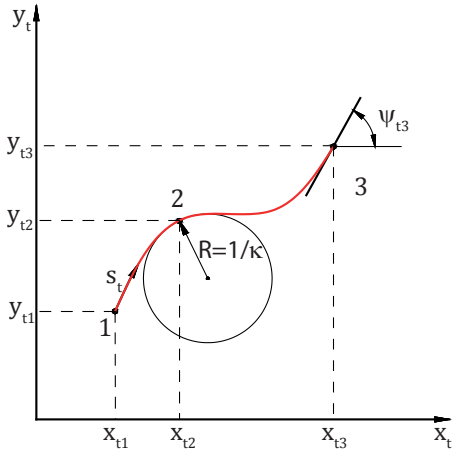

Figure 2.30.: Illustration of the values of the look-up table

$$\psi_t = \arctan \frac{y_{t(i+1)} - y_{t(i)}}{x_{t(i+1)} - x_{t(i)}}, \tag{2.101}$$

where the indices i denotes the number of data set and N is the total number of data sets. The curvature κ_t may be calculated according to Equation (2.99).

The next step is to calculate the current position of the vehicle s_v. The distance covered along the desired path s_v can be calculated according to Equation (2.102):

$$s_v = \int \frac{v_x \cos(\psi - \psi_t) - v_y \sin(\psi - \psi_t)}{1 - \kappa_t \left[(y - y_t)\cos(\psi_t) - (x - x_t)\sin(\psi_t)\right]}, \tag{2.102}$$

where s_v is the distance of the vehicle covered along the desired path in [m], v_x and v_y are the longitudinal or lateral vehicle speed in [m/s], respectively. The angle ψ depicts the rotation of the vehicle coordinate system relative to the global reference system in [rad], ψ_t is the tangent angle of the desired path in [rad], κ_t is the curvature of the desired path in [1/m], x and y are the global position coordinates of the vehicle in [m] and x_t and y_t are the position coordinates of the desired path in [m].
In order to get the desired position x_t, y_t, path curvature κ_t and the tangent angle ψ_t a linear interpolation is performed with the help of the look-up table, shown in Table 2.1.

Lateral Preview Distance $d_{p,lat}$

The lateral driver model also works with a preview distance $d_{p,lat}$. But in contrast to the longitudinal preview distance, the lateral one is define according to [CS09]:

$$d_{p,lat} = v_x \cdot T_p, \tag{2.103}$$

where $d_{p,lat}$ is the lateral preview distance in [m], v_x is the longitudinal vehicle speed in [m/s] and T_p is the preview time in [s]. The preview time may be selected by the user

and should be between 0.75 [s] and 2 [s]. This preview distance is afterwards divided into five equidistant evaluation points. That means that a [1x5] preview vector is generated which looks as shown in Equation (2.104):

$$\mathbf{s}_{p,lat} = \mathbf{s}_v + \begin{bmatrix} 0 \\ 0.25 \\ 0.5 \\ 0.75 \\ 1 \end{bmatrix} d_{p,lat}, \tag{2.104}$$

where $\mathbf{s}_{p,lat}$ is the lateral preview vector in [m], $\mathbf{s}_v$ is a [1x5] vector containing the distance covered along the desired path in [m] and $d_{p,lat}$ is the velocity depending lateral preview distance also in [m].

The lateral driver controller consists of two control parameters, which are explained in detail in the following:

Heading Angle Control

The heading angle controller is comparing the current vehicle-heading angle ψ with the tangent angle ψ_t of the desired trajectory ahead of the vehicle. As it can be seen in Figure 2.31, the lateral preview distance $d_{p,lat}$ is divided into five equidistant data points. The generated preview vector is then used to perform a lookup on the desired path table and to compare its values with the current car heading angle. The heading angle error is defined according to Equation (2.105):

$$e_{\psi,i} = \psi_t - \psi. \tag{2.105}$$

Since there are five data points to compare, a heading error vector is created:

$$\mathbf{e}_\psi = \begin{bmatrix} e_{\psi,1} \\ e_{\psi,2} \\ e_{\psi,3} \\ e_{\psi,4} \\ e_{\psi,5} \end{bmatrix} = \begin{bmatrix} \psi_{t,1} \\ \psi_{t,2} \\ \psi_{t,3} \\ \psi_{t,4} \\ \psi_{t,5} \end{bmatrix} - \begin{bmatrix} \psi \\ \psi \\ \psi \\ \psi \\ \psi \end{bmatrix}.$$

In order to get an average heading error value, the heading error vector is multiplied with a weighting vector w_ψ. Consequently, the final heading angle error e_ψ may be calculated according to Equation (2.106):

$$e_\psi = \begin{bmatrix} e_{\psi,1} \\ e_{\psi,2} \\ e_{\psi,3} \\ e_{\psi,4} \\ e_{\psi,5} \end{bmatrix} \cdot \begin{bmatrix} a_{\psi,1} \\ a_{\psi,2} \\ a_{\psi,3} \\ a_{\psi,4} \\ a_{\psi,5} \end{bmatrix}, \tag{2.106}$$

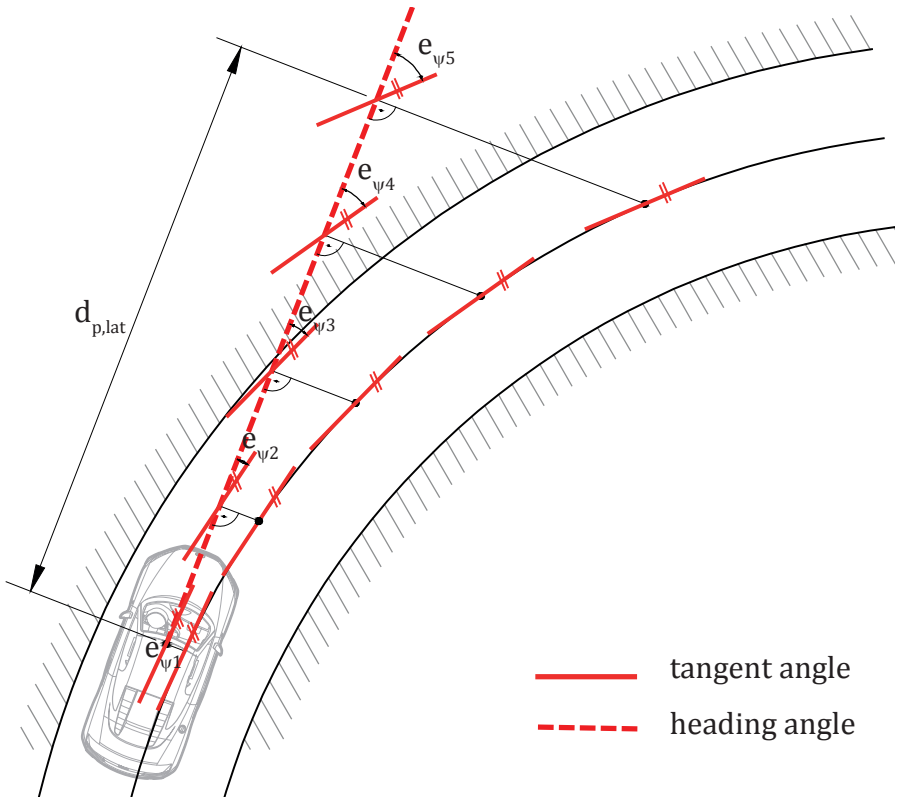

Figure 2.31.: Lateral driver model - Heading angle control

where $a_{\psi,i}$ are weighting coefficients.
In order to get a steering angle, the heading angle error is used as input for a simple P-controller according to Equation (2.107):

$$\delta_\psi = K_{p,\psi} \cdot e_\psi, \tag{2.107}$$

where δ_ψ is the steering angle due to the heading angle error in [rad] and $K_{p,\psi}$ is the proportional gain of the P-controller. The proportional gain $K_{p,\psi}$ is chosen according to [CS09]

Position Deviation Control

The second controller used according to [CS09] is the position deviation controller, which compares the current and the future vehicle position when keeping the current heading angle ψ with the position of the desired path ahead. Similarly to the heading angle control, the same lateral preview vector is used in order to have a lookup on the coordinates of the desired path x_t and y_t. These coordinates are then compared with the future position of the vehicle, if it keeps the current heading angle. The vectors containing

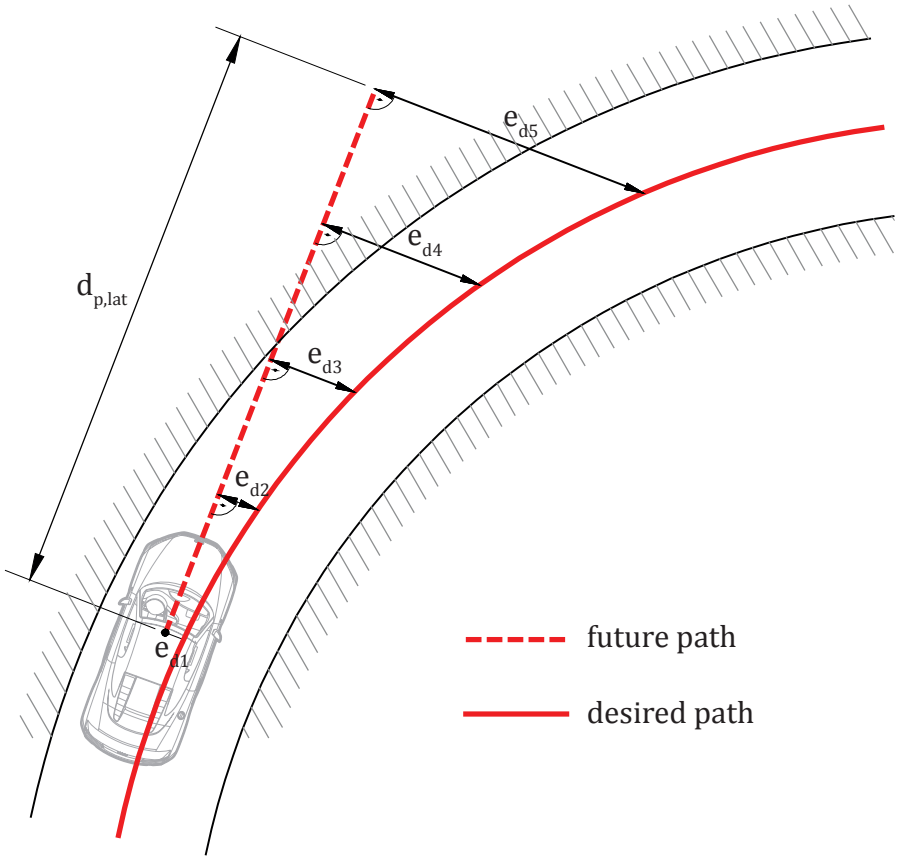

Figure 2.32.: Lateral driver model - Position deviation control

$\mathbf{x}_f$ and $\mathbf{y}_f$ containing the future position of the vehicle can be calculated according to (2.108) to (2.109):

$$\mathbf{x}_f = \mathbf{x} + d_{p,lat} \begin{bmatrix} 0 \\ 0.25 \\ 0.5 \\ 0.75 \\ 1 \end{bmatrix} \cos\psi, \tag{2.108}$$

$$\mathbf{y}_f = \mathbf{y} + d_{p,lat} \begin{bmatrix} 0 \\ 0.25 \\ 0.5 \\ 0.75 \\ 1 \end{bmatrix} \sin\psi, \tag{2.109}$$

where $\mathbf{x}$, $\mathbf{y}$ are vectors containing the current vehicle position in [m], ψ is the current heading angle in [rad] and $d_{p,lat}$ is the lateral preview distance in [m]. The vector with

the position error $\mathbf{e}_d$ can be determined by

$$\mathbf{e}_d = (\mathbf{y}_t - \mathbf{y}_f)\cos\psi - (\mathbf{x}_t - \mathbf{x}_f)\sin\psi.$$

where $\mathbf{y}_t$ and $\mathbf{x}_t$ is a [1x5] vector containing the position of the desired path in [m]. Moreover $\mathbf{x}_f$ and $\mathbf{y}_f$ is also a [1x5] vector containing the future position of the vehicle in [m].
Finally, the position deviation error is used as input for a simple P-controller, after multiplying it with the weighting vector w_d, similarly to Equation (2.106). The coefficients do not have to be the same as for the heading angle approach. Consequently, the steering angle δ_d due to the position deviation can be written according to Equation (2.110):

$$\delta_d = K_{p,d} \cdot e_d, \tag{2.110}$$

where $K_{p,d}$ is the proportional gain of the position deviation controller in [rad/m], chosen according to [CS09], and e_d is the weighted position deviation error in [m].

Total Steering Output

The last step is to combine both the steering angle δ_ψ due to the heading angle error and the steering angle δ_d because of the position deviation error. This results in the following expression for the total steering angle δ_t:

$$\delta_t = \delta_\psi + \delta_d. \tag{2.111}$$

In order to create a realistic driver model, the influence of the traveling speed on the steering behavior is considered, as well. The characteristics of the vehicle are also taken into account, as far as understeering or oversteering is concerned. In general, the average driver reduces the amount of steering as the speed of the vehicle increases according to [CS09]. The steering tendency of the vehicle is defined according to [HW10b]:

$$K = \frac{\partial\delta}{\partial a_y} := \frac{m_v}{l_{12}}\left(\frac{d_r}{dF_{y0,f}} - \frac{d_f}{dF_{y0,r}}\right), \tag{2.112}$$

where K is the stability factor of the vehicle in [kgrad/N], m_v is the total vehicle mass in [kg], l_{12} is the wheelbase in [m], d_f and d_f is the distance of the CoG to the front or rear axle, respectively also in [m], and $dF_{y0,f,r}$ are the lateral tyre stiffness of the front and rear wheel in [N/rad].
According to [Kra08], the relation between the yaw rate $\dot{\psi}$ and the the steering angle δ for a linear single track model is:

$$K_{\dot{\psi},\delta} = \frac{\dot{\psi}}{\delta} = \frac{v_x}{l_{12}} \cdot \frac{1}{1 + K v_x^2}, \tag{2.113}$$

where v_x is the vehicle's longitudinal speed in [m/s], l_{12} is the wheelbase in [m] and K is the stability factor.

Last but not least, the steering angle response of the driver model can be calculated according to (2.113):

$$\delta = \frac{1}{K_{\dot{\psi},\delta}} \delta_t. \tag{2.114}$$

In order to limit the steering angle at the wheel, the following limiter is used:

$$\delta = \min\left(\text{abs}(\delta), \delta_{max}\right) \cdot \text{sign}(\delta), \tag{2.115}$$

where δ_{max} is the maximum steering angle at the wheel in [rad].

2.5.2.2. Lateral Driver Model Type II

The second driver model is based on the idea of [Kra08]. In contrast to the driver model presented in Section 2.5.2.1, this approach is not working with global coordinates; instead, it transforms every data point into the vehicle-fixed reference system. Thus, for every numeric iteration step, a number of transformations have to be carried out. It should also be mentioned that this model is only a mathematical approach without considering any cognitive driver perception.
This consists of two main parts, which are linked together in order to describe and control the vehicle's path. According to [Kra08], the first part is called the fundamental system of the driving kinematics, which describes the movement of the vehicle. On the other hand, the lateral dynamics completes the driving kinematics.

Driving Kinematics

First of all, the plain movement of the vehicle has to be transformed so that all positions of objects are defined in the vehicle-fixed coordinate system $\{0, x, y, z\}$ not as before in the inertial reference system $\{0_0, x_0, y_0, z_0\}$. This is done with the help of a differential transformation. Without a detailed derivation, the transformation of a point P into the vehicle-fixed coordinate system can be written according to Equation (2.116):

$$\underbrace{\begin{bmatrix} x(r,s) \\ y(r,s) \\ 1 \end{bmatrix}}_{{}_V\mathbf{x}(r,s)} = \underbrace{\begin{bmatrix} \cos\theta_v(s) & \sin\theta_v(s) & 0 \\ -\sin\theta_v(s) & \cos\theta_v(s) & 0 \\ 0 & 0 & 1 \end{bmatrix}}_{\mathbf{T}_{rot}(s)} \underbrace{\begin{bmatrix} 1 & 0 & -X_v(s) \\ 0 & 1 & -Y_v(s) \\ 0 & 0 & 1 \end{bmatrix}}_{\mathbf{T}_{trn}(s)} \underbrace{\begin{bmatrix} {}_0x_P(r) \\ {}_0y_P(r) \\ 1 \end{bmatrix}}_{{}_0\mathbf{x}_P(r)} \tag{2.116}$$

where ${}_V\mathbf{x}(r,s)$ is position vector relative to the vehicle-fixed coordinate system, ${}_0\mathbf{x}_P(r)$ is the position vector of an object in the inertial reference system, $\mathbf{T}_{rot}$ is the rotational transformation matrix, $\mathbf{T}_{trn}$ is the translational transformation matrix, r and s are parameters of the curve according to Figure 2.33: Equation (2.116) has to be partially differentiated with respect to the curve parameter r and s according to Equation (2.5.2.2) to (2.117):

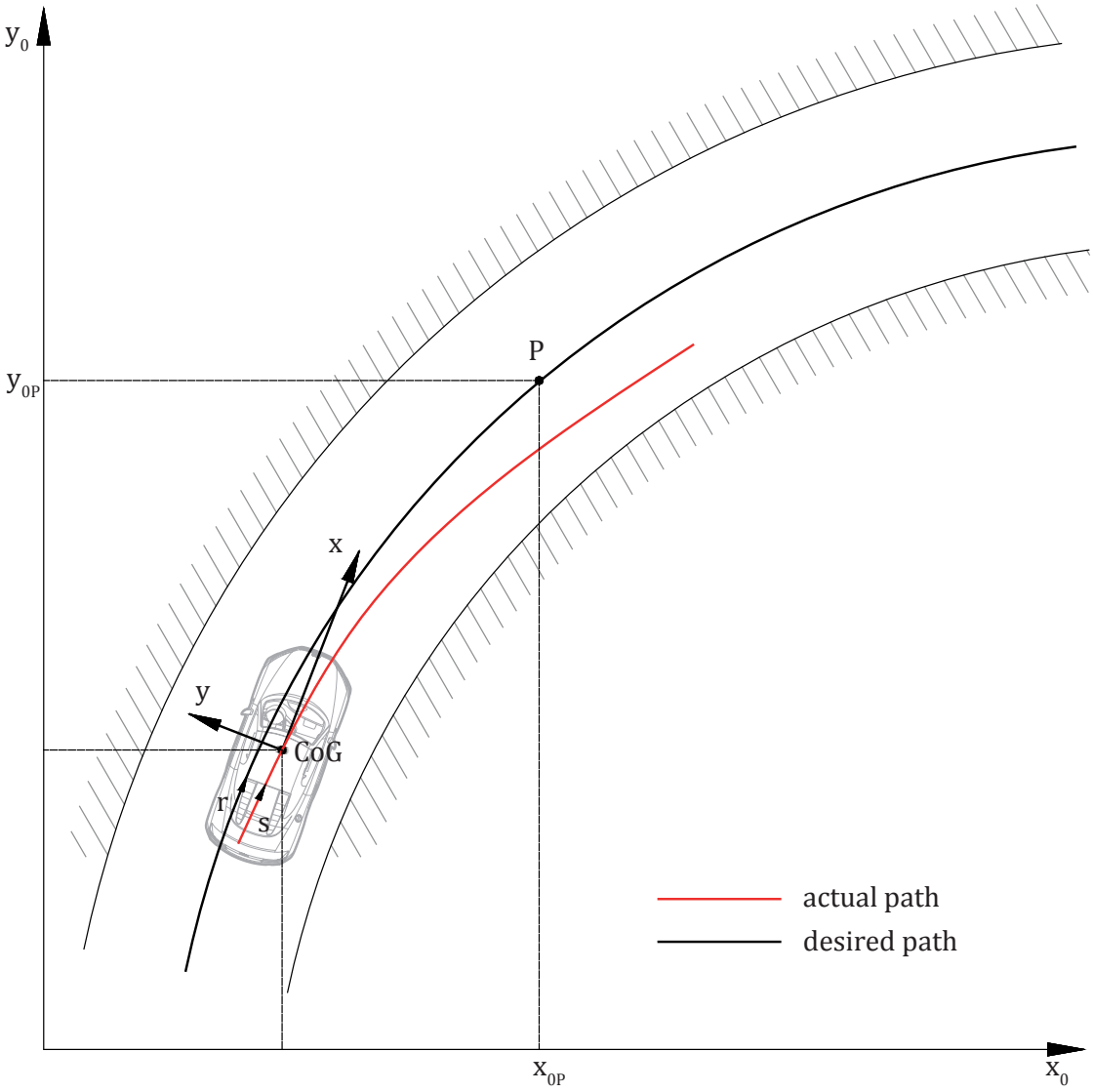

Figure 2.33.: Coordinates of a plain vehicle movement with fixed trajectory

Differentiation with respect to the curve parameter r is without derivation according to [Kra08]:

$$\frac{\partial}{\partial r}\begin{bmatrix} x(r,s) \\ y(r,s) \\ 1 \end{bmatrix} = \begin{bmatrix} \cos(\theta_P(r) - \theta_V(s)) \\ \sin(\theta_P(r) - \theta_V(s)) \\ 0 \end{bmatrix}$$

with $\theta_\Delta(r,s) = \theta_P(r) - \theta_V(s)$ the equation may be rearranged to:

$$\frac{\partial}{\partial r}\begin{bmatrix} x(r,s) \\ y(r,s) \\ 1 \end{bmatrix} = \begin{bmatrix} \cos(\theta_\Delta(r,s) \\ \sin(\theta_\Delta(r,s) \\ 0 \end{bmatrix} \tag{2.117}$$

Moreover, it holds that

$$\frac{\partial}{\partial r}\theta_\Delta(r,s) = \frac{\partial}{\partial r}\theta_P(r) - \frac{\partial}{\partial r}\theta_V(s) = \kappa_P(r).$$

Differentiation with respect to the curve parameter s is without derivation:

$$\frac{\partial}{\partial s}\begin{bmatrix} x(r,s) \\ y(r,s) \\ 1 \end{bmatrix} = \begin{bmatrix} \kappa_V(s) \cdot y(r,s) - 1 \\ -\kappa_v(s) \cdot x(r,s) \\ 0 \end{bmatrix} \tag{2.118}$$

Once again it also holds that

$$\frac{\partial}{\partial s}\theta_\Delta(r,s) = \frac{\partial}{\partial s}\theta_P(r) - \frac{\partial}{\partial s}\theta_V(s) = -\kappa_V(s).$$

where $\kappa_V(s)$ is the curvature of the vehicle path with a certain steering angle in [1/m] and $\kappa_P(r)$ is the curvature of an object in [1/m].

The fundamental system of the driving kinematics is determined with the help of the rule of total differentials according to Equation (2.119):

$$d\mathbf{x} = \frac{\partial \mathbf{x}}{\partial r}dr + \frac{\partial \mathbf{x}}{\partial s}ds.$$

$$\begin{aligned} dx(r,s) &= \cos\theta_\Delta(r,s)dr + (y(r,s)\kappa_V(s) - 1)\,ds, \\ dy(r,s) &= \sin\theta_\Delta(r,s)dr - x(r,s)\kappa_V(s)ds, \\ d\theta_\Delta(r,s) &= \kappa_P(r)dr - \kappa_V(s)ds. \end{aligned} \tag{2.119}$$

Lateral Vehicle Dynamics

This chapter explains how to use the fundamental system of driving kinematics in order to develop a lateral driver controller. First of all, a relation between these two parts has to be found. In (2.120), the simple correlation is shown.

$$\psi = \theta_V - \beta, \tag{2.120}$$

where β is the sideslip angle in [rad], ψ is the yaw angle in [rad] and θ_V is the path angle also in [rad].
According to the fundamental system, derived before, the only parameter influenced is the curvature of the vehicle path κ_V:

$$\kappa_V(s) = \frac{d}{ds}\theta_V(s) = \frac{d}{ds}\left(\psi(s) + \beta(s)\right). \tag{2.121}$$

where θ_V is the angle of the longitudinal speed vector relative to the global coordinate system. But the significant angle of the vehicle is the yaw angle ψ. Considering that fact, the fundamental system of driving kinematics may be rearranged to Equation (2.122) to Equation (2.124):

$$dx = \cos\theta_\Delta(r,s)dr + \left(y(r,s)\frac{\partial}{\partial s}\psi(s) - \cos\beta(s)\right)ds, \tag{2.122}$$

$$dy(r,s) = \sin\theta_\Delta(r,s)dr - \left(x(r,s)\frac{\partial}{\partial s}\psi(s) - \sin\beta(s)\right)ds, \tag{2.123}$$

$$d\theta_\Delta = \kappa_P(r)dr - \frac{\partial}{\partial s}\psi(s). \tag{2.124}$$

This system of total differentials has to be transformed into a system of ordinary differential equations. For this the underdetermination can be used, since for the three kinematical parameters x, y and θ_Δ, only two Equations (2.122) and (2.123) are available. Setting $x = \text{const}$ leads to $dx = 0$. Thus, Equation (2.122) can be used as in order to evaluate dr according to Equation (2.125):

$$dr = \left(\cos\beta - y\frac{\partial}{\partial s}\psi(s)\right)\frac{1}{\cos\theta_\Delta}ds. \tag{2.125}$$

With the help of the following substitutions

$$\begin{aligned} d\mathbf{s} &= \mathbf{v}dt, \\ x &= d_{p,lat}, \\ v_x &= \mathbf{v}\cos\beta, \\ v_y &= \mathbf{v}\sin\beta, \end{aligned}$$

where $d\mathbf{s}$ is the differential vector of the vehicle path in [m], $\mathbf{v}$ is the speed vector of the vehicle in [m/s] and β is the sideslip angle in [rad], the relevant ordinary differential equations can be calculated according to Equation (2.126) to (2.127):

$$\dot{y}(t) = \left(v_x(t) - y(t)\dot{\psi}(t)\right)\tan\theta_\Delta(t) - d_{p,lat}\dot{\psi}(t) + v_y(t), \tag{2.126}$$

$$\dot{\theta}_\Delta(t) = \left(v_x(t) - y(t)\dot{\psi}(t)\right)\frac{\kappa_P(t)}{\cos\theta_\Delta(t)} - \dot{\psi}(t). \tag{2.127}$$

The steering angle is evaluated with the help of a simple proportional controller and with the help of the Ackermann relation.

$$\delta(t) = -l_{12}\cdot K_p\cdot y(t),$$

Criterion	w_c [%/100]	Type I	Type II
Real-time capability	0.45	5	4
Implementation	0.1	4	3
Velocity dependent preview distance	0.25	5	0
Traceability	0.2	5	5
Sum	1	4.9	3.1

Table 2.2.: Benefit analysis

where $\delta(t)$ is the steering angle in [rad], l_{12} is the wheelbase of the vehicle in [m], K_p is the proportional gain of the P-controller in [rad/m] and $y(t)$ is the lateral deviation of the preview point from the desired path at the preview distance $d_{p,lat}$in [m]. The approach how to evaluate the curvature of the path κ_P was introduced in Section 2.5.1.5.

2.5.2.3. Comparative Analysis of Lateral Driver Models

After explaining two different types of lateral driver models, a benefit analysis is carried out, in order to choose the more suitable one.

As mentioned in Section 2.5.2, the main criteria are:

- Real-time capability,
- simple implementation,
- velocity dependent preview distance,
- easy reproducible.

These criteria have different weighting coefficient w_c, which were carefully chosen by the author of the present thesis in order to meet all expectations. The factors multiplied with a value between zero and five, where five is the best and zero the worst, a weighted result can be determined. The approach with the highest result is assumed to be more suitable. Table 2.2 shows the weighting coefficients w_c and the author's rating.

Since Type I has a higher value of benefit, this approach has been implemented in the simulation tool. However, both lateral driver models differ strongly in only one criterion, the velocity dependency of the preview distance $d_{p,lat}$.

2.5.3. Future Prospect: Path Planning

A useful extension of the implemented driver model is a path planning algorithm, which may be used for future driver assistance systems. According to [HS07], the simulation environment is modeled by a potential field hazard map. The suggested method is based on virtual beams that are deflected by the influence of this potential field hazard map. To ensure that the vehicle remains on a certain side of the road, the virtual road is

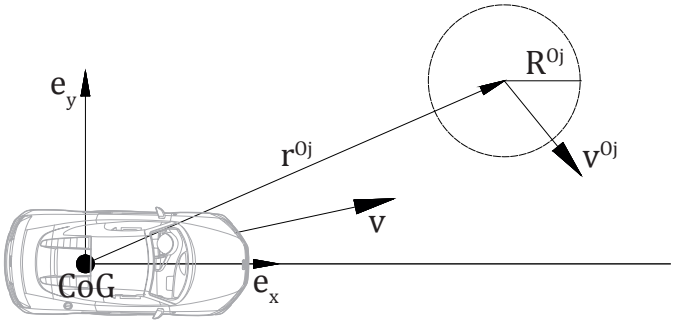

Figure 2.34.: Hazard potential of a moving obstacle
[HS07]

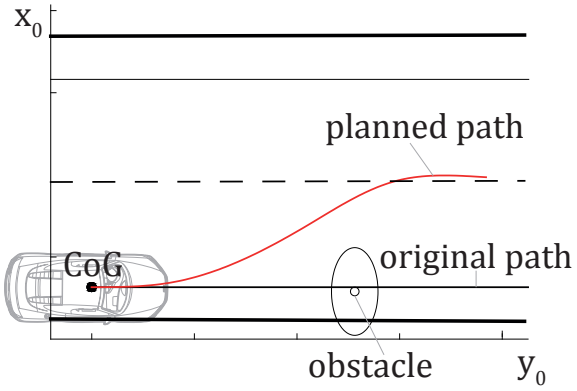

Figure 2.35.: Visualization of a path-planning scenario
[HS07]

modeled by separate logarithmic potentials for the right and left border. All other objects, like other road users or other obstacles, have a hazard potential, as well.

Figure 2.34 shows an obstacle which is moving with constat speed $\mathbf{v}^{Oj}$ in front of another car. The radius R^{Oj} displays its hazard potential. The driver in the vehicle, with the moving speed $\mathbf{v}$, chooses its traveling path in order to minimize the hazard potential.

In detail, a virtual beam interacts with the environment as follows: The beam is deformed by the load, which is calculated by the gradient of the total potential field in each point along the beam. Since the driver chooses the path with the minimal hazard potential, as shown in Figure 2.35, a collision-free travel may be ensured. According to [HS07], this novel approach has a couple of free model parameters, with which an adaption to the respective application can be done.

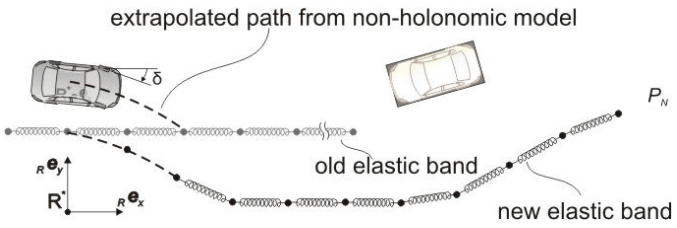

Figure 2.36.: Path-planning with elastic bands [BSB07]

A similar approach is applied in [BSW07], [SB05] and [BSB07], instead of a virtual beam, an elastic band is used, as shown in Figure 2.36. The elastic band deflects due to the hazard field as explained above.

By combining one of the path-planning approaches with a driver model, an "autopilot" can be designed, as it is tested in the "Stadtpilot" project, according to [SWLM11].

2.6. Parameterizations of different Vehicle Classes

In order to gain a knowledge about the distribution of vehicles driven on European roads, the cars are divided into segments according to Kraftfahrt-Bundesamtes's statistics. Further information can be assessed in [Kra11].

2.6.1. Grouping

The segmentation done by the "Kraftfahrt-Bundesamtes" in the following briefly KBA is extended by a heavy truck, a two axle bus. This grouping results in the following classes:

1. Minis
2. Subcompact cars
3. Compact cars
4. Medium-sized cars
5. Upper medium-sized cars
6. Luxury class cars
7. Sport's Utility Vehicles, SUV
8. Utilities
9. Two-axle heavy truck

10. Two-axle bus

For all these classes, plenty of parameters have to be defined in order to feed the vehicle simulation model with this data. Some information was taken from the data sheet of the specified vehicle types, but for other important parameters, especially the position of the center of gravity and the yaw inertia of the vehicle measurements, and estimation formulas had to be used.

2.6.2. Evaluation of the Position of the Center of Gravity

In reference to the classical mechanics, the position of the CoG can be obtained with the following method. The position of the CoG can be calculated by summing all mass fractions with its position vector as shown in Equation (2.128):

$$\mathbf{r}_{CoG} = \frac{1}{m} \sum_i m_i \mathbf{r}_i, \tag{2.128}$$

where $\mathbf{r}_{CoG}$ is the position vector of the CoG in [m], m is the total mass of the body in [kg], m_i is a mass fraction of the body in [kg] and $\mathbf{r}_i$ is the position vector of the mass fraction m_i in [m]. Moreover, the sum of the mass fractions m_i has to equal the total mass m of the body. This approach can also be applied to evaluate the CoG of different vehicles, especially when the whole car with its components and materials is fully available in a CAD model. The CAD programme can calculate the resulting CoG out of many components by using this method. Since it is not easy to get such precise CAD models, other methods have to be found.
The position of the CoG is one of the most important parameters in this simulation model, since it directly influences the handling behavior. That is why it is essential to evaluate it precisely. Unfortunately, most car manufacturers do not publish any information on the vehicle's weight distribution. In order to get the position of the CoG the following method is used.

The position of the CoG is defined by three parameters. First, the longitudinal distance from the center line of the front axle, second the transverse distance from the vertical symmetry plane of the vehicle and, last but not least, the vertical distance (height) above the horizontal level when the tyres are inflated as specified for the vehicle. The single track model only needs the distance from the front axle to the CoG and its height.

2.6.2.1. Longitudinal Distance from the Center Line of the Front Axle

The measurement of the shortest distance to the front axle can be done with weighing machines. Figure 2.37 shows the used test assembly in order to measure the total weight of the vehicle and the weight acting on each axle.

By adding every of the four wheel loads N_{ij} in [N], the total weight G in [N] of the specific car can be measured, compare Equation (2.129).

$$G = N_{fr} + N_{fl} + N_{rr} + N_{rl} \tag{2.129}$$

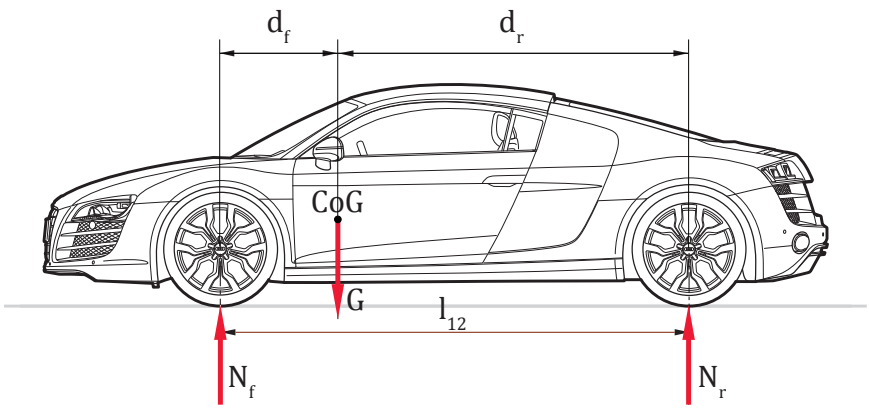

Figure 2.37.: Test set-up for evaluation position of CoG [AG11]

By calculating the equilibrium of moments at the front axle, it is possible to obtain the distance from the front axle to the CoG, as long as the wheelbase l_{12} in [m] is known, see (2.130). Data about the wheelbase is mostly given in the data sheet of the specific vehicles.

$$d_f = \frac{N_r}{G} \cdot l_{12} \tag{2.130}$$

The same can be done in order to get the distance from the rear axle to the CoG, which leads to the following equation:

$$d_r = \frac{N_f}{G} \cdot d_f \tag{2.131}$$

Another approach to determine the distance from the rear axle to the CoG is to use the simple correlation, as shown in Equation (2.132).

$$l_{12} = d_f + d_r \tag{2.132}$$

Although the position of the CoG in the y-coordinate direction is not needed for the present single track model, it should be mentioned that the distance can be obtained similarly. One just has to use the sum of the wheel loads of the left and right vehicle side, and then calculate the equilibrium of moments.

2.6.2.2. Evaluation of the Height of CoG above Ground

The height of the CoG above the ground is another very important parameter of the whole vehicle simulation model. Inertia forces due to acceleration/deceleration or cornering maneuvers in combination with the height of the CoG result in a dynamic wheel load transfer, which influences the dynamic behavior of the specific vehicle.

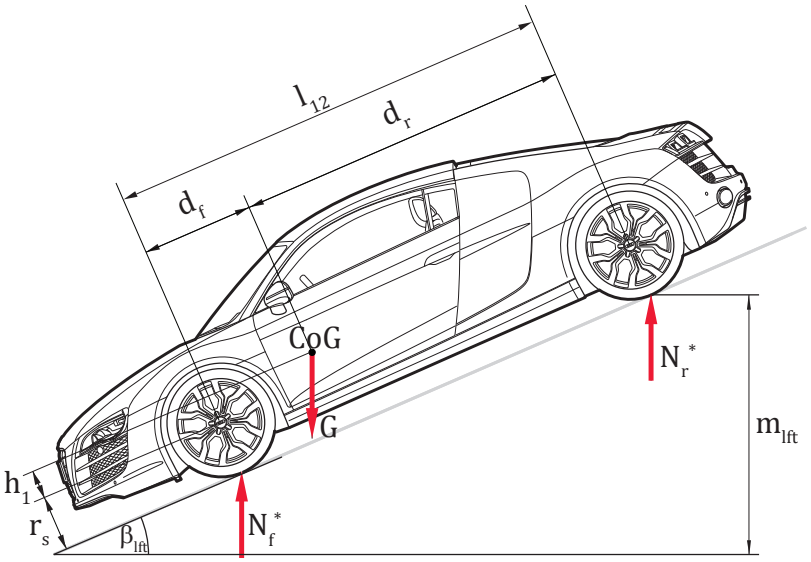

Figure 2.38.: Test set-up for evaluation height of CoG [AG11]

In order to evaluate this parameter, the following method can be used:
While the vehicle's rear axis is lifted, the tyre load at the front axle is measured. Using the horizontal position of the CoG evaluated in Section 2.6.2.1, the vertical position of the CoG can be calculated from the forces and moment equilibrium. From the calculation emerges that the static tyre diameter d_s is needed as well.

First of all, the sum of the measured loads at the front and rear axle shall be equal to the total weight measured in Section 2.6.2.1. If that is not given, the measurement devices and the arrangement should be controlled. That fact is shown in Equation (2.133).

$$N_f + N_r = N_f^* + N_r^*, \tag{2.133}$$

where N_f and N_r are the axle loads in the horizontal measurement position in [N]. N_f^* and N_r^* are the values of the position in [N] as shown in Figure 2.38. In order to calculate the lifting angle β_{lft} the lifting height m_{lft} has to be measured precisely. With the help of the trigonometric relationship, the lifting angle β_{lft} can be expressed as stated in Equation (2.134).

$$\beta_{lft} = \arcsin\left(\frac{m_{lft}}{l_{12}}\right) \tag{2.134}$$

The lifting height m_{lft} has to result in a lifting angle β_{lft} between 15° - 20° according to [Nat00]. To ensure this lifting angle, either a ditch has to be used, or the front axle should be in an elevated position to overcome the risk of damaging the front bumper. Moreover, the vehicle should remain constant after it has reached the required lifting

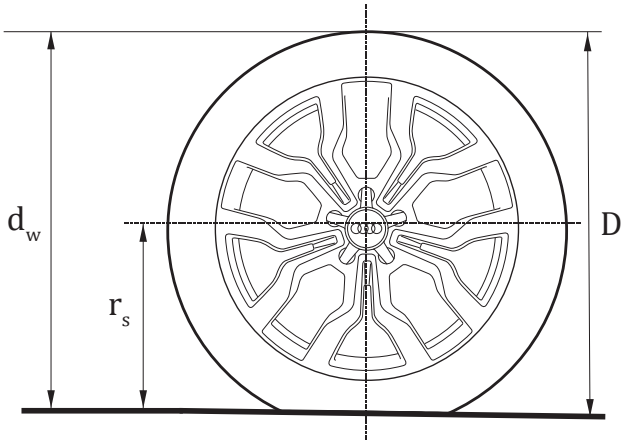

Figure 2.39.: Static tyre diameter

height. By using this measurement arrangement, the CoG's height can be calculated accordingly to (2.136).

The equilibrium of moments about the front axle leads to Equation (2.135):

$$-G \cdot d_f \cdot \cos\beta_{lft} + G \cdot h_1 \cdot \sin\beta_{lft} + N_r \cdot l_{12} \cdot \cos\beta_{lft} = 0 \tag{2.135}$$

where h_1 is the height of the CoG of the body alone, without the tyres, in [m].

$$h_{CoG} = r_s + h_1 = r + \left(d_f - l_{12} \cdot \frac{N_r^*}{N_f^* + N_r^*} \right) \cdot \frac{1}{\tan\beta_{lft}} \tag{2.136}$$

where r_s is the static tyre radius in [m], which can be also estimated by using Equation (2.137).

$$r_s = D - \frac{d_w}{2} \tag{2.137}$$

where d_w is the tyre diameter of the unformed wheel in [m] and D is the diameter of the wheel due to the static deflection in [m], see also Figure 2.39.

According to [Nat00], another method can be applied in order to evaluate the height of the CoG. This method is called tilting method, but will not be covered further within this paper.

The lifting method and the tilting method require special measurement arrangements which are not easy accessible. Moreover, there is always a high risk of damaging parts of the vehicle. For that reason, another approach is used, in order to estimate the height of the CoG. According to [Bur82], the height of the CoG can be approximated by the following formula, see Equation (2.138).

$$\frac{h_{CoG}}{l_{12}} = 0.26 - 0.04 \cdot \frac{m_v}{1000kg} \tag{2.138}$$

Segment [ ]	Manufacturer [ ]	Type [ ]	h_{CoG} [m]
Compact cars	BMW	120d	0.533
SUV	BMW	X5 40d	0.499

Table 2.3.: Comparison of the height of CoG

Rearranging Equation (2.138) leads to a direct expression of the height of the CoG.

$$h_{CoG} = l_{12} \cdot \left(0.26 - 0.04 \cdot \frac{m_v}{1000kg}\right), \tag{2.139}$$

where l_{12} is the wheelbase in [m], h_{CoG} is the height of the center of gravity in [m] and m_v is the total mass of the vehicle in [kg].

Although the approach mentioned in Equation (2.139) is used to estimate the height of the CoG, it has to be pointed out that it is necessary to question its results. For example, by looking at Table 2.3, which shows two different vehicle classes of the same manufacturer. The big SUV BMW X5 40d is much higher than the small BMW 120d. For that reason, it would be odd if the small 120d had a higher position of the CoG than the X5.

This fact results in a different approach, especially when calculating the height of big SUVs, see Figure 2.40. Sometimes, the static tilt angle is given in data sheets. As Figure 2.40 presents, the static tilt angle is reached if the resulting weight G in acting on the CoG go exactly through the wheel contact point. If the tilt angle α_{tlt} becomes bigger than the angle shown, the car will roll over sideways. Table 2.4 gives some examples of cars including tilt angle and the resulting height of CoG. In combination with the track of the specific car the height of CoG can be calculated with Equation (2.140):

$$\tan \alpha_{tlt} = \frac{trc}{2h_{CoG}}, \tag{2.140}$$

where trc is the track of the car in [m]. Rearranging Equation (2.140) leads to the following expression:

$$h_{CoG} = \frac{1}{2} \frac{trc}{\tan \alpha_{tlt}} \tag{2.141}$$

But in order to get to Equation (2.140), some simplifications have to be made. First of all, the suspension of the vehicle and the influence of passengers and payload is neglected. Moreover, the position of the CoG in y-direction is exactly in the middle of the track. Besides, the influence of the tyres is left unconsidered. Due to the facts mentioned above, and the fact that the static tilt angle α_{tlt} is rarely given in data sheets, this method was not used in this work, but for the sake of completeness it should also be mentioned. Table 2.4 shows all SUVs which are mentioned in the parameter list and its height of the CoG, calculated with Equation (2.141).

The tilt angle α_{tlt} was obtained from the NHTSA homepage [NHT11].

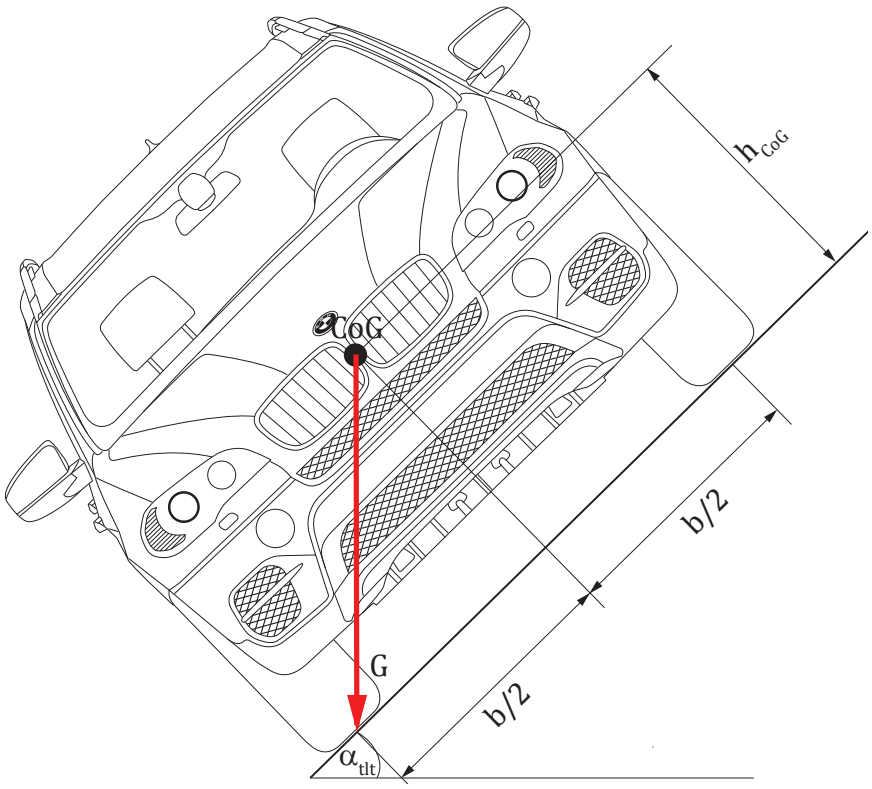

Figure 2.40.: Alternative method to evaluate height of CoG [BMW11]

Manufacturer [ ]	Type [ ]	Tilt angle [deg]	Track [m]	h_{CoG} [m]
Audi	Q5 2.0Tdi	50.3	1.617	0.671
BMW	X1 18d	48.8	1.500	0.657
BMW	X3 20d	48.9	1.616	0.705
BMW	X5 40d	47.7	1.644	0.748
VW	Tiguan 2.0Tdi	50.9	1.569	0.638

Table 2.4.: Height of CoG calculated with the vehicle's specific tilt angle

At the end of this subchapter, a simple estimation is performed, in order to get a notion how big the divergence is when using different approaches to calculate the height of CoG. By sticking to the demand of the Institute of Highway Engineering and Transport Planning that the vehicle should accelerate at maximum with two [m/s^2] and an averaged deceleration of 5.76 [m/s^2], which corresponds to the minimal legal deceleration, according to [Ano01], the failure can be estimated according to Equation (2.143). Since the height of the CoG only influences the tyre normal loads N_{fl}, N_{fr}, N_{rl} and N_{rr} in this vehicle model, Equation (2.142) has to be investigated:

$$_W F_{z,f} = m_v \cdot (g \cdot d_r - a_x \cdot h_{CoG})/(d_f + d_r) + F_{dwn}, \tag{2.142}$$

where $_W F_{z,f}$ is the tyre normal load at the front axle in [N], m_v is the total mass of the vehicle in [kg] and a_x is the acceleration or rather the deceleration of the vehicle in x - direction in $[m/s^2]$. By setting all parameters and values constant except the acceleration and the height of the CoG and by neglecting the downforce F_{dwn} the maximum difference can be obtained by using Equation (2.143):

$$F_{z,f} = c_2 \cdot (g \cdot d_r - a_x \cdot h_{CoG}) \tag{2.143}$$

where c_2 is a constant, a_x is equal to the biggest allowed absolute value of four $[m/s^2]$ and varying height of CoG between 0.499 [m] and 0.748 [m], which equals the values for the BMW X5 40d, the failure e_{rel} is according to Equation (2.144) 15 [%] as far as the tyre vertical forces are concerned.

$$e_{rel,x} = \frac{(g \cdot d_r - a_{x,max} \cdot h_{CoG,max}) - (g \cdot d_r - a_{x,max} \cdot h_{CoG,min})}{g \cdot d_r - a_{x,max} \cdot h_{CoG,max}} \tag{2.144}$$

where g is the gravitational acceleration in [m/s^2], d_r is the distance between rear axle and the position of the CoG in x-direction in [m]. The same procedure has to be carried out with the lateral acceleration. Since the lateral acceleration is limited to six [m/s^2] by the present driver model, the error may be calculated by:

$$e_{rel,y} = \frac{(-0.6 \cdot m_v \cdot a_{y,max} \cdot trc_f) \cdot (h_{CoG,max} - h_{CoG,min})}{0.5 \cdot F_{z,f} - 0.6 \cdot m_v \cdot a_{y,max} \cdot h_{CoG,max} \cdot trc_f},$$

where $e_{rel,y}$ is the relative error in lateral direction in [%] and $a_{y,max}$ is the maximum lateral acceleration in [m/s^2].

The resulting relative error due to a variation in the height of CoG is about twenty-nine [%], as far as the lateral acceleration is concerned. According to this error estimation, it can be said that the failure in comparisons to the simplifications done with the tyre model are adequate, but if a more sophisticated model is used, more accurate considerations with respect to the position of the CoG have to be made.

2.6.3. Determination of Yaw Inertia

Firstly, the mass inertia shall be explained in general. Then follows a discussion of the yaw axis, with a special emphasis on a method which can be used to obtain this important parameter.

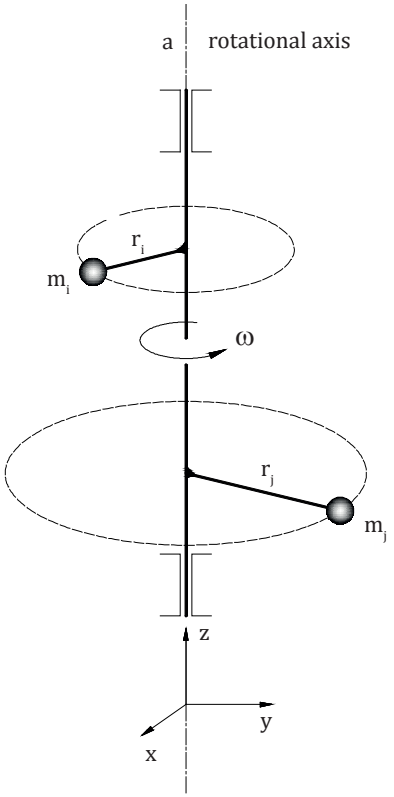

Figure 2.41.: Explanation of the mass inertia [SGHW08c]

The mass inertia is defined as the resistance to rotational movement of vehicle in classical mechanics. In general, it depends on the distribution of the mass and the location of the rotational axis. According to [SGHW08a], the mass inertia is defined as follows:

$$I_a = \sum_i m_i r_i^2, \tag{2.145}$$

where I_a is the mass inertia about the rotational axis a in [kgm^2], m_i is the mass fraction in [kg] and r_i is the vertical distance of the mass fraction m_i to its rotational axis in [m]. The correlation in Equation (2.145) is displayed in Figure 2.41.

The yaw inertia is another essential parameter for the used vehicle model. But there exists the same problem as in Section 2.6.2.2, the value is not given in any data sheets and the manufacturer refuse to tell. For that reason, a suitable estimation formula has to be found in order to obtain this essential parameter. Other vehicle simulation programmes, like PC Crash, are using the following formula, stated in Equation (2.146):

$$I_{zz} = 0.1269 \cdot m_v \cdot l_{12} \cdot L, \tag{2.146}$$

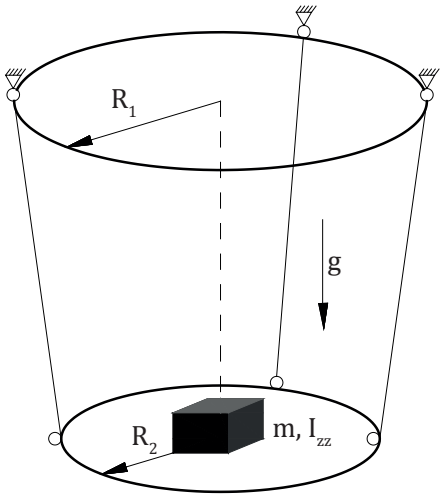

Figure 2.42.: Mass inertia determination - Natural force element (gravitation) [WG07]

where I_{zz} is the yaw inertia in [kgm^2], m_v is the total mass of the vehicle in [kg], l_{12} is the wheelbase in [m] and L is the total length of the vehicle in [m]. The formula stated in Equation (2.146), is mentioned in [Bur82] and valid for vehicles up to 1500 [kg] in total, which is nowadays the kerb weight of a compact car. Nonetheless, it is still used in simulation programmes like PC Crash, since there are no data available and the measurement of it is very time-consuming. This formula has to be verified if the values are comparable, especially in the SUV segment. According to [MCI97], otherwise Equation (2.146) is well rated in comparison to other methods, although only American cars were considered in that study.
If accurate data is needed, there exist a few measurement arrangements to determine the mass inertia of the vehicle about all three vehicle coordinate axis. According to [WG07] the following main measurement arrangement may be distinguished:

1. **Acceleration due to a natural force element (gravitation)**
   This measurement arrangement, developed by Kamm [WG07], was originally able to determine the yaw inertia only. The yaw inertia was measured with the help of a bifilar pendulum. The evaluation of the yaw inertia is carried out by measuring the harmonic period T. By using Equation (2.147), the yaw inertia can be calculated (without derivation):

$$I_{zz} = m\frac{gR_1R_2}{4\pi^2}T^2, \tag{2.147}$$

   where m is the mass of the object in [kg], g is the gravitation in [m/s^2], R_1 and R_2 are the radius of the rotation in [m] and T is the harmonic period in [s]. The measurement principle can be seen in Figure 2.42.

   Prerequisites are the geometry of the arrangement, and the mass of the measured

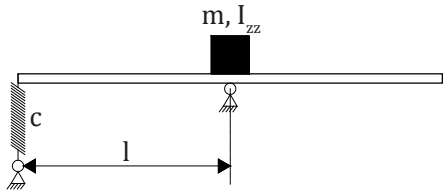

Figure 2.43.: Mass inertia determination - Passive force element [WG07]

object. A more modern measurement arrangement which can determine all mass inertias is situated at the Technical University in Milan, Italy. The measurement arrangement consists of a cubical-shaped frame, which is mounted with three or four wires. With the help of inclination sensors, acceleration sensors and angular velocity sensors, all ten mass inertia parameters, the mass, the position of the CoG, and the six mass inertias can be evaluated.

2. **Acceleration due to a passive force element**
   A typical example of this approach is situated at the Cranfield University in Great Britain. The measurement arrangement consists of a spheric air bearing, a frame mounted on it, and a hydraulic elevator. The center of the air bearing forms together with an additional bearing the rotational axis. The mass inertia is determined by measuring the period of oscillation for little deflections. Some springs mounted on the frame create momentums which act against this deflection. The mass inertia can be calculated with Equation (2.148):

$$I_{zz} = \frac{c \cdot l^2 \cdot T^2}{4\pi^2}, \tag{2.148}$$

   where I_{zz} is the mass inertia about the z-axis in [kgm^2], c is the stiffness of the spring in [N/m], l is the distance between the rotational point and the point where the spring is mounted on the frame in [m] and T is the period of oscillation in [s]. Figure 2.43 shows the principal measurement arrangement.

3. **Acceleration due to an active force element**
   This group is based on the direct measurement of the acting forces on the measured object. As it is displayed in Figure 2.44, the measurement arrangement consists of a defined movement mechanism and force sensors. One test bench is located at the company AB-Dynamics, Great Britain [WG07]. This approach is able to measure all ten mass inertia parameters like the mass, the position of the CoG and the six mass inertias. The mass inertia can be derived by Equation (2.149):

$$I_{zz} = \frac{Fl}{\ddot{\varphi}}, \tag{2.149}$$

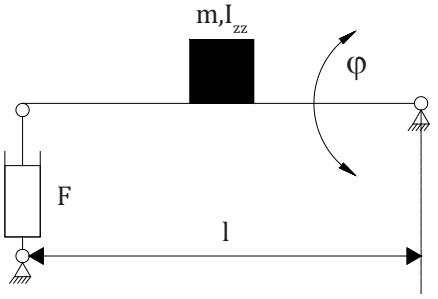

Figure 2.44.: Mass inertia determination - Active force element [WG07]

where I_{zz} is the mass inertia about the z-axis in [kgm^2], F is the force applied by a force element in [N] and $\ddot{\varphi} = \dot{\omega}$ is the angular acceleration about the rotational axis a in [rad/s^2].

To sum it up, the determination of the needed parameters is essential for every vehicle model. The more precise the parameters can be obtained, the more accurate the simulation output is likely to be. However, one has to consider the required effort to receive precise parameters. Due to the simplified tyre model it is not success-oriented to determine some parameters more precisely.

2.7. Sensitivity Analysis

As explained before, the parameters are essential to run the simulation properly. A few estimations have to be made, as not all required values are given in the data sheets. This fact leads to a certain amount of uncertainty. This chapter deals with the influence of all parameters and its size of variance. For that reason a specific test course is used which is, as Figure, 2.45 shows, a simple cornering maneuver.

Data received by data sheets is considered as accurate and thus not analyzed. For that reason, only parameters, which are not described in data sheets or which have to be measured, are investigated. That means that the position of the CoG in vertical and horizontal direction, the total vehicle weight, the yaw inertia, and the aerodynamic coefficient is analyzed a bit further.

First of all, the total vehicle weight has to be discussed, since it has a strong influence on the vehicle dynamics. As mentioned in Section 2.6.2, the vehicle weight is measured with four weighting machines, one on each tyre. Thus, it is possible to determine the total weight of the vehicle. According to the manufacturer of the weighting machines, the precision is $\pm$ 5 [kg] for less than 500 [kg] on each machine [Mes11]. Therefore, the result can vary by 20 [kg] in total. For the sensitivity analysis, this allowed inaccuracy is the lowest value, the highest value is calculated by the inaccuracy of the weighting machines plus an average passenger of 80 [kg], in other words plus 100 [kg], for one specific vehicle. Since the differences between the corresponding state variables are little

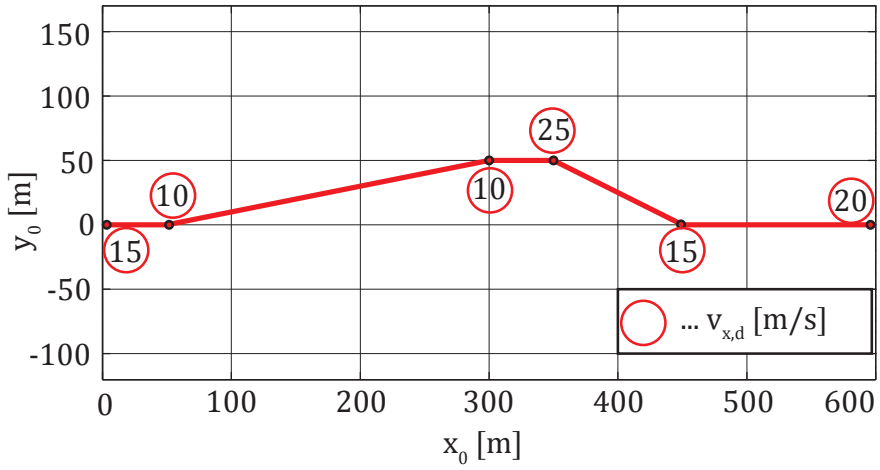

Figure 2.45.: Test course for the sensitivity analysis

relative to the figure resolution, the characteristic values for the lower and highest value are only pointed out in Table 2.5. Because the focus is on the exact description of a desired path only the deviation in x and y position are analyzed. Whereas the deviation is calculated at the same time step. The position error in x and y direction is calculated according to the following equations:

$$|e_{x,max}| = |x_{i,d}(t) - x_{i,v}(t)| \tag{2.150}$$

$$\bar{e}_x = \sum_i (x_{i,d}(t) - x_{i,v}(t)) \tag{2.151}$$

$$|e_{y,max}| = |y_{i,d}(t) - y_{i,v}(t)| \tag{2.152}$$

$$\bar{e}_y = \sum_i (y_{i,d}(t) - y_{i,v}(t) \tag{2.153}$$

where $|e_{x,y,max}|$ is the maximum absolute error due to the x and y deviation in [m], $\bar{e}_{x,y}$ is the mean value of the x and y deviation in [m], $x_{i,d}$ and $y_{i,d}$ is x and y position of the desired path in [m], $x_{i,v}$ and $y_{i,v}$ describe the actual position of the vehicle also in [m].

vehicle mass [kg]	$\lvert e_{x,max}\rvert$ [m]	$\bar{e}_x$ [m]	$\lvert e_{y,max}\rvert$ [m]	$\bar{e}_y$ [m]
m_v -20 kg	0.2605	0.1007	0.0725	-0.012
m_v (reference)	0	0	0	0
m_v +100 kg	0.1096	-0.0341	0.0214	0.0016

Table 2.5.: Sensitivity analysis - Position deviation when varying the vehicle mass

In Table 2.5 it can be seen that the varying mass influences the longitudinal position - but the difference is very little. The difference is even smaller if one considers the lateral

movement as well.

Next, the position of the CoG should be discussed briefly. According to [SGHW08c], the CoG of a system is moving as the total mass is combined in it and all external forces are acting on this point. This statement allows to assume that a variation of the position of the CoG may have a strong impact on the vehicle's behavior. This will be also proven in the following with the help of one specific vehicle, where a variation of ± 10 kg on each axle is assumed. This value is according to the uncertainty given by the producer of the weighting machines, as stated by [SGHW08c].
According to Table 2.6, a variation of the axle load by 10 [kg], in other words a variation of the longitudinal position of the CoG, with constant total vehicle weight results in the following position deviation:

front axle mass [kg]	$\lvert e_{x,max} \rvert$ [m]	$\bar{e}_x$ [m]	$\lvert e_{y,max} \rvert$ [m]	$\bar{e}_y$ [m]
$m_{f,axle}$ -10 kg	0.2743	0.1117	0.1030	-0.0155
$m_{f,axle}$ (reference)	0	0	0	0
$m_{f,axle}$ +10 kg	0.2314	0.0777	0.0657	-0.0086

Table 2.6.: Sensitivity analysis - Position deviation when varying the x position of the CoG

The position gap when changing the axle load is marginal, as it can be seen in Table 2.6 in both aspects the longitudinal and lateral movement.

Next the influence of the height of the CoG is investigated in detail. For that purpose the height of CoG is varied between 0.4 [m] and 0.8 [m] and compared with the value calculated with the estimation formula used in Section 2.6.2.2.

h_{CoG} [m]	$\lvert e_{x,max} \rvert$ [m]	$\bar{e}_x$ [m]	$\lvert e_{y,max} \rvert$ [m]	$\bar{e}_y$ [m]
$h_{CoG} = 0.4$	0.2524	0.0894	0.0658	-0.0094
$h_{CoG} = 0.65$ (reference)	0	0	0	0
$h_{CoG} = 0.8$	0.2747	0.1006	0.075	-0.013

Table 2.7.: Sensitivity analysis - Position deviation when varying the height of the CoG

The difference caused by changing the height of CoG remains little. This fact is also supported by Equation (2.144).

The calculation of the aerodynamic drag is also afflicted with uncertainty, since the aerodynamic coefficient is not given in every specific data sheets. In reference to [MW04a], an average car has an aerodynamic coefficient of about 0.3 and below. In order to investigate the impact on different c_x-values, the value should vary between 0.26 and 0.8 for a specific car. The lower threshold may be a flow optimized passenger car, and the upper threshold can be a normal truck. In Table 2.8 it can be seen that the variation of

c_x [-]	$\lvert e_{x,max} \rvert$ [m]	$\bar{e}_x$ [m]	$\lvert e_{y,max} \rvert$ [m]	$\bar{e}_y$ [m]
$c_x = 0.26$	0.1450	0.0263	0.0278	-0.0063
$c_x = 0.3$ (reference)	0	0	0	0
$c_x = 0.8$	0.3784	0.1533	0.1062	-0.0146

Table 2.8.: Sensitivity analysis - Position deviation when varying the aerodynamic drag

the aerodynamic drag only influences the longitudinal movement. The higher the aerodynamic drag is, the bigger the driving resistance gets and the less acceleration capacity is available. This results in a lower speed at a certain time step which also explains the bigger longitudinal deviation with higher c_x-values.
Last but not least, the yaw inertia should be discussed. Due to the time-consuming and complex measurement arrangement, an estimation formula was used in order to determine its value. In order to gain a notion of the influence of the yaw inertia on the position of the vehicle, the measured inertia about the z-axis is compared with the estimation formula used in this work for a specific vehicle. According to the estimation formula in Equation (2.146), the yaw inertia is about 2564 [kgm^2], the measured data is 3006 [kgm^2], according to a test report [HHE10]. This means a deviation of about 15%. Consequently, for the sensitivity analysis a range of $\pm$ 15% of the measured value is used according to Table 2.9

yaw inertia I_{zz} [kgm^2]	$\lvert e_{x,max} \rvert$ [m]	$\bar{e}_x$ [m]	$\lvert e_{y,max} \rvert$ [m]	$\bar{e}_y$ [m]
$I_{zz} = 3006$ - 15%	0.2044	0.0795	0.0542	-0.0077
$I_{zz} = 3006$ (reference)	0	0	0	0
$I_{zz} = 3006$ + 15%	0.2355	0.0756	0.0571	-0.0094

Table 2.9.: Sensitivity analysis - Position deviation when varying the yaw inertia

Table 2.9 shows that the deviation caused by a change in the yaw inertia is marginal. In general, it can be pointed out that a change of the numerated parameters within certain limits does not effect the position of the vehicle dramatically. Consequently, the vehicle model with its parameter should be accurate enough to fulfill its purpose in a urban traffic flow simulation.

3. Evaluation and Discussion

This section deals with the applied vehicle and driver model in detail. First, the behavior of the model should be tested with really simple driving maneuvers, such as braking and accelerating without steering, afterwards the explained testing methods are a bit more complex. Next, the accuracy of the path following is analyzed. Finally, some driving maneuvers are compared with another, more advanced simulation programm called "MOVES^2", in [RNFD11].

3.1. Basic Evaluation of the Vehicle Model and the Driver Model

In order to test the applied vehicle and driver model, the following simple testing routines are applied. It has to be mentioned that all test routines are done with the same vehicle parameters, thus transparency may be ensured.

- Simple Acceleration on a straight line
- Simple Deceleration on a straight line
- Driving with constant speed in an arbitrarily direction

3.1.1. Acceleration and Braking Maneuvers

This testing method demonstrates the capability of the vehicle model and the driver model to adapt to a change in speed. It proves that the driver model is always able to follow a certain speed profile and shows the limits of the vehicle model.

Figure 3.1 shows an example of this simple acceleration testing. The dashed red line in the velocity-over-time-diagram displays the desired velocity profile, the solid blue line shows the simulation results of the specific vehicle. The gradient of the desired speed is too high for the specific vehicle after five [s], since its real acceleration capability is limited to 2.7 [m/s^2] at maximum. Consequently, the vehicle needs the span of time Δt more to reach the desired speed. This phenomenon is explained with (2.26). The tested car is an Opel Combo with a relative high vehicle mass and an engine with a very limited performance. This results in the limited acceleration capability shown in Figure 3.1.
The same testing procedure is carried out for a braking maneuver. Here, it also shows that the braking capability or, in other words, the maximum deceleration of the vehicle also depends on the specific vehicle mass and the used brake system as explained in Section 2.5.1.2. But it can be said that the braking capability is always higher than the acceleration capability, due to the simplifications done for the brake system.

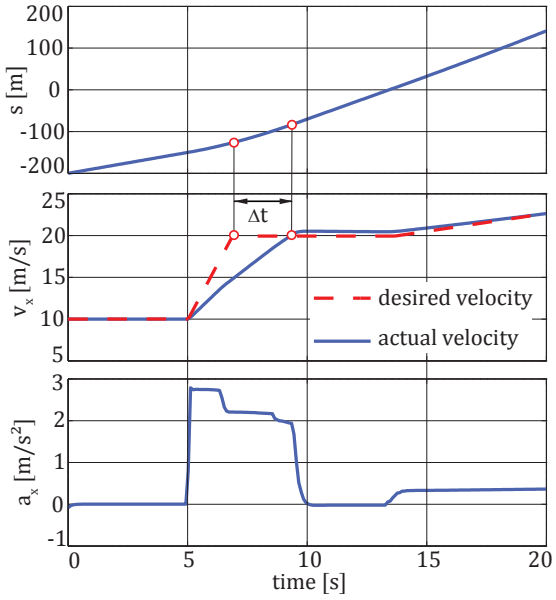

Figure 3.1.: Simple acceleration testing

3.1.2. Driving with constant speed in different directions

This testing method sounds quite straightforward, but the implementation shows that it is rather complex. The driver model needs specific information, shown in Section 2.5.2.1, in order to follow a certain path. For that reason, trigonometric functions have to be used. This testing approach should show if these functions are implemented correctly, and thus that the driver model works properly. The testing pointed out that especially the needed range of the arctan-function has to be defined properly, since this function is originally only defined in the range of $\pm\pi/2$ without an ensuing further examination. In order to avoid problems in the Matlab code, the atan2-function is used. This functions calculates the angle by looking at both the absolute values and the algebraic signs of the x and y coordinates. Consequently, a correct description of a plane path can be ensured. Figure 3.2 shows the tested paths. Both positive and negative directions parallel to the coordinate axis are successfully tested.

3.2. Path following ability of the Driver Model

The aim of this chapter is to evaluate how precise the driver and vehicle model can follow a given trajectory. For that reason, a suitable evaluation criterion has to be found. The deviation error per equidistant time step, but also the deviation error per traveled distance are possible evaluation criteria. In Figure 3.3, the red dashed line shows the desired path in the global coordinate system and the solid blue one displays

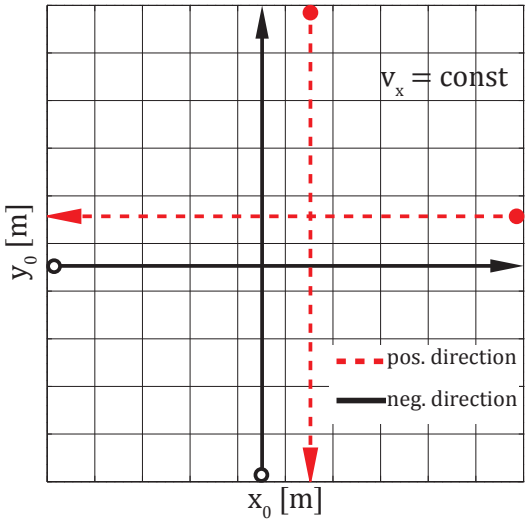

Figure 3.2.: Driving with constant speed in different directions

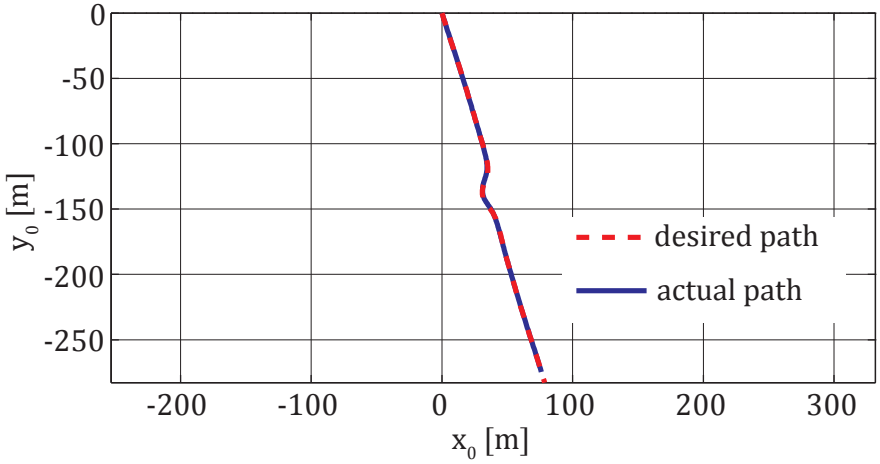

Figure 3.3.: Comparison of a given trajectory and the one chosen by the driver model

the path chosen by the driver model. The given trajectory is determined in real traffic measurements, with a high accuracy GPS and shows a path along a roundabout. By only looking at the figure, the path deviation error seems minimal, but in order to deliver some qualitative facts, both data sets are compared in detail. First, the deviation error in x direction in global coordinates is analyzed, which is defined according to (3.1):

$$x_e = x_d - x_{drv}, \tag{3.1}$$

where x_d is the global position of the path in x-direction in [m] and x_{drv} is the x coordinate of the path chosen by the driver model also in [m]. The analysis delivers the following facts:

$$\begin{aligned} x_{e,max} &= 1.5622[\text{m}] \\ x_{e,min} &= -0.18[\text{m}] \\ x_{e,mean} &= 0.6225[\text{m}] \end{aligned}$$

The error in the global y-direction is similarly defined to Equation (3.1):

$$y_e = y_d - y_{drv}, \tag{3.2}$$

where y_d is the global position of the path in y-direction in [m] and y_{drv} is the y-coordinate of the path chosen by the driver model also in [m].

$$\begin{aligned} y_{e,max} &= -5.021[\text{m}] \\ y_{e,min} &= 0.0048[\text{m}] \\ y_{e,mean} &= -2.1553[\text{m}] \end{aligned}$$

The pythagorean mean error is defined by Equation (3.3):

$$e_{pyt} = \sqrt[2]{x_e^2 + y_e^2} \tag{3.3}$$

Inserting the corresponding data sets, the pythagorean error can be calculated to:

$$\begin{aligned} e_{pyt,max} &= 5.2584[\text{m}] \\ e_{pyt,min} &= 0[\text{m}] \\ e_{pyt,mean} &= 2.2564[\text{m}] \end{aligned}$$

This approach is one way to evaluate the position error, but with this method, it is not possible to distinguish, if the error arises due to inaccuracy of the longitudinal or lateral driver model. Consequently, another approach is applied as well. It distinguishes between longitudinal and lateral errors by transforming every data set into the vehicle-fixed coordinate system and solve it with fixed time steps according to Figure 3.4: In order to get the right position of the path relative to the vehicle, both a transversal and a rotational transformation have to be combined. With the help of Equations (3.4) to (3.5), the transformation is carried out and consequently, it is easy to distinguish between longitudinal and lateral control error.

$$_0\begin{bmatrix} x \\ y \end{bmatrix} = \mathbf{r}_e - \mathbf{r}_b, \tag{3.4}$$

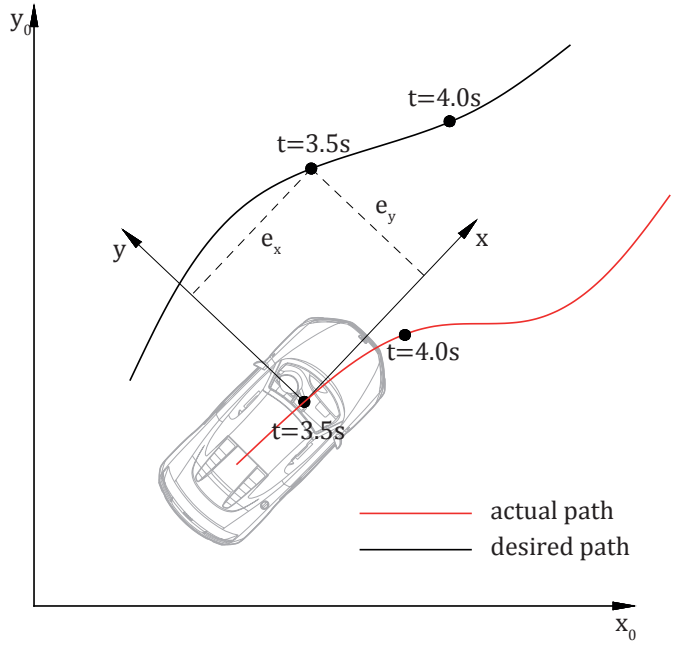

Figure 3.4.: Path following ability - Fixed time step

test scenario	$\lvert e_{x,max}\rvert$ [m]	$\bar{e}_x$ [m]	$\lvert e_{y,max}\rvert$ [m]	$\bar{e}_y$ [m]
Roundabout 180	6.8014	2.8395	0.7815	0.0508
Roundabout 270	2.9137	1.3083	0.6464	-0.13

Table 3.1.: Path following ability - Absolute errors

test scenario	$e_{x,rel,max}$ [%]	$e_{x,rel,min}$ [%]	$e_{y,rel,max}$ [%]	$e_{y,rel,min}$ [%]
Roundabout 180	0.92	1.46E-5	1.91	-1.66
Roundabout 270	0.65	-2.076E-3	0.6	-1.34

Table 3.2.: Path following ability - relative errors

$$\begin{bmatrix} x \\ y \end{bmatrix}_V = {}^0_V\mathbf{T} \cdot \begin{bmatrix} x \\ y \end{bmatrix}_0, \tag{3.5}$$

where $\mathbf{r}_b$ and $\mathbf{r}_e$ are the global position vectors in[m], the indices e and b stands for end or begin respectively, ${}^0_V\mathbf{T}$ is the transformation matrix in order to transform data from the global reference system into the vehicle-fixed coordinate system.

The deviation error of the course in Figure 3.3 is shown in Table 3.1 and 3.2. Additionally, the errors for a 270 degree roundabout are also analyzed according to Figure 3.5.

where $e_{x,y,max,min}$ is the maximum or minimum error in [m] and $\bar{e}_{x,y}$ is the mean

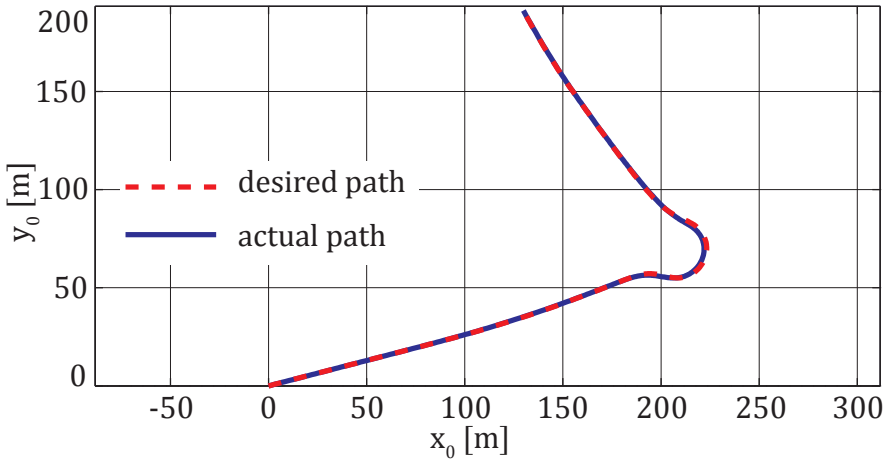

Figure 3.5.: Path following ability - 270 degree roundabout maneuver

deviation error also in [m]. $e_{x,y,rel,max,min}$ is the maximum or minimum relative position error in [%]. The relative errors are defined as follows:

$$e_{x,rel,max} = \frac{e_{x,max}}{\sum |x_{trv}|}, \tag{3.6}$$

$$e_{x,rel,min} = \frac{e_{x,min}}{\sum |x_{trv}|}, \tag{3.7}$$

where $e_{x,max,min}$ is the maximum or minimum deviation error in [m] and x_{trv} is the traveled way in x-direction also in [m]. The same formula is used in order to get the lateral errors, only the y-values have to be used instead of the x-values.

3.3. Needed Path Description Accuracy

As described in Section 2.5.2.1, the used driver model needs data points in order to follow a certain path. The more datapoints are available, the more accurate the path following of the driver is. More datapoints automatically imply that the simulation has to deal with more information, which results in a longer simulation time. Two examples are analyzed in this section in order to find out how many datapoints are needed to optimize the simulation time while guaranteeing high path following accuracy: a 180° and a 270° roundabout maneuver.

3.3.1. 270 degree Roundabout Maneuver

The first driving maneuver is shown in Figure 3.6. It is a 270 degree roundabout maneuver, where the speed is changing in every time step. The dashed red line shows the desired path, which was evaluated in real traffic. The solid blue line shows the actual

test scenario	$\lvert e_{x,max} \rvert$ [m]	$\bar{e}_x$ [m]	$\lvert e_{y,max} \rvert$ [m]	$\bar{e}_y$ [m]
Roundabout 270	38.5328	14.3334	7.6462	0.8156

Table 3.3.: Needed path description - Absolute error values of a 270 roundabout maneuver

test scenario	$e_{x,rel,max}$ [%]	$e_{x,rel,min}$ [%]	$e_{y,rel,max}$ [%]	$e_{y,rel,min}$ [%]
Roundabout 270	0.78	-1.7383E-4	1.21	-1.27

Table 3.4.: Needed path description - Relative error values of a 270 roundabout maneuver

path chosen by the driver model due to its settings. Finally, the dashed green line shows the discrete number of datapoints used to optimize the simulation time. In this example, it is possible to reduce the number of datapoints from 344 to only 15 points. This means a reduction of about 95.6%, which consequently speeds up the simulation procedure. As it can be seen, the dashed green line creates some kind of envelope for the chosen path. The first test has shown that especially in a curve, the data points should not be exactly on position of the desired path, but a bit outside of the curve. Moreover, the simulation has proven that especially at the beginning of a curve, the need of data tends to be higher, in order to guarantee a precise path following. This can be explained according to (2.99). The used driver model needs the curvature as an input. Since the curvature of the simplified road is calculated out of three adjoint datapoints, it is important to increase the number of points in relevant regions, such as the beginning of a curve or a heavy change in the desired heading angle. This circumstance is considered in the path optimization done in Figure 3.6. The optimization is completed with a displacement of about two meters of datapoints to the outer area of the curve. It has to be said that the optimization is carried out manually and not with an algorithm, so the optimized path description does not automatically mean that it is the absolute optimum - it is simply more precise than the other ones.
The error analysis compared with the measured data set can be seen in Table 3.3 and 3.4:

The relative high deviation errors are noticeable, but result from the comparison of equal time steps. This means that the datapoints are always compared at the same time step of both the actual path and the desired path. This may result in a higher deviation, if the driver model is not able to keep the desired speed. Since the vehicle is slower, it covers a shorter distance and consequently, the longitudinal and lateral deviation can be higher. In the shown example above the reason is the reduction of datapoints. The driver model is missing information, since only such datapoints have the information of the desired path position and the desired speed and between such datapoints, the required values are linearly interpolated. As Figure 3.9 shows, the actual speed profile is lower than the measured one over a long simulation time. Consequently, the longitudinal and the lateral deviation increase. This problem can be avoided by adding some additional information points in order to fit the speed profile to the original one.

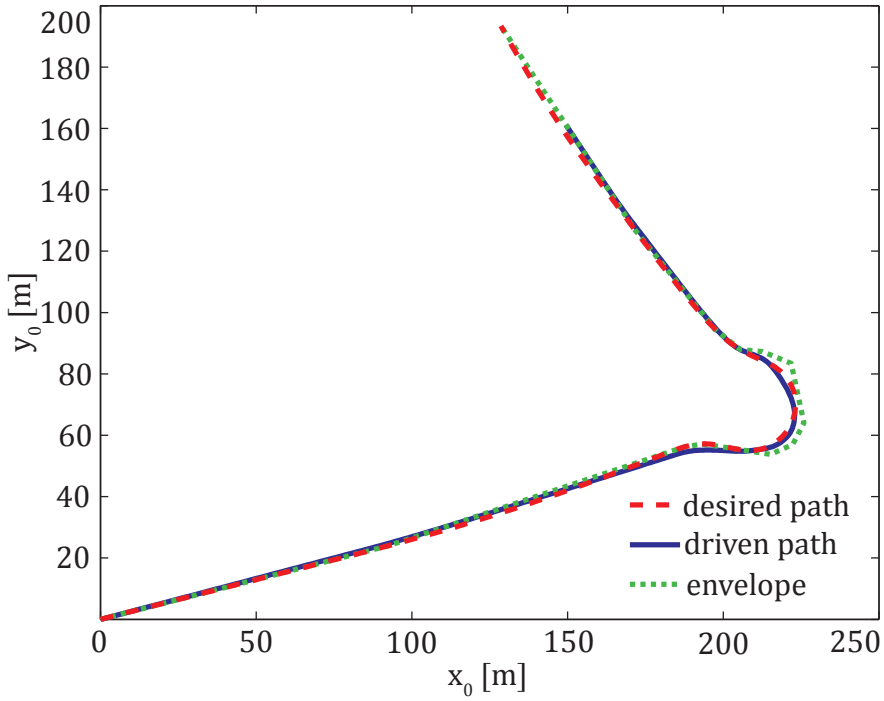

Figure 3.6.: Needed path description accuracy - 270 degree roundabout maneuver

3.3.2. 180 degree Roundabout Maneuver

The second driving maneuver is also a roundabout, but now only with an angle of 180 degrees. All facts discussed above are also valid for this example. That means that in order to optimize the path following ability, an envelope is needed and of course, the more datapoints are available, the more precise the driver model works. The maneuver shown in Figure 3.8 illustrates the desired path with the dashed red line, the solid blue line is the actual path and the dashed green one is the so-called envelope. The number of datasets used can be reduced by about 95% from 260 to 13 datapoints. Additionally, the error values can be seen in Table 3.5 and 3.6. It holds again that the longitudinal and lateral deviations are compared relatively large. This can be explained as for the 270 degree roundabout maneuver above. In Figure 3.9, the deviation of the speed profile to the desired speed is shown, which is the main factor why the deviation in longitudinal and lateral vehicle direction is relatively high.

To sum up, it can be pointed out that the driver model may follow a path better, if a so-called envelope is designed with a deviation to the desired path of about two [m]. This may increase the path following ability, but in order to improve the speed following ability additional datapoints are needed, if there is a sudden speed change, since the operating mode of the driver model only allows linear interpolation between two adjoint

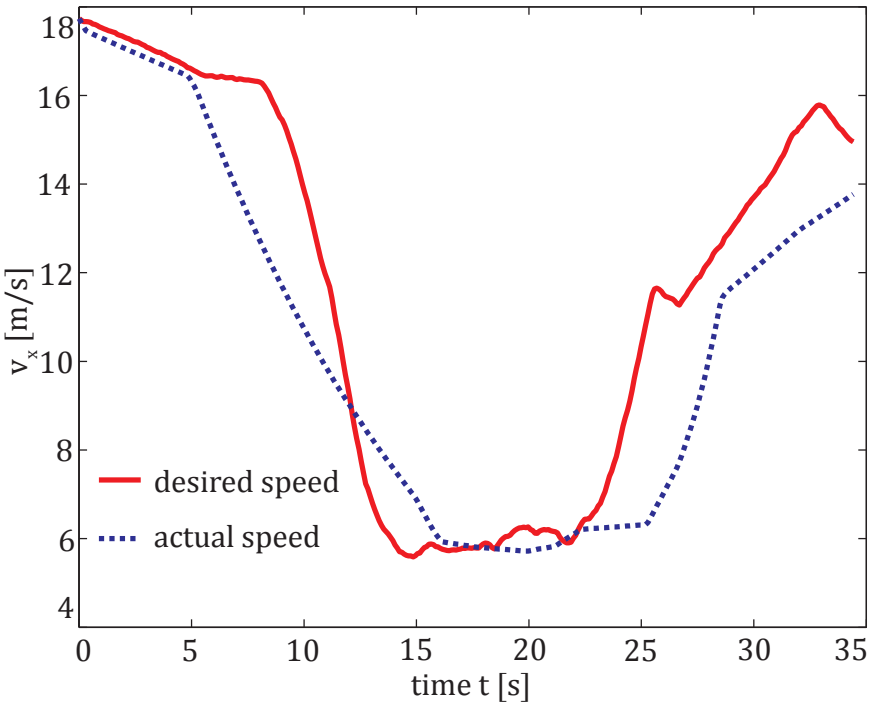

Figure 3.7.: Needed path description accuracy - Comparison speed profile

test scenario	$\lvert e_{x,max} \rvert$ [m]	$\bar{e}_x$ [m]	$\lvert e_{y,max} \rvert$ [m]	$\bar{e}_y$ [m]
Roundabout 180	33.9491	12.7812	4.3304	0.0306

Table 3.5.: Needed path description - Absolute error values of a 180 roundabout maneuver

test scenario	$e_{x,rel,max}$ [%]	$e_{x,rel,min}$ [%]	$e_{y,rel,max}$ [%]	$e_{y,rel,min}$ [%]
Roundabout 180	1.02	-1.8411E-3	2.25	-1.55

Table 3.6.: Needed path description - Relative error values of a 180 roundabout maneuver

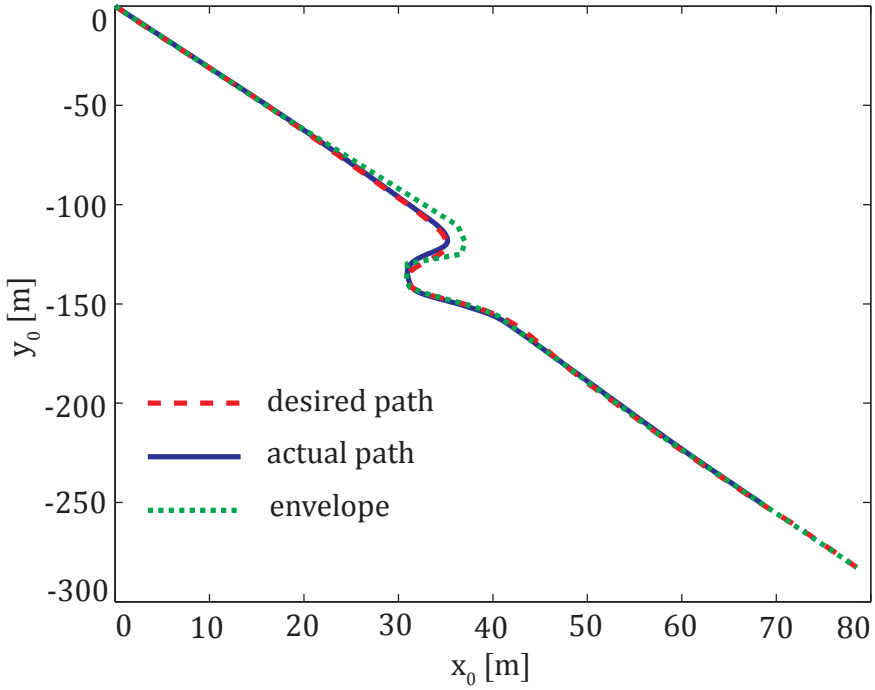

Figure 3.8.: Needed path description accuracy - 180 degree roundabout maneuver

points. But by increasing the number of datapoints, it always has to be considered that the simulation time is extended. Thus, a compromise between the path and speed following accuracy and the real-time capability has to be found. According to [CS09], the distance between the datapoints should almost be equal.

3.4. Vehicle Dynamics - Evaluation and Comparison

The following section deals with the evaluation of the vehicle model and how accurate the non-linear single track model is compared to a more advanced simulation model called "$MOVES^2$". For that reason, some driving maneuvers are chosen to compare the main vehicle dynamics state variables. In order to avoid deviations due to different driver models, the evaluation is done with open-loop maneuvers, where the drive control input is predefined.
The following driving maneuvers are discussed in detail:

- Steering ramp according to DIN ISO 7401
- Steady-state cornering with increasing velocity according to DIN ISO 4138
- Transient Driving maneuver with varying steering angle and varying velocity

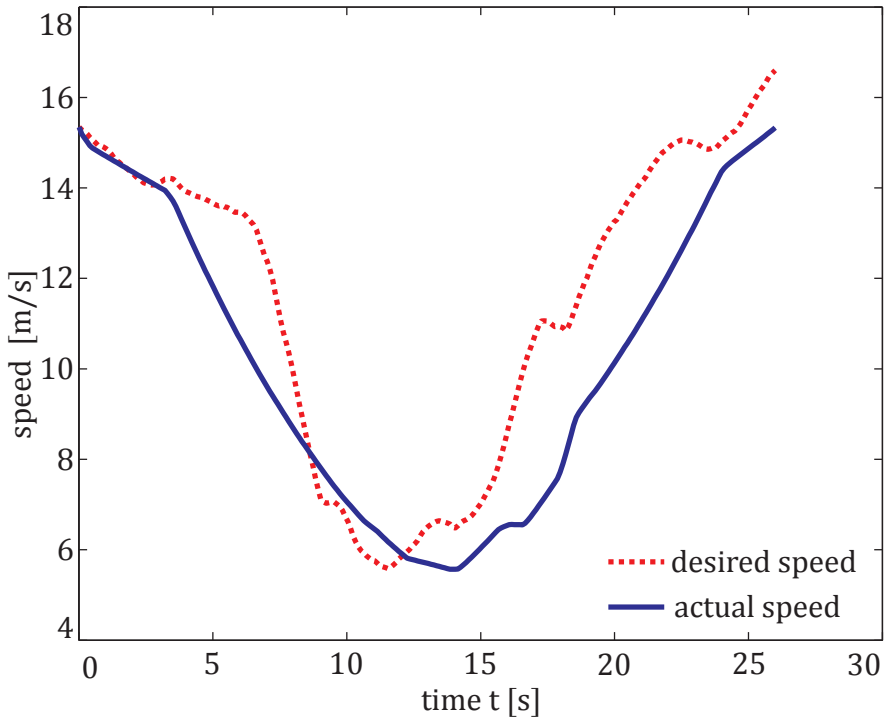

Figure 3.9.: Needed path description accuracy - Comparison speed profile

3.4.1. Sudden steering angle change DIN ISO 7401

This evaluation procedure is carried out with a longitudinal velocity of 20 [m/s] and a step steer input from zero to three degrees at the front wheel. The main state variables, such as the yaw rate $\dot{\psi}$, the lateral acceleration a_y, the sideslip angle β and the position x_0 and y_0, are then compared with those of a more complex vehicle simulation model. The following figures show the mentioned variables in comparison and are afterwards discussed in detail. The steering angle time histories can be seen in Figure 3.10. The steering profile in Figure 3.10 includes a region of transition of 0.3 [s], where the steering angle increases to its maximum value. In general, it can be said that the trend of all vehicle state variables corresponds quite well to the data calculated with "$MOVES^2$". In order to compare the data, a relative error for all vehicle dynamical state variables is calculated for the steady state, which is defined as follows:

$$e_{rel,var} = \frac{var_{NLV} - var_{ref}}{var_{ref}}, \tag{3.8}$$

where $e_{rel,var}$ is the relative error for a specific state variable in [%], var_{NLV} is a variable calculated with the present non-linear single track model and var_{ref} is the same variable calculated with "$MOVES^2$" for the same time step.

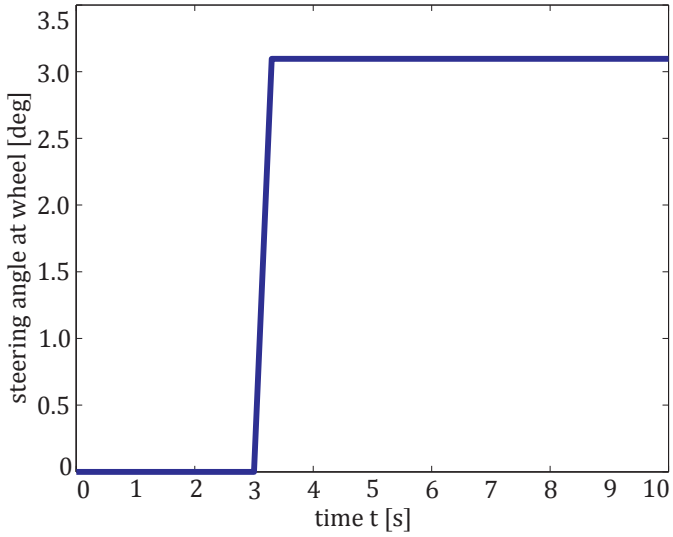

Figure 3.10.: Steering ramp - Steering angle over time

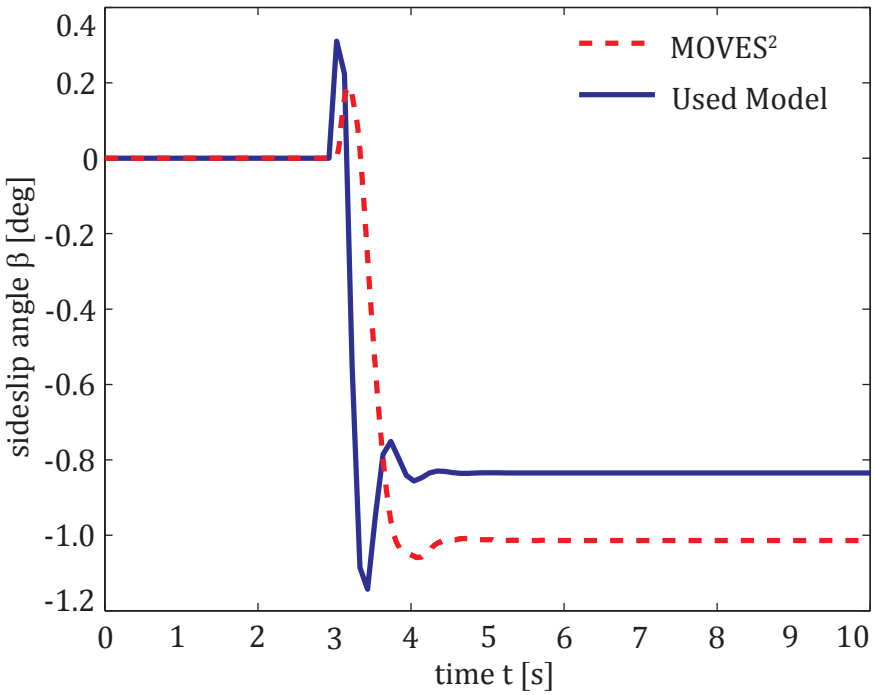

Figure 3.11.: Steering ramp - Sideslip angle over time

Figure 3.11 shows the sideslip angle time history. The solid blue line shows the trend of the sideslip angle calculated with the non-linear single track model. Compared with the dashed red line, which is evaluated with "$MOVES^2$", the trend corresponds with the used model, although the amplitude differs strongly at some time steps . The relative error in the steady state can be calculated according to Equation (3.9):

$$e_{rel,\beta} = \frac{\beta_{NLV} - \beta_{ref}}{\beta_{ref}} \cdot 100\% = -17,69\%. \tag{3.9}$$

This means that the output of the used model in the steady state is about 17.69% lower than the more complex model as far as the sideslip angle is concerned.
Moreover, the shape of the state variable at the beginning of the steering ramp is very interesting. At the first few milliseconds, the sideslip angle increases to its maximum positive value, and afterwards, the negative steady state value of the variable is set. It is necessary to go into greater detail in order to explain this phenomenon coherently. According to [Mat07] the frontal lateral tyre force F_{yf} increases nearly proportional with the steering angle δ. After 0.3 [s], the steering angle reaches its maximum value and consequently, the frontal slip angle α_f does not increase anymore. The fast development of the frontal lateral tyre force results in an abrupt rise of the yaw rate ω_z. In contrast, the slip angle at the rear wheel builds up a bit later, and with its development, the yaw rate decreases to its final steady state value. The delay of the development of the rear slip angle is the reason for the trend of the sideslip angle characteristics at the first few milliseconds. Another explanation may also be given by regarding the first few milliseconds of the steering change as an impulse. The immediate development of the frontal lateral tyre force can be seen as an impulse, whereas the whole vehicle starts to rotate about the center of percussion T_s. Consequently, at the first moment the rear wheel is not affected by the impulse. Afterwards, the instantaneous center of rotation moves forward. Depending on the longitudinal position of the CoG, the effect can be amplified or damped. For a front-heavy vehicle, the center of percussion is at the beginning behind the rear axle on the vehicle longitudinal axis and consequently, the trend of the state variable at the beginning of the maneuver is amplified, according to [Mat07].
Next, the yaw rate ω_z time history, which can be seen in Figure 3.12, is analyzed a bit further. Once again, the trend of the state variable corresponds to reference model, but the amplitude is different. The relative error is evaluated according to Equation (3.10):

$$e_{rel,\omega_z} = \frac{\omega_{z,NLV} - \omega_{z,ref}}{\omega_{z,ref}} \cdot 100\% = 4.31\%. \tag{3.10}$$

The output of the used model is also a bit too low in the steady state, but not that high as it is the case when analyzing the sideslip angle. The vehicle dynamical state variable of the used model is 4.31% lower than the reference model. By looking at the differential equation of $\dot{\omega}_z$, the variables which influence the yaw rate can be identified.

$$\dot{\omega}_z = \frac{1}{I_{zz}} \left({}_V F_{y,f} \cdot d_f - {}_V F_{y,r} \cdot d_r \right)$$

Since steering causes an immediate change of the lateral tyre forces, the inclination has to be higher than in reality, since in reality there is always a delay between steering angle change and the development of the lateral tyre forces. Consequently, the inclination of the state variable is flatter. In order to get a more realistic simulation output, the steering ramp has a transition region where the steering angle increases to its desired level according to [MW04b]. Further, the position of the CoG and the yaw inertia of the vehicle also affect the amplitude of the yaw rate ω_z.

Next, the overshooting behavior of the state variable is explained. The amplitude of this overshoot depends on the longitudinal vehicle velocity . With a high longitudinal vehicle speed, the damping factor D_f becomes smaller than one. Consequently, disturbances like a steering ramp for instance, fade away oscillating according to [MW04b]. The damping measure is defined according to:

$$D_f = \frac{d}{c},$$

where the damping constant d and undamped eigenfrequency c can be evaluated with the help of the eigenvalue analysis of the autonomous vehicle system according to [HW10b]. In Figure 3.12, it can be seen that the damping factor D_f is rather low since an oscillation can be identified.The relation between the damping measure D_f and the yaw rate in order to explain the overshoot is also valid for the lateral acceleration a_y and the sideslip angle β.

The next vehicle dynamical state variable discussed and shown in Figure 3.13 is the lateral acceleration caused by the steering ramp. Since the state variables are in a tight relation to the lateral acceleration and vice versa, the trend corresponds quite well to the advanced vehicle model. The relative error in the steady state is according to Equation (3.11) 4.42%.

$$e_{rel,a_y} = \frac{a_{y,NLV} - a_{y,ref}}{a_{y,ref}} \cdot 100\% = 4.42\%. \tag{3.11}$$

Last but not least, the traveled path is analyzed in detail. Figure 3.14 shows the path covered by the present vehicle model in the solid blue line, which is compared with the reference in the red dashed line. As it can be seen, there is a deviation between both vehicle models. The difference is explained by the velocity and the steering angle at the front wheel, which are directly used from the data of the reference model. At first sight, this fact does not seem to provide any problems, but since "$MOVES^2$" is a complex full vehicle model according to Section 2.2.4, there are different steering angles at both front wheels. Thus, it is assumed that the steering angle at the front wheel for the single track model δ_{NLV} is simply the mean of both front steering angles of the more complex model according to Equation (3.12):

$$\delta_{NLV} = \frac{1}{2}\left(\delta_{f,r,MOVES^2} + \delta_{f,l,MOVES^2}\right), \tag{3.12}$$

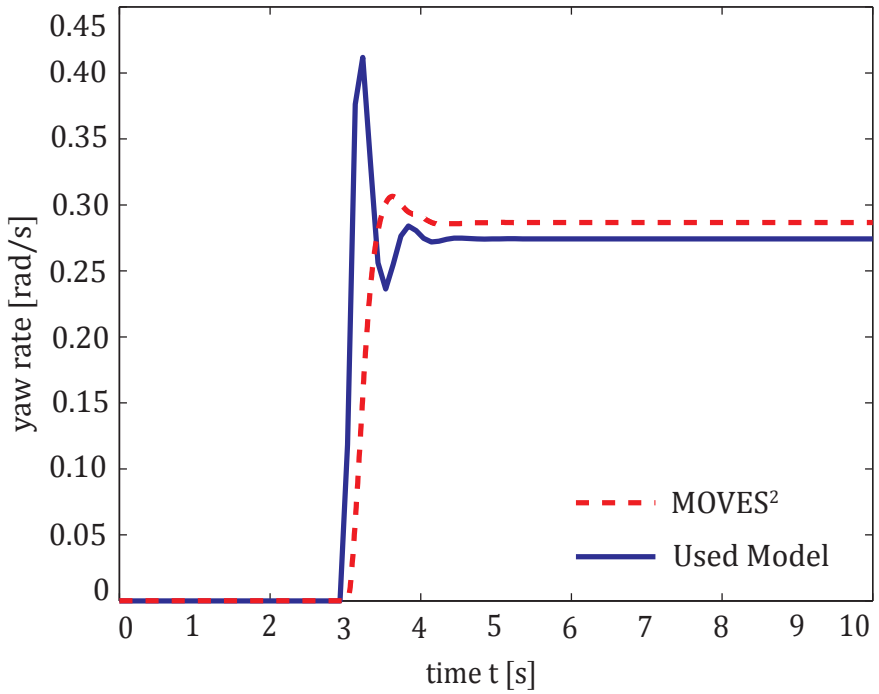

Figure 3.12.: Steering ramp - Yaw rate over time

where the indices f, r, l denote the front right and left wheel. Although this approach is a suitable approximation it does not calculate the effective steering angle at the front wheel. Consequently, a small position deviation due to this fact may occur. Moreover, the present vehicle model does not consider any elasticities neither of the suspensions nor of the steering mechanism. Overall, the trend of the position corresponds with the reference. Of course, the uncertainty of the steering angle at the front wheel of the single track model affects all the other state variables discussed for this driving maneuver. Figure 3.13 shows that the lateral acceleration is about six [m/s^2], that means according to [HW10b], the non-linearity of the tyre characteristics should be considered. But the used tyre model is primarily designed for non-critical maneuvers, and thus only operating in the linear area of the tyre. This fact is another reason for difference of the mentioned state variables to its reference values. The steady state amplitudes of the mentioned state variables may also be calculated with the help of the following relations if the radius of the driving maneuver is known.

$$a_y = \frac{v_x^2}{R}, \tag{3.13}$$

$$\omega_z = \frac{v_x}{R}. \tag{3.14}$$

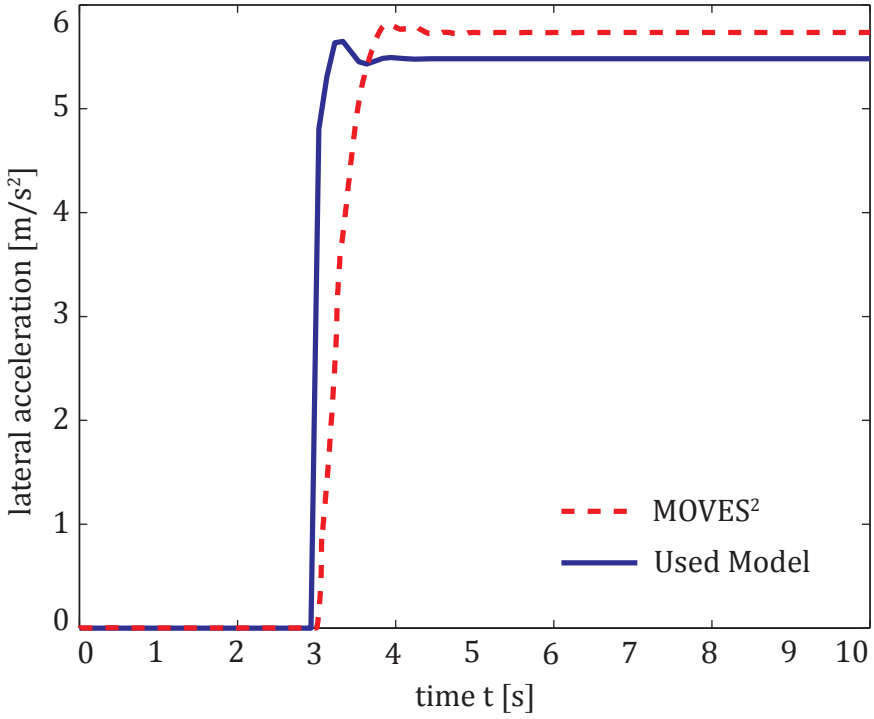

Figure 3.13.: Steering ramp - Lateral acceleration over time

Since the longitudinal vehicle speed v_x and radius of the desired circle are constant during the whole test cycle, the state variables a_y and ω_z are no longer variables. They become parameters. The only state variable remaining is the sideslip angle β.

3.4.2. Steady-state cornering with increasing velocity DIN ISO 4138

The next test method is a steady-state cornering with increasing velocity. The longitudinal vehicle velocity is a linear function of the simulation time and has got an initial value of three [m/s]. The velocity function can be written according to (3.15):

$$v_{(t)} = 0.1 \cdot t + 3, \tag{3.15}$$

where t is the simulation time in [s] and $v_{(t)}$ is the longitudinal vehicle velocity in [m/s]. The vehicle should drive on a circle with a radius of 50 [m]. Thus, the vehicle has to adapt the steering angle in order to manage such a driving maneuver where the speed permanently increases until its maximum value of 20 [m/s]. Since the whole simulation model is primarily designed for closed-loop maneuvers, the model needs the values of the longitudinal vehicle speed and of the corresponding steering angle at the front wheel for every time step. The velocity input is done straightforward, since there is a linear relation to the simulation time according to (3.15). The steer input is calculated with the same

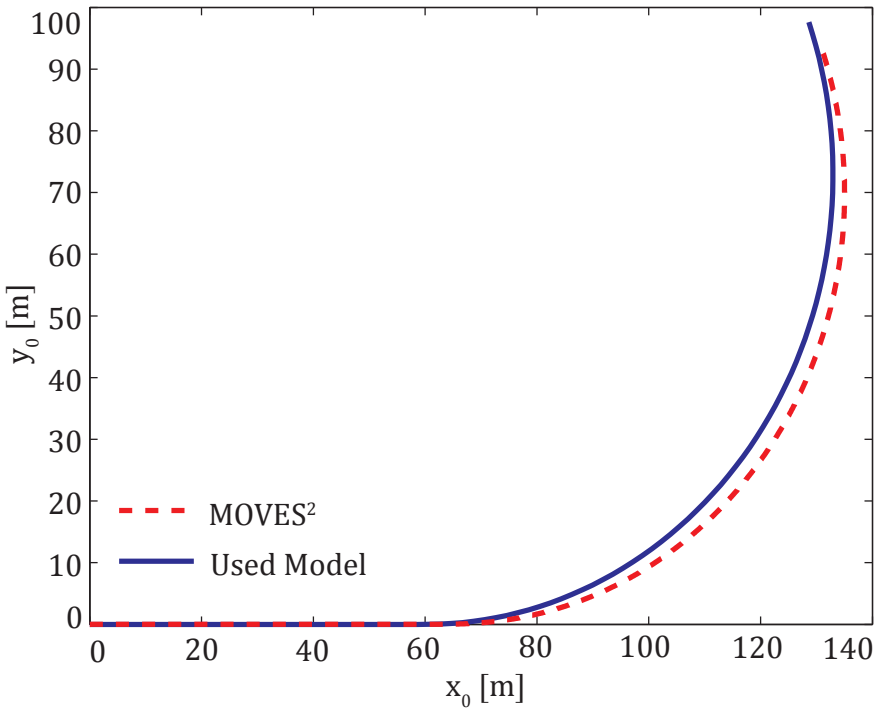

Figure 3.14.: Steering ramp - Global position

method used in Equation (3.12). Consequently, the steering angle at the front wheel and the velocity perform as shown in Figure 3.15: From a certain longitudinal speed, the additional steering angle needed to keep the desired path increases non-linearly. This phenomenon is called understeering. The additionally needed steering angle with increasing vehicle speed in a circle can also be explained with Equation (3.16), according to [HW10b]:

$$\delta = \underbrace{\frac{d_f + d_r}{R}}_{\approx \delta_A} + \underbrace{\frac{m_{veh} a_y}{d_f + d_r} \left(\frac{d_r}{dY_{0,f}} - \frac{d_f}{dY_{0,r}} \right)}_{= \Delta\delta}, \tag{3.16}$$

where δ_A is the Ackermann steering angle in [rad], $\Delta\delta$ is the additional steering angle due to the lateral acceleration a_y in [rad] and R is the radius of the driving maneuver in [m].

These two inputs result in the following characteristic curves. The first characteristic curve shows the sideslip angle β in dependency to the lateral acceleration a_y, shown in Figure 3.16. The dashed red line shows the reference values, which were evaluated with real world data. The solid blue line shows the sideslip angle of the present model. As it can be seen, the values correspond well with the reference especially in the region of low lateral acceleration until about six [m/s^2]. After that, the difference gets progressively

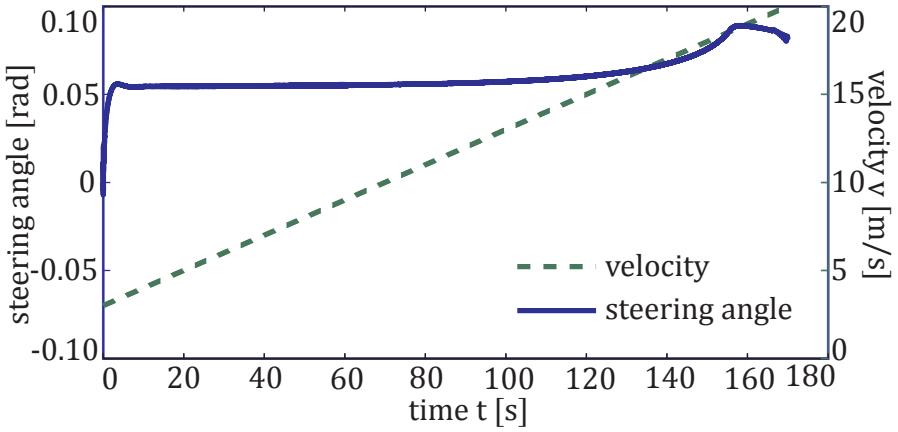

Figure 3.15.: Steady-state cornering input - Steering angle and vehicle velocity over time

worse. The developing gap arises due to the simplifications especially for the tyre model. This fact is used in order to explain the limitation of the maximum lateral allowable acceleration $a_{y,max}$ during cornering used for evaluation the maximum longitudinal vehicle velocity in Equation (2.97). The trend also corresponds quite well with the measurement data in [MW04c]. Starting with a positive sideslip angle, the value becomes zero with increasing lateral acceleration, and afterwards negative. The shape of the curve can also be explained by using Equation (3.17) according to [HW10b] and [MW04c]:

$$\beta = \underbrace{\frac{d_r}{R}}_{\beta_0} - \underbrace{\alpha_r}_{\Delta\beta}, \tag{3.17}$$

where β is the sideslip angle in [rad], d_r is the longitudinal distance of the CoG to the rear axle in [m], R is the radius of the circle in [m] and α_r is the slip angle at the rear wheel in [rad]. The symbol β_0 denotes the sideslip angle only due to geometric data and $\Delta\beta$ is the additional sideslip angle due to the increasing lateral acceleration. By applying Equation (3.17) on the used test scenario β_0 is according to Equation (3.18) 0.0282 [rad]:

$$\beta_0 = \frac{d_r}{R} = \frac{1.41}{50} = 0.0282 \tag{3.18}$$

By comparing the calculated value with the maximum value of the used model output in Figure 3.16, there is a correspondence. With increasing rear slip angle α_r, the sideslip angle β decreases.

The second state variable plotted over the lateral vehicle acceleration a_y is the yaw rate ω_z. Once again, it may be seen that the trend of the variable follows the reference well until a lateral acceleration of about six [m/s^2]. Afterwards, the deviation increases permanently.

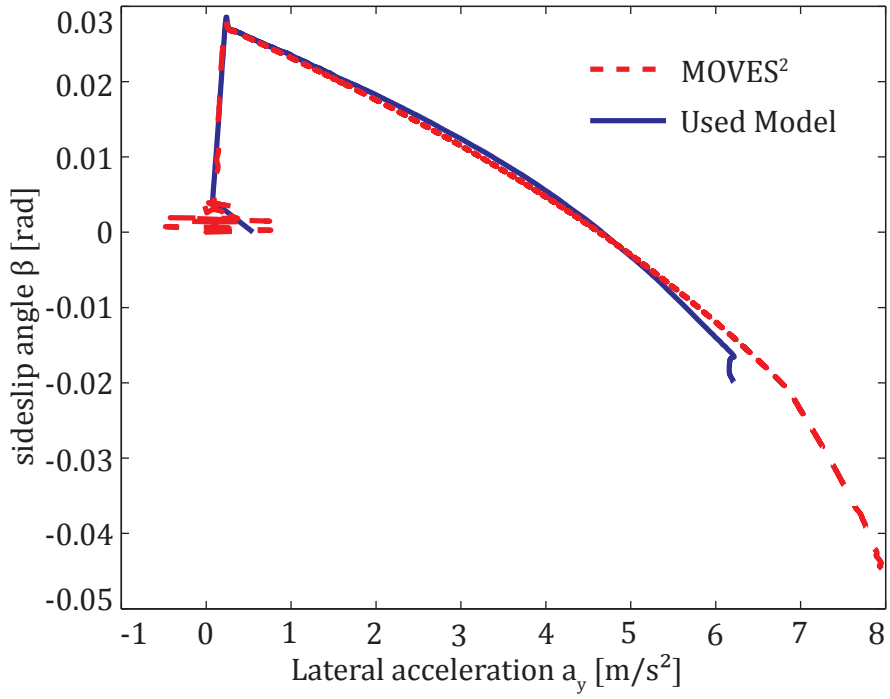

Figure 3.16.: Steady-state cornering - Sideslip angle over lateral acceleration

In conclusion to this test method, the state variables of the used vehicle model correspond well with the more advanced vehicle model and the trend of the specific variables perform similarly as shown in [MW04c] on page 597. Moreover, in [MW04c] the influence of the position of the CoG and its influence on the state variables is discussed. According to the author, a front-heavy vehicle has the shown overshoot characteristic, while a back-heavy vehicle shows an asymptotic characteristic. Since the tested car is strongly front-heavy, this fact can also be used in order to explain the trend of the vehicle. Last but not least, the shape of the steering ramp also affects the state variables. A more abrupt steering ramp increases the initial trend of the vehicle variables discussed in this section. In general, it can be said that with a higher vehicle velocity not only the steady state values, but the overshoots grow bigger as well.

3.4.3. Transient Driving Maneuver

This evaluation method shows the accuracy of the vehicle model as far as the vehicle dynamic state variables are concerned. The real world test was conducted on a test course in the city of Melk, Austria, with an Audi A4 Avant 1.8TFSI. As it can be seen in Figure 3.18 and 3.19, the basic trend of the state variables correspond well with the measurement data. Only the amplitude differs to those of the measured data. The reason for this deviation may be that the test course was not flat, which was not considered

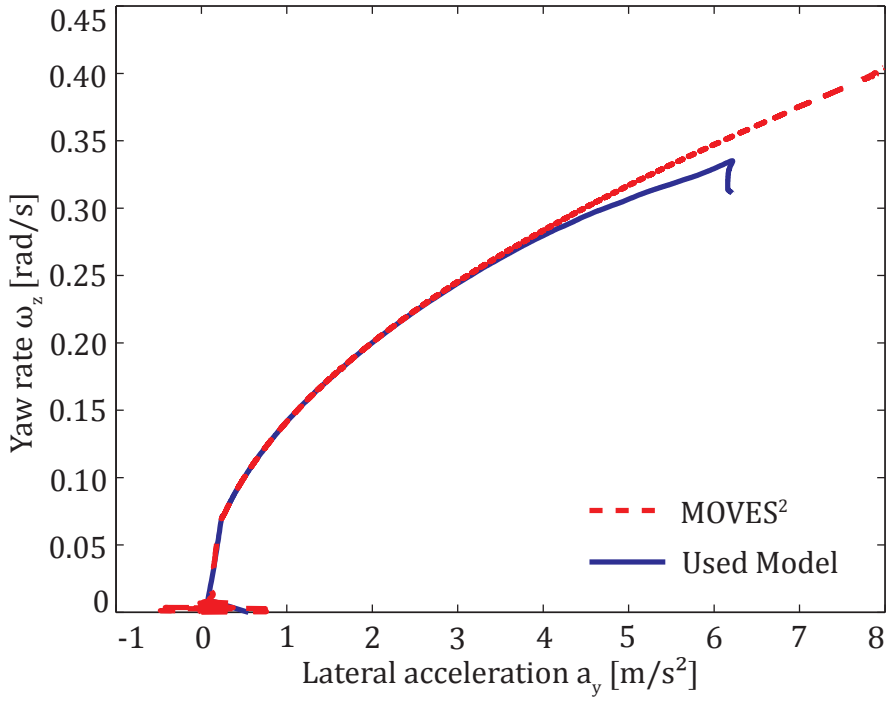

Figure 3.17.: Steady-state cornering - Yaw rate over lateral acceleration

in addition by the used measurement arrangement. The preprocessing of the needed input data, such as the vehicle speed v_x and the steering angle δ affects the results as well. Another reason for the difference can be that the steering wheel ratio is assumed to be constant in order to get the steering angle at the front wheel, which also effects the results. Thus, no elasticities of the steering mechanism are considered.

At the end of this chapter, a short summary of all the test scenarios and its results shall be given. In general, the values correspond well with those of a more complex vehicle model, but the difference strongly depends on the test. A high dynamic test such as the steering ramp, shows a bigger gap as for example a steady-state cornering maneuver. The cornering maneuver shows that the present single track model is sufficiently accurate unless the lateral acceleration does not exceed a certain threshold. Since the model is primarily designed for inner city driving maneuvers without any emergency driving situations, the inaccuracy will be kept within reasonable limits. Additionally, the implemented driver model does not allow lateral acceleration above five [m/s^2]. In the paper according to [RNFD11], the decreasing accuracy with a lower model complexity is also supported.

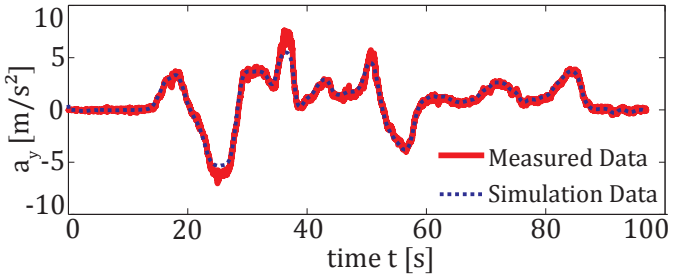

Figure 3.18.: Transient driving maneuver - Lateral acceleration over time

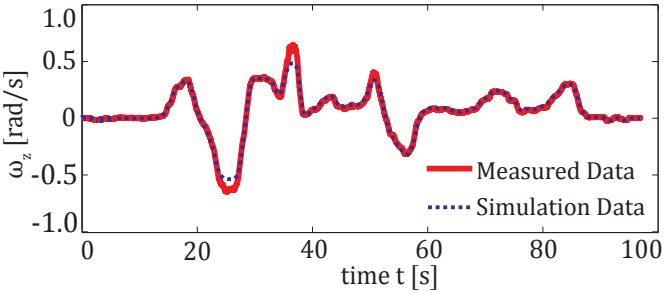

Figure 3.19.: Transient driving maneuver - Yaw rate over time

4. Summary

4.1. Conclusion

The use of simulation models in the development stage is not only a major development tool for the vehicle manufacturers, but also for experts in infrastructure planning. The major advantage of simulations is the possibility to carry out a huge amount of different test scenarios in a very short time. Consequently, costs for real world testings can be saved.

At the very end of the present diploma thesis, the most important facts shall be summarized.

This work deals with the problem of creating an efficient and real-time capable vehicle and driver model for the application in traffic flow simulation. As mentioned before the main emphasis lies on the real-time capability. This requisite affects the whole vehicle and driver modeling and consequently, some model simplifications have to be made. Thus, a compromise between model accuracy and required simulation resources has to be accomplished. I the level of accuracy is too high, the real-time capability cannot be ensured. For that reason, such complex vehicle models are mainly used in the development phase of vehicles in order to reduce development costs, to speed up that stage and to gain information about the future vehicle behavior in the early stage of vehicle development. Such virtual mock-ups [1] substitute the costly physical model more and more - in every reasonable sector. On the other hand, if the model complexity is reduced too much, which enhances the real-time capability, it has no real benefit in comparison to the vehicle models currently used in traffic flow simulations.
In order to meet both requirements, a catalogue of the main specifications was defined. The main facts are pointed out once again.

- Real-time capability for both, the vehicle and the driver model, combined with an adequate and realistic reproduction of the vehicle dynamics and the driver behavior
- A vehicle model for non-critical driving maneuvers
- The limitation of the longitudinal speed to 50 [km/h], which meets almost all inner-city driving maneuvers
- The implementation of a suitable driver model

[1] short VMU; is a high detailed model, which allows to investigate a problem on the computer screen

- The definition of suitable vehicle classes and the determination of its parameters

At first, these requirements resulted in a non-linear single track model with a simplified tyre model, but the evaluation with the help of more complex vehicle models showed that with such a model configuration a comparison was hardly possible. Consequently, the vehicle model was extended with a simple pitch and roll model. With those two extensions, it is possible to consider both, the longitudinal and the lateral change of load.

Chapter 3.4 shows how accurate the used vehicle model is in comparison to other more sophisticated models. In order to exclude possible errors due to the used driver model, all vehicle dynamics testing scenario are exclusively studied with driver-independent open-loop maneuvers. Although some simplifications have been made, the accuracy, especially in the region of low lateral accelerations, meets almost all expectations. But at higher lateral acceleration, the deviation increases disproportionately high. Moreover, it shows the benefits and the drawbacks of the present vehicle model. Nevertheless, the implemented vehicle model considers the physical effects more accurately than the currently used vehicle model for traffic flow simulations at the project partner, especially at lower lateral vehicle accelerations a_y. Moreover, the implemented driver model supports the model accuracy, since it may limit the lateral acceleration to a certain threshold, which is logically below the point where the vehicle model has its limits. Moreover, the driver model can follow a desired path autonomously. Consequently, a complicated evaluation of the needed steering angle δ and the needed pedal position p is not necessary. With the help of the fictitious driver parameters K_p, T_N, T_p, W_ψ, $K_{p,\psi}$, K_{v_ψ}, W_d, $K_{p,d}$, which are explained in detail in the programme code, the driver behavior can be adapted. Although only one driver type has been defined according to [CS09], the results are more than acceptable. In order to assess the error due to vehicle parameters uncertainties, an error analysis has been carried out.

Overall, it may be said that the present vehicle and driver model meets all requirements defined at the project kickoff. The evaluation has shown that an application in the area of traffic flow simulation is recommendable, since it improves the accuracy without affecting the real-time capability compared with the currently used model.

4.2. Future Work / Prospects

After the successful implementation of a real-time capable vehicle and driver model, some suggestions about future extensions or model improvements shall be given.
Although the real-time capability is ensured, the vehicle and driver model may be adapted to the specific application. This means that different parts of the simulation programme are optimized for its respective application. The integrator may be adapted to the specific user case, for example. In the present simulation model, an implicit integrator is implemented for stability reasons. If the initial speed is higher than about five [m/s], an explicit integrator can be used, since in this case, the explicit one performs faster, without any stability problems according to [HEW11].

Another very interesting extension of the driver model could be a path planning algorithm, explained in Section 2.5.3. The combination of a suitable driver model with such a path planning approach may be used for an "autopilot". Such a system may enhance the driving comfort and the safety. Such an "autopilot" is nowadays tested in the so-called "Stadtpilot" project of the Technical University Braunschweig, Germany, according to [SWLM11], [WSM10a] and [WSM10b].

Moreover, in order to be able to study the influence of different driving styles, groups of driver types have to be defined and the correlating driver parameters for the driver model have to be identified. By using different driver types, a more realistic distribution of the road users is ensured. Consequently, the traffic flow simulations may become even more realistic.

List of Figures

List of Tables

Bibliography

[AG11] Audi AG. Audi R8 Coupé / R8 Spyder Katalog, 2011.

[Amm97] D. Ammon. *Modellbildung und Systementwicklung in der Fahrzeugdynamik*. B.G. Teubner, 1997.

[Ano01] Anonymous. Einheitliche Vorschriften für die Genehmigung der Personenkraftwagen hinsichtlich der Bremsen, 2001.

[Ble11] B. Blei. Der Shared Space in Graz wird noch barrierefrei. Available at http://derstandard.at/1318726387968/Sonnenfelsplatz-Der-Shared-Space-in-Graz-wird-noch-barrierefrei, 21.10.2011 2011. Accessed on 10.2011 2011.

[BMW11] BMW. Der BMW X5., 2011.

[BSB07] T. Brandt, T. Sattel, and M. Böhm. Combining haptic human-machine interaction with predictive path planning for lane-keeping and collision avoidance systems. In *IEEE Intelligent Vehicles Symposium, Proceedings*, pages 582–587, 2007.

[BSW07] T. Brandt, T. Sattel, and J. Wallaschek. Towards vehicle trajectory planning for collision avoidance based on elastic bands. *International Journal of Vehicle Autonomous Systems*, 5(1-2):28–46, 2007.

[Bur82] H. Burg. Approximation von Trägheitsmomenten bei Personenkraftwagen. Technical report, 1982.

[CS09] C. I. Chatzikomis and K. N. Spentzas. A path-following driver model with longitudinal and lateral control of vehicle's motion. *Forschung im Ingenieurwesen/Engineering Research*, 73(4):257–266, 2009.

[ESP11] T. Eberl, R. Stroph, and A. Pruckner. Analyse unterschiedlicher Bedienkonzepte der Fahrzeuglängsführung bei Eletromobilität. In *Proceedings of 2. Münchner Automobiltechnisches Kolloquium*. VDI, 12.04.2011 2011. München.

[FV10] M. Fellendorf and P. Vortisch. *Microscopic Traffic Flow Simulator VISSIM* , pages 63–93. Fundamentals of Traffic Simulation. Springer Science+Business Media, LLC 2010, 2010.

[Gen97] G. Genta. *Motor vehicle dynamics: modeling and simulation.* World Scientific, 1997.

[HEW11] W. Hirschberg, A. Eichberger, and H. M. Waser. Modellbildung und Simulation in der Fahrzeugdynamik, 2011. Institute of Automotive Engineering.

[HFS11] W. Huang, M. Fellendorf, and R. Schoenauer. Social Force based Vehicle Model for 2-dimensional Spaces. Technical report, 2011.

[HHE10] T. Horrmann, T. Hüsemann, and L. Eckstein. Parameterermittlung an einem Gesamtfahrzeug. Technical report 106100, Forschungsgesellscahft Kraftfahrwesen mbH Aachen, 2010 2010.

[HRW07] W. Hirschberg, G. Rill, and H. Weinfurter. Tire model TMeasy. *Vehicle System Dynamics*, 45:101–119, 2007.

[HS07] T. Hesse and T. Sattel. Path-planning with virtual beams. In *Proceedings of the American Control Conference*, pages 3904–3905, 2007.

[HW07] M. Hardy and K. Wunderlich. Evacuation Management Operations (EMO) Modeling Assessment: Transportation Modeling Inventory. Technical report, Research and Innovative Technology Administration, ITS Joint Program Office, 2007.

[HW10a] W. Hirschberg and H. M. Waser. Fahrzeugdynamik. Lecture notes, 2010. Institute of Automotive Engineering.

[HW10b] W. Hirschberg and H. M. Waser. Fahrzeugdynamik. Lecture notes, 2010. Institute of Automotive Engineering.

[Joh77] G. Johannsen. *Der Mensch im Regelkreis: Lineare Modelle.* Oldenbourg, 1977.

[Kra08] U. Kramer. *Kraftfahrzeugführung: Modelle - Simulation - Regelung.* Carl Hanser Verlag München, München, 2008.

[Kra11] KraftfahrtBundesamt. Neuzulassungen von Personenkraftwagen im Dezember 2010 nach Segmenten und Modellreihen, 2011. Accessed on 08/01 2011.

[Mat07] W. Matschinsky. *Kurvenfahrt*, chapter 7, pages 171–230. Radführungen der Straßenfahrzeuge. Springer-Verlag Berlin Heidelberg 1998,2007, Deutschland, 3rd edition, 2007.

[MCI97] D. D. MacInnis, W. E. Cliff, and K. W. Ising. Comparison of moment of inertia estimation techniques for vehicle dynamics simulation. In *SAE Special Publications*, volume 1237, pages 99–117, 1997.

[Mes11] HKM Messtechnik. Transportable Radlastwaage RW 8.1 Produktinfo, 22.08.2011 2011. Accessed on 21.08.2011 2011.

[MW04a] M. Mitschke and H. Wallentowitz. *Aerodynamik des Kraftfahrzeuges*, pages 51–61. Springer-Verlag Berlin Heidelberg New York, 4th edition, 2004.

[MW04b] M. Mitschke and H. Wallentowitz. *Dynamisches Verhalten*, pages 584–641. Dynamik der Kraftfahrzeuge. 4th edition, 2004.

[MW04c] M. Mitschke and H. Wallentowitz. *Kreisfahrt bei konstanter Fahrgeschwindigkeit*, chapter XVIII.1, pages 556–583. Dynamik der Kraftfahrzeuge. 4th edition, 2004.

[MW04d] M. Mitschke and H. Wallentowitz. *Reifen*, pages 3–49. Springer-Verlag Berlin Heidelberg New York, 4th edition, 2004.

[MW04e] M. Mitschke and H. Wallentowitz. *Zweispurmodell, Vierradfahrzeug*, pages 710–795. Dynamik der Kraftfahrzeuge. 4th edition, 2004.

[Nat00] United Nations. Determination of vehicle's CG position, 2000.

[NHT11] NHTSA. National Highway Traffic Safety Administration, 08/16/2011 2011. Accessed on 08/16 2011.

[RNFD11] A. E. Rojas Rojas, H. Niederkofler, X. Bas Ferrer, and J. Duernberger. Modular modeling of vehicle with inovative powertrain systems. In *Proceedings of the 13th EAEC European Automotive Congress*, June 13-16 2011. Valencia.

[RS40] P. Riekert and T. E. Schunck. Zur Fahrmechanik des gummibereiften Kraftfahrzeugs. *Archive of Applied Mechanics*, 11(3):210–224, -06-01 1940.

[SB05] T. Sattel and T. Brandt. Ground vehicle guidance along collision-free trajectories using elastic bands. In *Proceedings of the American Control Conference*, volume 7, pages 4991–4996, 2005.

[SGHW08a] J. Schröder, D. Gross, W. Hauger, and W. Wall. *Bewegung eines starren Körpers*, pages 115–188. Technische Mechanik 3. Springer Berlin Heidelberg, 2008.

[SGHW08b] J. Schröder, D. Gross, W. Hauger, and W. Wall. *Bewegung eines starren Körpers; Technische Mechanik 3*, pages 115–188. Springer Berlin Heidelberg, 2008.

[SGHW08c] J. Schröder, D. Gross, W. Hauger, and W. Wall. Kinetik eines Systems von Massenpunkten, 2008.

[SGHW08d] J. Schröder, D. Gross, W. Hauger, and W. Wall. *Relativbewegung des Massenpunktes; Technische Mechanik 3*, pages 269–284. Springer Berlin Heidelberg, 2008.

[SHB+10a] D. Schramm, M. Hiller, R. Bardini, D. Schramm, M. Hiller, and R. Bardini. *Einspurmodelle*, pages 243–275. Modellbildung und Simulation der Dynamik von Kraftfahrzeugen. Springer Berlin Heidelberg, 2010.

[SHB+10b] D. Schramm, M. Hiller, R. Bardini, D. Schramm, M. Hiller, and R. Bardini. *Mathematische und kinematische Grundlagen; Modellbildung und Simulation der Dynamik von Kraftfahrzeugen*, pages 25–50. Springer Berlin Heidelberg, 2010.

[SHB+10c] D. Schramm, M. Hiller, R. Bardini, D. Schramm, M. Hiller, and R. Bardini. *Räumliche Gesamtfahrzeugmodelle; Modellbildung und Simulation der Dynamik von Kraftfahrzeugen*, pages 325–378. Springer Berlin Heidelberg, 2010.

[SHB+10d] D. Schramm, M. Hiller, R. Bardini, D. Schramm, M. Hiller, and R. Bardini. *Zweispurmodelle*, pages 277–323. Modellbildung und Simulation der Dynamik von Kraftfahrzeugen. Springer Berlin Heidelberg, 2010.

[SWLM11] F. Saust, J. M. Wille, B. Lichte, and M. Maurer. Autonomous vehicle guidance on Braunschweig's inner ring road within the stadtpilot project. In *IEEE Intelligent Vehicles Symposium, Proceedings*, pages 169–174, 2011.

[Wal05] H. Wallentowitz. *Längsdynamik von Kraftfahrzeugen*. 2005.

[WG07] H. Wallentowitz and S. Gies. *Harald Goertz: Identifikation von Fahrzeugträgheitsparametern in Fahrversuchen und auf Prüfständen*. Forschungsgesellschaft Kraftfahrwesen mbH Aachen (fka), Aachen, 2007.

[WSM10a] J. M. Wille, F. Saust, and M. Maurer. Comprehensive treated sections in a trajectory planner for realizing autonomous driving in Braunschweig's urban traffic. In *IEEE Conference on Intelligent Transportation Systems, Proceedings, ITSC*, pages 647–652, 2010.

[WSM10b] J. M. Wille, F. Saust, and M. Maurer. Stadtpilot: Driving autonomously on braunschweig's inner ring road. In *IEEE Intelligent Vehicles Symposium, Proceedings*, pages 506–511, 2010.

[Zot11] P. Zotter. Entwicklung eines Bremspedalkraftsimulators für Brake-by-wire Bremssysteme , 2011.

A. Vehicle Parameters

Table A.1.: Vehicle Parameters - Part I

Type	A_x [m^2]	c_x [-]	$\xi_{a,f}$ [%]	$\xi_{a,r}$ [%]	$\xi_{b,f}$ [%]	$\xi_{b,r}$ [%]	trc_f [m]	trc_r [m]	l_{12} [m]	d_f [m]	d_r [m]	h_{CoG} [m]	m_v [kg]	I_{zz} [kgm^2]
Minis														
Fiat 500	2.09	0.32	100	0	70	30	1.414	1.408	2.3	0.886	1.414	0.496	1106	1145
Smart Fortwo	1.95	0.37	0	100	70	30	1.283	1.385	1.867	1.052	0.815	0.417	916	543
Ford Ka	2.11	0.34	100	0	70	30	1.399	1.387	2.3	0.811	1.489	0.508	976	1031
Renault Twingo	1.96	0.35	100	0	70	30	1.414	1.4	2.367	0.869	1.498	0.518	1027	1111
Subcompact Cars														
VW Polo Trendline	2.04	0.32	100	0	70	30	1.454	1.453	2.47	0.944	1.526	0.531	1122	1396
SKODA Fabia Kombi	2.11	0.33	100	0	70	30	1.436	1.426	2.462	0.998	1.464	0.525	1164	1455
Opel Corsa	2.09	0.3	100	0	70	30	1.485	1.478	2.511	0.976	1.535	0.535	1173	1495
Ford Fiesta	2.08	0.32	100	0	70	30	1.493	1.481	2.489	0.973	1.516	0.532	1154	1440
BMW Mini 1.6 Benzin	1.92	0.33	100	0	70	30	1.24	1.21	2.595	1.590	1.005	0.552	1180	1596
Audi A1 1.6 Tdi Ambition	2.04	0.32	100	0	70	30	1.477	1.471	2.83	1.444	1.386	0.530	1815	1558
Compact Cars														
Audi A3 2.0Tdi Sportback	2.13	0.32	100	0	70	30	1.534	1.507	2.578	0.974	1.604	0.523	1432	2011
VW Golf Highline 1.4 TSI	2.22	0.31	100	0	70	30	1.541	1.514	2.578	0.972	1.606	0.528	1384	1901
BMW 120d	2.1	0.3	0	100	70	30	1.474	1.507	2.66	1.365	1.295	0.533	1491	2194
Opel Astra	2.11	0.32	100	0	70	30	1.544	1.558	2.685	1.128	1.557	0.533	1538	2316
Ford Focus 1.6 Diesel	2.26	0.3	100	0	70	30	1.535	1.531	2.65	0.972	1.678	0.541	1394	2043
Medium-sized Cars														
Audi A4 Avant 2.0 Tdi	2.19	0.27	100	0	70	30	1.564	1.551	2.808	1.204	1.604	0.548	1623	2720
Audi RS5 4.2 FSI	2.18	0.33	40	60	70	30	1.588	1.575	2.751	1.157	1.594	0.506	1902	3087
VW Passat Variant	2.29	0.3	100	0	70	30	1.552	1.551	2.712	1.073	1.639	0.540	1521	2497
BMW 316d Kombi	2.17	0.27	0	100	70	30	1.506	1.535	2.76	1.325	1.435	0.546	1558	2470
C-Klasse	2.17	0.26	0	100	70	30	1.549	1.552	2.76	1.272	1.488	0.507	1905	3063
Upper-medium-sized Cars														
Audi A6 2.7 Tdi Lim.	2.3	0.26	100	0	70	30	1.627	1.618	2.912	1.165	1.747	0.543	1834	3331
BMW 525d Lim	2.26	0.27	0	100	70	30	1.6	1.627	2.83	1.444	1.386	0.530	1815	3157
E-Klasse	2.24	0.26	0	100	70	30	1.583	1.604	2.874	1.401	1.473	0.526	1928	3423
Luxury-class Cars														
Audi A8	2.41	0.26	50	50	70	30	1.644	1635	2.992	1.346	1.646	0.531	2065	4028
BMW 730d	2.41	0.29	0	100	70	30	1.611	1.65	2.99	1.488	1.502	0.537	2014	3843
SUV														
Audi Q5	2.65	0.33	50	50	70	30	1.617	1.613	2.807	1.264	1.543	0.526	1815	2993
VW Tiguan 2.0 Tdi 4 Motion	2.55	0.38	50	50	70	30	1.569	1.571	2.604	1.069	1.535	0.498	1720	2516
BMW X1 18d	2.34	0.32	50	50	70	30	1.5	1.529	2.76	1.404	1.356	0.526	1732	2702
BMW X3 20d	2.5	0.35	50	50	70	30	1.616	1.632	2.81	1.365	1.445	0.516	1911	3167
BMW X5 40d	2.87	0.34	50	50	70	30	1.644	1.65	2.933	1.463	1.470	0.499	2248	4064
Utilities														
VW Caravelle Trendline	2.09	0.33	100	0	70	30	1.628	1.628	3	1.234	1.766	0.529	2094	3900
Sprinter	6.30	0.36	0	100	70	30	1.71	1.716	4.325	1.973	2.352	0.691	2504	10094
Truck Class														
Truck 2 axles 18t	9.2	0.6	0	100	70	30	2.00	1.80	4.7	3.006	1.694	1.250	18000	87280
Bus Class														
Bus 2 axle	6	0.6	0	100	70	30	2.00	1.80	6.3	2.1	4.2	1.4	15000	165000

Table A.2.: Vehicle Parameters - Part II

Type	i_G [-]								i_{fd}	P_{rated} [kW]	ω_{rated} [rpm]	ω_{min} [rpm]	ω_{max} [rpm]
	1	2	3	4	5	6	7	8					
Minis													
Fiat 500	3.909	2.158	1.345	0.974	0.744				3.35	62.5	5500	1000	6000
Smart Fortwo	13.23	9.604	6.899	5.235	3.8	2.73			3.92	45	5250	1000	6000
Ford Ka	3.58	1.93	1.28	0.95	0.76				4.25	51	5400	1000	6000
Renault Twingo	14.889	8.179	5.562	4.111	3.277				1	75	5500	1000	6000
Subcompact Cars													
VW Polo Trendline	3.615	1.955	1.281	0.975	0.778				4.06	51	5400	1000	6000
SKODA Fabia Kombi	3.77	2.1	1.39	1.03	0.81				3.882	51	5400	1000	6000
Opel Corsa	3.545	2.143	1.429	1.121	0.892				4.18	51	5600	1000	6500
Ford Fiesta	3.58	1.93	1.28	0.95	0.76				4.059	60	5500	1000	6000
BMW Mini 1.6 Benzin	3.308	1.913	1.258	0.943	0.806				4.158	72	6000	1000	6500
Audi A1 1.6 Tdi Ambition	3.778	2.118	1.269	0.865	0.66				3.158	66	4200	1000	5000
Compact Cars													
Audi A3 2.0Tdi Sportback	3.77	2.09	1.32	0.92	0.9	0.76			3.68	103	4200	1000	5000
VW Golf Highline 1.4 TSI	3.778	2.063	1.455	1.107	0.875	0.733			3.647	90	5000	1000	6000
BMW 120d	5.14	2.83	1.804	1.257	1	0.831			2.563	130	4000	1000	5500
Opel Astra	4.58	2.96	1.91	1.45	1	0.75			3.23	74	6000	1000	6500
Ford Focus 1.6 Diesel	3.58	2.04	1.41	1.11	0.88				4.06	74	6000	1000	6500
Medium-sized Cars													
Audi A4 Avant 2.0 Tdi	3.778	2.05	1.321	0.97	0.757	0.625			3.741	125	4200	1000	5000
Audi RS5 4.2 FSI	3.692	2.238	1.559	1.175	0.915	0.745	0.617		4.375	331	8250	1000	8500
VW Passat Variant	3.778	2.063	1.25	0.844	0.625				3.389	77	4400	1000	5000
BMW 316d Kombi	4.002	2.108	1.38	1	0.78	0.645			3.071	85	4000	1000	5500
C-Klasse	4.38	2.86	1.92	1.37	1	0.82	0.73		2.47	150	4200	1000	5000
Upper-medium-sized Cars													
Audi A6 2.7 Tdi Lim.	3.556	1.905	1.241	0.882	0.659	0.558			3.875	150	4000	1000	5000
BMW 525d Lim	4.11	2.25	1.4	1	0.8	0.66			3.46	150	4000	1000	5500
E-Klasse	4.38	2.86	1.92	1.37	1	0.82	0.73		2.47	150	4200	1000	5000
Luxury-class Cars													
Audi A8	4.714	3.143	2.106	1.667	1.285	1	0.839	0.667	3.204	273	6800	1000	7200
BMW 730d	4.17	2.34	1.52	1.14	0.87	0.69			2.563	180	4000	1000	5500
SUV													
Audi Q5	3.778	2.05	1.321	0.97	0.757	0.625			4.657	125	4200	1000	5000
VW Tiguan 2.0 Tdi 4 Motion	3.949	2.303	1.556	1.164	0.86	0.688			4.046	125	4200	1000	5000
BMW X1 18d	5.14	2.83	1.8	1.26	1	0.83			2.79	105	4000	1000	5500
BMW X3 20d	4.11	2.25	1.4	1	0.8	0.66			3.73	135	4000	1000	5500
BMW X5 40d	4.71	3.14	2.11	1.67	1.29	1	0.84	0.67	3.15	225	4400	1000	5500
Utilities													
VW Caravelle Trendline	3.769	2.087	1.324	0.919	0.902	0.757			3.684	132	4000	1000	5000
Sprinter	5.1	2.78	1.75	1.25	1	0.81			2.47	195	3800	1000	5000
Truck Class													
Truck 2 axles 18t	13.8	9.49	6.53	4.57	3.02	2.08	1.43	1.00	3.70	225	1900	800	4000
Bus Class													
Bus 2 axle	3.43	2.01	1.42	1.00	0.83	0.59			2.50	191	2300	1000	4500

B. Tyre Parameters

Table B.1.: Tyre Parameters

Type	$f_{z,nom}$ [N]	$Y_{max,f_{z,nom}}$ [N]	$Y_{max,2f_{z,nom}}$ [N]	$Y_{inf,f_{z,nom}}$ [N]	$Y_{inf,2f_{z,nom}}$ [N]	$dY_{0,f_{z,nom}}$ [N/deg]	$dY_{0,2f_{z,nom}}$ [N/deg]	a_R [-]	r_d [m]
Vehicle tyre 185/60 R15, p=2.3 bar	2500	2720	4990	2600	4700	900	1400	0.01	0.285
Truck tyre 315/80 R22.5, p=8.25 bar	35000	24500	42000	24500	42000	250000	340000	0.006	0.538